IMPROVING pH AND TEMPERATURE STABILITY OF UREASE FOR UREOLYSIS-INDUCED CALCIUM CARBONATE PRECIPITATION

by

Arda Akyel

A dissertation submitted in partial fulfillment
of the requirements for the degree

of

Doctor of Philosophy

in

Chemical Engineering

MONTANA STATE UNIVERSITY
Bozeman, Montana

July 2022

DEDICATION

This dissertation is wholeheartedly dedicated to my beloved mom, sister, grandmother, grandfather, and wife, who gave strength when I thought of giving up and continually provided their morale and support.

ACKNOWLEDGEMENTS

The process of earning a doctorate is arduous and lengthy. First and foremost, I would like to thank my wife and my family for constant support, encouragement, and understanding; it would not have been possible to get my doctorate without them.

I would like to thank my advisors, Dr. Robin Gerlach and Dr. Adrienne Phillips, for their motivation and guidance throughout my graduate studies. Thanks to all the staff, researchers, and students in the Center for Biofilm Engineering (CBE) for their collaborative support whenever I needed it, especially Pınar Günyol for her support while I was finalizing my dissertation. Thanks to the U.S. Department of Energy, grant Numbers DE-FE0026513 and DE-SC0010099, the National Science Foundation (NSF) (Award #2036867), Montana State University's Center for Biofilm Engineering, Thermal Biology Institute, Norm Asbjornson College of Engineering, Vice President for Research, Graduate Education, and Economic Development, and Wayne and L. Eileen Coursey for support throughout my studies.

Finally, I thank my other committee members for their guidance and support Drs. Ellen Lauchnor, Dana Skorupa and Stephan Warnat.

TABLE OF CONTENTS

TABLE OF CONTENTS CONTINUED

TABLE OF CONTENTS CONTINUED

TABLE OF CONTENTS CONTINUED

LIST OF TABLES

Table Page

LIST OF TABLES CONTINUED

Table Page

LIST OF TABLES CONTINUED

Table Page

LIST OF FIGURES

Figure Page

LIST OF FIGURES CONTINUED

Figure Page

LIST OF FIGURES CONTINUED

Figure Page

LIST OF FIGURES CONTINUED

Figure Page

LIST OF FIGURES CONTINUED

Figure Page

LIST OF FIGURES CONTINUED

Figure Page

LIST OF FIGURES CONTINUED

Figure Page

LIST OF FIGURES CONTINUED

Figure Page

LIST OF FIGURES CONTINUED

Figure Page

ABSTRACT

Ureolysis-induced calcium carbonate ($CaCO_3$) precipitation (UICP) is a promising technology that takes advantage of urea hydrolysis. During UICP, the enzyme urease hydrolyzes urea, and calcium carbonate can precipitate in the presence of calcium (Ca^{2+}). This process is also known as biomineralization, and urease is found in several bacterial and plant cells.

Urease must be active to enable biomineralization engineering applications such as sealing leakage pathways around wells for CO_2 sequestration. However, biotechnological reactions are limited by physicochemical conditions (temperature, pH, toxic compounds, etc.), and conditions in practice can be suboptimal.

Sporosarcina pasteurii and jack bean meal (JBM) ureolytic activities were investigated while simulating potential environmental stresses such as high temperature and pH conditions. Urease was extracted from bacterial cells to evaluate bacterial urease as an alternative to plant-based ureases. Ureolytic activities and thermal inactivation for both bacterial- and plant-based ureases were similar. Urease became thermally inactivated at elevated temperatures (> 50 °C), and urease activity also decreased when pH values moved away from circumneutral pH conditions, *i.e.*, at pH values < 5 and > 9.

Urease stability was improved through immobilization for temperatures up to 60 °C and pH values between 3.7 and 4.7. While suspended urease did not demonstrate any residual activity after a one-hour exposure to pH 4.1 at 60 °C, immobilized urease remained active after the exposure.

The studies presented here suggest that UICP technology may be used in a broad range of applications, and urease stability can be improved. The use of bacterially derived urease could be cost-competitive. UICP technology not only has the potential to solve various engineering challenges, but it also has the potential to replace traditional cement technologies and contribute to a more sustainable future.

CHAPTER ONE

INTRODUCTION

Background

The research presented in this dissertation describes investigations related to ureolysis-induced calcium carbonate precipitation (UICP) and its potential for engineering applications. Research suggests that the UICP technology can be applied using plant- and bacterial-based ureases to form biocement that may be used in sustainable building materials, soil stabilization, and subsurface sealing applications, among other uses; this process is also referred to as ureolytic biomineralization herein. For an effective application of ureolytic biomineralization, sustained urease activity is essential because urease is an essential catalyst for the reactions to occur. Ureases can be subject to reversible or irreversible inhibition, *e.g.,* through denaturation of the enzyme or at non-optimal temperature or pH conditions. This dissertation investigates the kinetics and stability of urease derived from plants and bacteria along with methods to improve the stability of urease.

This research was supported by the U.S. Department of Energy (DOE) and the National Energy Technology Laboratory (NETL) under funding Award Number DE-FE0026513 "Wellbore Leakage Mitigation Using Advanced Mineral Precipitation Strategies" and the DOE Small Business Technology Transfer (STTR) Program under DE-FG02-13ER86571 "Using Biomineralization Sealing for Leakage Mitigation in Shale during CO_2 Sequestration". Any opinions, findings, conclusions, or recommendations expressed herein are those of the authors and do not necessarily reflect the views of the DOE. Additional support was provided by Montana State University's Center for Biofilm Engineering, Thermal Biology Institute, Norm

Asbjornson College of Engineering, and Vice President for Research, Graduate Education and Economic Development, as well as through the National Science Foundation (NSF) (Award #2036867) FMSG: Biologically Assembled and Recycled Construction and Structural Materials (BRICS).

Dissertation Overview

This dissertation explored urease capabilities and stability at temperature and pH conditions, mimicking field conditions of potential subsurface and other engineering applications. The dissertation begins with a literature review of "Key Applications of Biomineralization" (Chapter 2), which was published as a chapter in a book titled "*Mineral formation by microorganisms: concepts and applications*" by Springer Nature (Akyel et al., 2022), discussing possible applications of biomineralization, such as for use in building materials, soil stabilization, bioremediation, and subsurface engineering solutions that have been realized or are currently under development. Chapter 3 describes a study investigating the thermal stability of jack bean meal (JBM) urease, resulting in a mathematical model describing the inactivation and urea hydrolysis rates as a function of temperature (Feder et al., 2020). Chapter 4 describes a strategy to find an alternative option to JBM urease; bacterial urease was extracted from *Sporosarcina pasteurii*. Growing bacteria, which does not require the use of agricultural resources, provides a strategy to produce urease quickly and potentially at the point of application. Producing urease bacterially at the point of application can reduce possible competition with food production and reduce the need to transport enzymes to the point of application. Chapter 4 assesses the thermal stability of bacterially produced urease and compares the results to jack bean urease with respect to their activity, stability, and cost. Chapter 5 investigates the ureolytic activity of JBM urease at low-pH conditions (pH 5.6-7.3) created by

pressurized CO_2, and low and high pH conditions (pH 3-12) created by synthetic buffers. Urease pH stability was further evaluated at room temperature (22 °C) and elevated temperature (60 °C), using suspended and immobilized forms of the enzyme. Chapter 6 summarizes the results of this dissertation work, summarizes the conclusions, and suggests future work to advance biomineralization-based technologies.

Chapter 2 is a book chapter that reviews literature about the potential biomineralization applications of the experimental results in the field. This chapter is published as "Key applications of biomineralization" in the first edition of the *Mineral formation by microorganisms: concepts and applications* (Akyel et al., 2022). A variety of engineering applications have already been tried or proposed, such as sustainable building materials (Achal & Kawasaki, 2016; Achal & Mukherjee, 2015; Castro-Alonso et al., 2019; Heveran et al., 2020; Ryparová et al., 2020), soil stabilization (Gowthaman et al., 2019; Kalkan, 2020; Mujah et al., 2017; Whiffin et al., 2007), or subsurface fracture sealing (Cunningham et al., 2019; Kirkland et al., 2021a; Phillips et al., 2013a; Phillips et al., 2018; Yudhowijoyo et al., 2018). This chapter describes the key applications and potential challenges of using biomineralization in three categories, 1) above-ground (*i.e.*, building materials), 2) near-ground (*i.e.*, soil stabilization), and 3) below-ground (*i.e.*, wellbore integrity).

Chapter 3 experimentally and mathematically assesses and describes the activity and inactivation of plant-based ureases at various temperatures. The ureolytic activities of JBM, cottonseed, pigeon peas, and soybean ureases were evaluated. JBM, which has the highest urease content among these plant-based sources, was chosen for in-depth analysis, and the ureolytic activity of JBM urease was investigated between 20-80 °C. With an increase in temperature, higher ureolytic activity was observed. However, above 60 °C, although urea hydrolysis rates

were higher, not all the present urea was hydrolyzed, indicating urease was inactivated at higher temperatures. The enzyme inactivation rates were calculated between 50-80 °C by exposing the enzyme to temperature conditions over various periods. Three enzyme inactivation models were investigated to determine an optimal way to model the experimental results. The determined urease kinetic parameters and the models help predict activity in desired field operations, allowing engineering applications to be designed. This work was published as "Temperature-dependent inactivation and catalysis rates of plant-based ureases for engineered biomineralization" in the journal *Engineering Reports* (Feder et al., 2020).

Chapter 4 discusses the methods to extract urease from bacterial cells, specifically *Sporosarcina pasteurii*, and explores the ureolytic activities at elevated temperatures. Methods, such as filtration and sonication, were investigated to separate urease from whole bacterial cells. The activity and inactivation of extracted bacterial urease were evaluated between 20 to 80 °C, and temperature-dependent reaction rates were calculated. Similar to JBM, as discussed in Chapter 3, the urease inactivation coefficients were calculated for *S. pasteurii* urease and compared with JBM. Cost comparisons per gram of urease were made using the urease content of JBM and *S. pasteurii*; potential advantages and disadvantages of each urease source were discussed. This chapter is in preparation for publication, and a target journal has not been selected yet.

In Chapter 5, JBM urease activity was investigated in the presence of pressurized CO_2, over a range of pH values, and at elevated temperatures. Pressurized CO_2 may result in low-pH conditions, and pH conditions play a role in ureolytic activity; ureolytic biomineralization can be an essential tool in the toolbox for sealing wells drilled for carbon sequestration purposes. Ureolytic activity was observed in the presence of pressurized CO_2 (up to 4 MPa), and the pH

increased over time with the ureolysis reaction. In the CO_2 studies (pH 5.6-9), the pH was not constant and increased over the course of an hour. Therefore, synthetic buffers (pH 3-12) were later used to assess ureolytic activity with minor pH variation. In another set of experiments, the recovery of ureolytic activity of suspended and carrier-immobilized enzymes was assessed by exposing the enzymes to low-pH and elevated temperature conditions (22 & 60 °C) before assessing the remaining ureolytic activity. Immobilization of urease provided the enzyme with better protection against low-pH and elevated temperature conditions compared to the enzyme's suspended form. This chapter is in preparation, and a target journal has not been selected yet.

The appendices contain supplemental work that has been published with the author of this dissertation as a co-author or is planned to be included in future publications. The work described therein has also contributed to the advancements in biomineralization technology and was conducted during this Ph.D. work. The appendices contain the abstracts and citations describing the enrichment and study of facultative and anaerobic consortia of haloalkaliphilic ureolytic micro-organisms capable of precipitating calcium carbonate (Skorupa et al., 2019) (Appendix A) and a numerical model for enzymatically induced calcium carbonate precipitation (Hommel et al., 2020) (Appendix B). Appendix C includes the abstract of a publication describing a field-scale demonstration of the ureolysis-induced calcium carbonate precipitation (UICP) technology for well sealing in the presence of CO_2-affected brine (Kirkland et al., 2021a). Appendix D includes the screening study on ceramic carriers to immobilize *S. pasteurii* cells and urease extract from *S. pasteurii* using sonication to investigate immobilization capabilities, potentially creating an alternative to JBM urease immobilization. Appendix E includes the screening study on pH stability of urease from *S. pasteurii* cells, similar to JBM pH stability experiments presented in Chapter 5. *S. pasteurii* urease activity drops significantly after

1-hr exposure to low-pH buffers compared to JBM urease. JBM urease was used for further investigations, and results are presented more in detail in Chapter 5.

Moreover, a patent application titled “Ureolysis-induced calcium carbonate precipitation for sealing channels and other uses” is pending with the USPTO for a U.S. patent and has the publication number: US 2022/0169908 A1 (Phillips et al., 2022).

CHAPTER TWO

KEY APPLICATIONS OF BIOMINERALIZATION

Contribution of Authors and Co-Authors

Manuscript in Chapter 2

Author: Arda Akyel

Contributions: Envisioned graphics, and major topics of the review. Wrote and revised manuscript.

Co-Author: Micah Coburn

Contributions: Drew graphics. Contributed to the writing, and development.

Co-Author: Adrienne J. Phillips

Contributions: Contributed to the revision of the manuscript with comments and feedback.

Co-Author: Robin Gerlach

Contributions: Contributed to the revision of the manuscript with comments and feedback.

Manuscript Information

Arda Akyel, Micah Coburn, Adrienne J. Phillips, Robin Gerlach

Microbiology Monographs: Concepts and Applications

Status of Manuscript:
____ Prepared for submission to a peer-reviewed journal
____ Officially submitted to a peer-reviewed journal
____ Accepted by a peer-reviewed journal
_X_ Published in a peer-reviewed journal

Springer Cham
ISSN: 1862-5576, Edition: 1

Abstract

Biomineralization is a natural process with significant potential for use in various engineering applications. Engineered biomineralization has been researched intensively, primarily to develop methods to control mineral formation by microorganisms to enable various technologies. Engineered microbial mineral formation processes have developed from theory and a proof-of-principle vision to a technology being applied in the marketplace. Biological manufacturing methods, such as engineered mineral precipitation, can significantly reduce energy intensive cement manufacturing activities and contribute to resource and climate conservation.

Introduction

Engineered biomineralization has been researched intensively for approximately two decades with a significant uptick in the past ten years. The controlled mineral formation by microorganisms has enabled technologies which were not available previously. As a result, numerous research articles and literature reviews have been written over the past decade, which summarize the research along with established or potential applications (Bang et al., 2010; Cunningham et al., 2011; El Mountassir et al., 2018; Krajewska, 2018; Phillips et al., 2013a; Phillips et al., 2018; Stocks-Fischer et al., 1999). The prior chapters of this book mostly focused on fundamental science and modeling related to understanding mineral formation by microorganisms. This chapter reviews key applications that have been realized or are currently under development. Key applications are categorized as (i) above-ground, (ii) near-ground and (iii) below-ground in this chapter. Above-ground applications consist of biological building products with potential to reduce energy intensive materials. Ground level applications consist of

surface and near-surface stabilization applications which can increase soil stability or treat toxic chemical contamination. Below-ground applications include enhanced oil recovery as well as the sealing of leakage pathways around wells.

Chemistry & Pathways

Biomineralization reactions can generally be classified into three categories: Biologically controlled mineralization, biologically induced mineralization, and biologically influenced mineralization (Dupraz et al., 2009a; Phillips et al., 2013a). Biologically induced mineralization, the precipitation of minerals as byproducts of microbial metabolism, is the most frequently used approach in application development; specifically, ureolysis-induced (aka ureolytic) biomineralization of calcium carbonates (explained in detail below) has been used most frequently in research and application development.

There are various types of minerals that can be produced by microorganisms, *e.g.,* carbonates, iron oxides, silicates, gypsum (Cecchi et al., 2018; Miot et al., 2009a; Miot et al., 2009b; Skorupa et al., 2019). At this point carbonate minerals, such as calcium carbonate, appear to be the most frequently used minerals produced for engineered biomineralization applications. A pre-requisite for the formation of minerals is that saturation for the mineral of interest is exceeded locally and at least temporally, and microbiological activities can influence saturation and promote mineral precipitation. For calcium carbonate ($CaCO_3$) mineralization, the saturation state (S) depends on Ca^{2+} and CO_3^{2-} concentrations as well as temperature, ionic strength, and other parameters that affect the solubility 'constants' (K_{SO}) (Equation 2.1) (Phillips et al., 2013a). When S is greater than 1, a system is considered supersaturated and precipitation is thermodynamically favorable (Stumm & Morgan, 2013). Supersaturation is required for precipitation, but supersaturation does not guarantee precipitation (Connolly & Gerlach, 2015)

because compounds such as organics (proteins, organic acids, chelators, etc.) can inhibit precipitation reactions (Aggarwal et al., 2013; Arp et al., 2001; Bentov et al., 2010).

$$S = \frac{\{Ca^{2+}\}\{CO_3^{2-}\}}{K_{SO}} \qquad \text{Equation 2.1}$$

Microbially catalyzed reactions that increase alkalinity and thus usually carbonate and bicarbonate concentrations are summarized in Table 2.1. Microorganisms can be responsible for carbonate generation using urea hydrolysis, nitrate reduction, sulfate reduction, photosynthesis, asparaginase hydrolysis, and iron reduction among other mechanisms. In the presence of certain cations, such as calcium (Ca^{2+}), this increase in carbonate alkalinity can induce the precipitation of carbonate minerals such as calcium carbonate ($CaCO_3$) (Equation 2) (Connolly & Gerlach, 2015; Phillips et al., 2013a).

$$Ca^{2+} + CO_3^{2-} \leftrightarrow CaCO_3 \qquad \text{Equation 2.2}$$

For each of the reactions listed in Table 2.1, microorganisms generate directly or indirectly inorganic carbon in the form of HCO_3^- or CO_3^{2-}, thus increasing alkalinity (Equation 3). Depending on the prevailing pH, bicarbonate (HCO_3^-) and/or carbonate (CO_3^{2-}) ion concentrations increase while hydroxyl ion (OH^-) production and proton (H^+) consumption occurs.

$$Alkalinity \approx HCO_3^- + 2CO_3^{2-} - OH^- + H^+ \qquad \text{Equation 2.3}$$

Calcium carbonate can precipitate in various forms, with calcite, aragonite, and vaterite being the most common forms observed (Krajewska, 2018; Mitchell & Ferris, 2006a). Transition from less crystalline phases, such as vaterite, to more crystalline phases, such as calcite, occurs through Ostwald ripening during which more thermodynamically stable mineral phases form from less stable intermediates (Connolly & Gerlach, 2015; Tourney & Ngwenya, 2009; Xiao et al., 2010).

There are many metabolic pathways used by microorganisms, which can result in calcium carbonate formation. Urea hydrolysis is likely the most frequently used pathway in engineering research and development, followed by nitrate reduction, but other metabolisms such as sulfate reduction, iron reduction, photosynthesis, and asparagine hydrolysis are also possible pathways (Connolly & Gerlach, 2015; Phillips et al., 2013a). Ureolytic biomineralization is somewhat unique among these metabolisms since it can act independently of growth and thus provides engineers with the opportunity to control mineral formation by adjusting urea and calcium concentrations and amounts while being able to rely on a fairly easily controlled catalyst: the enzyme urease. Urease is a ubiquitous enzyme, essential in nitrogen metabolism and has functions in nitrogen provision, detoxification and organismal defense (Feder et al., 2020; Krajewska, 2009a; Lauchnor et al., 2015). Urease is found in many different organisms, including bacteria, plants and fungi (Feder et al., 2020; Krajewska, 2009a; Lauchnor et al., 2015).

Table 2.1: Microbially catalyzed reactions that increase alkalinity and thus carbonate and bicarbonate concentrations with potential for engineered biomineralization applications

Biomineralization Type	**Reaction**	**Microorganisms e.g.**	**References e.g.**
Urea Hydrolysis	$CO(NH_2)_2$ (Urea) + $H_2O \rightarrow NH_2COOH + NH_3$ NH_2COOH (carbamic acid) + $H_2O \rightarrow NH_3 + H_2CO_3$ $2NH_3 + H_2O + H_2CO_3 \leftrightarrow 2NH_4^+ + OH^- + \mathbf{HCO_3^-}$	*Sporosarcina pasteurii, Bacillus sphaericus*	(Connolly & Gerlach, 2015; De Muynck et al., 2011; Phillips et al., 2013a)
Asparaginase Hydrolysis	$C_4H_8N_2O_3$ (asparagine) + $H_2O \rightarrow C_4H_6NO_4^- + NH_4^+$ $C_4H_6NO_4^-$ (aspartate) + $H_2O \rightarrow C_3H_7NO_2$ (alanine) + $\mathbf{HCO_3^-}$	*Bacillus megaterium*	(Lee & Park, 2018; Li et al., 2015)
Iron Reduction	$8FeO(OH) + CH_3COO^- + 15H^+ \rightarrow 8Fe^{2+} + 2\mathbf{HCO_3^-} + 12H_2O$	*Geobacter* sp., *Shewanella* sp.	(Connolly & Gerlach, 2015; Li et al., 2019)
Photosynthesis	$\mathbf{HCO_3^-} \rightarrow CO_2 + OH^-$ (CO_2 fixation) $\mathbf{HCO_3^-} + OH^- \leftrightarrow \mathbf{CO_3^{2-}}$	cyanobacteria, algae	(Arp et al., 2001)

Table 2.1: Continued

Biomineralization Type	**Reaction**	**Microorganisms e.g.**	**References e.g.**
Oxidation of organic Ca-salts (*e.g.*, Ca-acetate)	$Ca(C_4H_6O_4) + 4O_2 \rightarrow Ca\mathbf{CO_3} + 3CO_2 + 3H_2O$	*Bacillus pseudofirmus*	(Jonkers et al., 2010; Sharma et al., 2017; van Paassen et al., 2010b)
Nitrate Reduction (*e.g.*, with acetate as electron donor)	$5CH_3COO^- + 8NO_3^- + 3H^+ \rightarrow 10\mathbf{HCO_3}^- + 4N_2 + 4H_2O$	*Pseudomonas calcis,*	(Boquet et al., 1973; Connolly & Gerlach, 2015; van Paassen et al., 2010b)
Sulfate Reduction (*e.g.*, with acetate as electron donor)	$CH_3COO^- + SO_4^{2-} \rightarrow 2\mathbf{HCO_3}^- + HS^-$	Sulfate Reducing Bacteria (SRB)	(Connolly & Gerlach, 2015; Van Lith et al., 2003; van Paassen et al., 2010b)

Parameters Affecting Mineral Formation by Microorganisms

Environmental parameters, such as temperature and pH, as well as the chemical environment influence microbial growth and activity (Mortensen et al., 2011; Qabany et al., 2012); the same factors can also influence mineral formation. Hence, each biomineralization application at each location will require a certain level of optimization to successfully adapt to the existing conditions and control saturation. In this section we focus on describing the influence of temperature and pH value on microbial activity, saturation conditions and thus mineral formation since these two parameters are some of the most important in the development and application of engineering applications.

Temperature is important since it affects microbial and enzyme activity; temperature can also affect the saturation state of a solution since solubility 'constants' are indeed temperature-dependent; temperature can also affect mineralogy and morphology of precipitates (Feder et al., 2020; Ferris et al., 2004; Skorupa et al., 2019). As outlined in Table 2.1, there are several metabolisms that can promote carbonate mineral precipitation. Some of these reactions are microbial growth-dependent while others simply rely on the activity of enzymes produced by microbes but might not be essential for growth. Microbial growth and enzyme activity usually increase with temperature until they peak and decrease again with further increasing temperature because enzymes and other essential cell components become damaged at higher temperatures. In general, the temperature range for effective microbial growth is narrower than the temperature range for acceptable enzyme activity. For example, the ureolytic bacterium, *Sporosarcina pasteurii*, can grow at temperatures from >0°C to around 40°C, while the enzyme urease

produced by *S. pasteurii* or derived from plants is capable of hydrolyzing urea at temperatures of up to ~75°C for at least several minutes (Feder et al., 2020; Skorupa et al., 2019).

Appropriate pH values are also critical; microbial and enzymatic activities, for instance, are sensitive to pH since both, high and low pH values can inhibit or permanently denature enzymes, and other essential microbial functions (Dupraz et al., 2009b; Fidaleo & Lavecchia, 2003; Krajewska, 2016; Lauchnor et al., 2015; Qin & Cabral, 1994). With regards to calcium carbonate precipitates, pH values indirectly influence the saturation state since carbonate concentrations are strongly dependent on pH values with increasing fractions of the dissolved inorganic carbon being present as carbonate (CO_3^{2-}) at higher pH values (Table 2.2).

Table 2.2: Carbonic acid diprotic dissociation and calcium carbonate precipitation

Reaction	**Equation**	**pKa***
Carbonic acid dissociation	$H_2CO_3 + OH^- \leftrightarrow HCO_3^- + H_2O$	6.3
Bicarbonate dissociation	$HCO_3^- + OH^- \leftrightarrow CO_3^{2-} + H_2O$	10.3
Calcium carbonate precipitation	$Ca^{2+} + CO_3^{2-} \leftrightarrow CaCO_3\ (Biocement)$	-

*note that pKa values are also dependent on temperatures and ionic strength; here the pKa values are provided for ~20°C and low ionic strength

Negatively charged bacterial surfaces or extracellular polymeric substances (EPS) can act as nucleation sites for mineral formation by accumulating calcium or other multivalent cations in close proximity to each other, thus effectively increasing their local concentrations (Mitchell &

Ferris, 2006b). In addition, bacterial cell wall functional groups such as hydroxyl and phosphate groups can become negatively charged at high pH values (Phillips et al., 2013a; Rodriguez-Navarro et al., 2003; Sharma et al., 2017). The resulting, increased number of nucleation points could enable more and/or larger crystal formation events (Rivadeneyra et al., 1996; Sharma et al., 2017). Indeed, when mineral formation was examined microscopically, minerals were observed mainly associated with the bacteria initially and bacteria were observed inside mineral precipitates later on, indicating that bacteria acted as nucleation site (Zambare et al., 2020).

Key Applications

In the remainder of this chapter, current and envisioned biomineralization technologies are summarized. The most mature technologies can be separated roughly into three categories: (i) above-ground, building and construction materials, (ii) near-ground surface, stabilization applications, and (iii) subsurface applications (Figure 2.1).

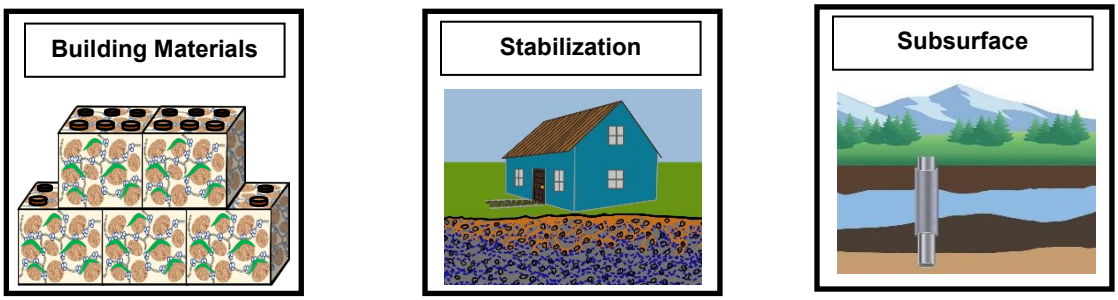

Figure 2.1: Schematic overview of the most technologically advanced applications of microbial biomineralization. The remainder of this chapter summarizes the state of the technology as well as recent research and development activities in these three main topic areas: (a) Building and Construction Materials, (b) Ground Stabilization Applications, and (c) Subsurface Applications.

The building and construction materials section covers the possibility of using biomineralization to create building materials, to remediate existing structures and the possibility of adding self-healing properties to existing or new building materials. The stabilization applications section discusses the expanding research and field demonstrations of utilizing microorganisms and enzymes to stabilize or immobilize soil, dust, and toxic mine tailings as an alternative to more traditional methods. Finally, engineering applications related to the deeper subsurface are highlighted. Biomineralization technology for deeper subsurface applications, *e.g.*, leaky well-sealing, has been developed over the past decades and has reached commercial sector application.

Different applications have different requirements with respect to time available for implementation, desired permeability, strength, toughness, etc. Thus, depending on the application, implementation strategies are likely to be different. Some applications may require the relatively rapid formation of strong bonds, *e.g.*, for building materials (bricks, foundations, etc.), while other applications, like self-healing concrete, require long-lasting biomineralization potential that can ramp up rapidly when needed to fill cracks in a structure once present (Seifan et al., 2016). Hence, it is important to understand how to control biomineralization to address the requirements inherent in these different applications.

Economics are one of the greatest hurdles in enabling the widespread use of biomineralization as an alternative to materials, such as cement which is well-established and relatively inexpensive. While biomineralization technologies are at this point more expensive, they have proven to be competitive due to their success rate, reliability, and relative ease of

implementation. Ureolytic biocementation could indeed prove to be a greener (*i.e.,* lower carbon emission) alternative since it largely avoids high temperature processes with exception of the production of urea, which is often produced through the combination of the Haber-Bosch process (Haber, 1905) for ammonia production and the Bosch-Meiser process for ammonia to urea conversion (Bosch & Meiser, 1922). Depending on the source of ammonia and CO_2 for these processes a significant amount of energy for heat and pressurization might be necessary. Other mineralization mechanisms, as outlined above, are also providing possible strategies but ureolysis-induced calcium carbonate precipitation is currently the most commonly used strategy for larger scale applications.

Building and Construction Materials

Cement production requires extensive, though well-established, high temperature processing and currently contributes 6-7% of the annual anthropogenic carbon emissions (Abdul-Wahab et al., 2016; Achal et al., 2015). Portland cement is used to produce concrete, likely the most commonly used building material in the world. Concrete is a mixture of cement, aggregate (*e.g.,* sand or gravel) and water, and overall, concrete is a durable, low-cost construction material with more than 10 billion tons used annually around the globe (Abdul-Wahab et al., 2016; Brown et al., 2014). Concrete is known for its high compressive strength but is characterized by a relatively low tensile strength. Thus, in many applications steel must be used to reinforce concrete. Under ideal conditions concrete prevents steel reinforcements from corrosion. However, cracks can form when concrete structures age or are mechanically damaged, experience freeze thaw cycles or other environmental stresses. The cracking of concrete is a

worldwide problem and, in a 2006 report, it was estimated that the annual cost for repair, protection and strengthening of concrete structures amounts to between $18 and $21 billion in the U.S. alone (Emmons & Sordy, 2006). Indeed, some large concrete structures such as bridges could be impractical to replace or will be extremely costly to repair (Gardner et al., 2018). Specifically cracks in cement can provide pathways for corrosive substance such as oxygen and water into the structures, which can lead to corrosion of the steel reinforcements. These damages can affect mechanical properties and durability of the concrete structure, consequently reducing the useful life of concrete (Achal et al., 2015).

Biological building materials are considered an alternative to concrete and biocementation is considered a viable strategy for maintenance and repair of existing concrete structures (Khodadadi et al., 2017; Van Tittelboom et al., 2010). These potentially more environmentally friendly and sustainable technologies do not require energy intensive Portland cement production. Instead, biocement requires two main constituents: (1) microorganisms (or enzymes) to initiate the biomineralization reactions and (2) aqueous solutions that provide the ingredients and proper conditions to enable the mineral precipitation. Biocement can be produced in place, using low energy methods while using local materials such as existing sand and gravel; however, a need still exists for somewhat energy-intensive raw-materials, such as $CaCl_2$ (ice-melt) and urea (fertilizer) if ureolysis-induced biomineralization is used. Both, urea and $CaCl_2$, production require energy, and comprehensive life-cycle and techno-economic analyses (LCAs and TEAs) comparing traditional Portland cement and biocement are, at this point, not available.

Biological Bricks, Grout and Mortar.Biomineralized Bricks: Bricks and pre-cast concrete parts are the most-used building materials in the world (Brown et al., 2014; Wong et al., 2018). They are part of our everyday world (Figure 2.2) and are designed to have great compressive strength, which is achieved through extensive manufacturing at temperatures above 1000°C. The company, bioMASON, is one of the first to produce biologically produced masonry products. Their current products can be used for exterior cladding, paving, flooring and on walls. These products contain approximately 85% by-product from granite quarrying and 15% calcium carbonate which is produced using ureolysis-induced calcium carbonate precipitation, thus decreasing the overall energy consumption. bioMASON's bioLITH tiles can be manufactured within approximately 72 hours and are reported to require only 3.5 % of the manufacturing energy of traditional engineered stone (bioMASON, 2020). bioMASON reports that this energy reduction is achieved by avoiding the heat treatment necessary for traditional clay brick manufacturing (bioMASON, 2020). bioMASON also reports that their products are lighter than natural stone, exceed performance in terms of CO_2 emissions and possess higher compressive strength.

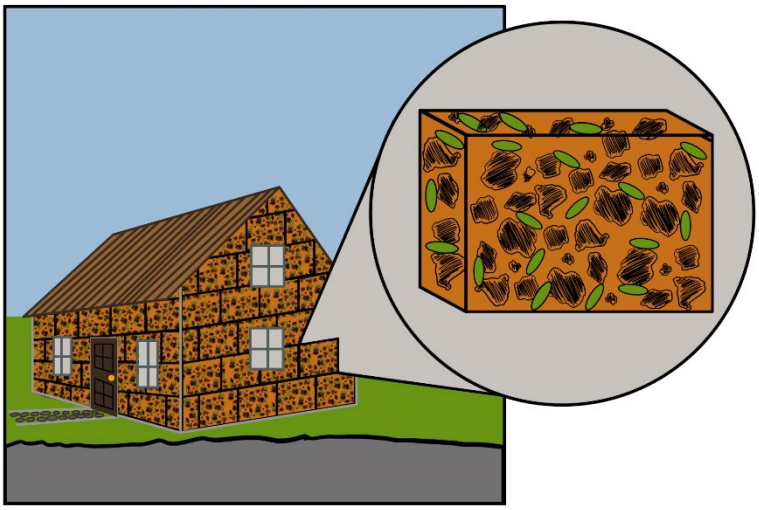

Figure 2.2: Eco-manufactured modular building materials (MBMs) are a new paradigm for sustainable construction. Bricks (orange), mortar (black lines) and grouts (not shown) can be produced through biomineralization processes. Biologically produced building materials can potentially overcome several limitations inherent to conventional cement manufacturing and usage, such as high energy manufacturing processes and lack of recyclability.

In a recent study Heveran et al. (2020) engineered a Living Building Material (LBM) using cyanobacteria to make biologically produced bricks. Cyanobacteria were placed in a sand-gelatin scaffold and the bacteria increased the stiffness through photosynthesis-driven biomineralization (*cf.* Table 2.1). The resulting products did not only provide strength but also demonstrated the ability to self-heal when deformed. Self-healing requires long term viability of microorganisms. This study suggests that lower temperatures and increased relative humidity (RH) increase cell survival with approximately 9% and 14% of cells being recoverable after 30 days at 4°C at 50% and 100% RH; lower recoveries were observed at ambient conditions (22°C and 24% RH) where cells were viable until day 7. The long-term viability of microbes must be

improved further so that LBMs can sustain their structural and biological functions for the lifetime of structures (*cf.* 'Concrete Remediation and Self-Healing Cement' section).

Biological Grout and Mortar: Grout and mortar are other materials commonly used in the construction industry. Grout and mortar are used for filling gaps between tiles and bricks among other uses. The difference between grout and mortar is that grout generally is being applied to fill and seal gaps between, *e.g.*, tiles but provides minimal structural support. Mortar is generally applied between bricks or under tiles and provides certain structural support during and after curing while also acting as a glue. Hence, grout must be able to penetrate and ultimately seal small gaps, while mortar must be viscous enough to support not only its own weight, but also that of masonry placed above it. Most grouts and mortar are Portland cement-based but synthetic grouts, such as acrylamide-, lignosulfonate- and polyurethane-based grouts are also in use; each of these compounds has its own environmental footprint (Achal & Kawasaki, 2016). Biomineral-based grouts and mortar, which are under development, have potential to reduce the environmental footprint relative to the traditional grouts and mortars.

Literature regarding the use of biomineralization to produce a biogrout for building materials, *e.g.*, tiling, is limited at this point. However, biogrouts have been demonstrated by multiple groups to have potential for concrete repair and self-healing applications. As mentioned above, grouts must readily fill gaps, voids and cracks, often with the goal of preventing the entry of water after curing. Hence, tile grouts generally require lower viscosities than mortar. *[Note: The terms 'grout', 'grouting', etc. are also used in the context of soil stabilization; the application of biomineralization-based grouting for soil stabilization is discussed in the next*

section ("b. Stabilization Applications")]. The biomineralization technology is water-based, thus low viscosity is one of its inherent characteristics. Minerals are generally precipitated through a biologically catalyzed, chemical reaction, allowing for the grout to develop in place. Biomineralization-based grouts might have advantages over traditional grouts since the microbes and enzymes are smaller than traditional cementitious grout particles and less viscous than, *e.g.*, synthetic grouts, and thus might more efficiently penetrate small gaps before precipitating and forming bonds. Indeed, it is suggested that biogrout can be less expensive than chemical grouting while achieving unconfined compressive strengths comparable to traditionally used products (Achal & Kawasaki, 2016; Li et al., 2015).

As mentioned above, mortar, in contrast to grout, needs to perform a structural function. Even during application, limited structural support needs to be provided to building components. For instance, mortar must maintain the spacing between masonry, such as bricks even during curing. Currently, there are no published works that specifically address the challenge of providing higher viscosity, mortar-like products using biomineralization methods. Furthermore, upon curing, significant structural strength (compressive strength) needs to be ensured along with other properties, such as fire resistance. Fire resistance of biobricks and biomortar is predicted to be comparable to traditional cement-based bricks and mortar since $CaCO_3$ is generally stable up to approximately 600°C after which decomposition of $CaCO_3$ to CO_2 and CaO occurs at increasing rates (Abdel-Gawwad, 2017). This decomposition also occurs in traditional cements and can result in decreases in compressive strength and other properties (Abdel-Gawwad, 2017).

The incorporation of organics into bio-bricks, -grout and -mortar must also be considered. While organics can increase viscosity and potentially elasticity, biomass, generally begins decomposing around 250°C and decomposes completely at temperatures around 500°C (Abdel-Gawwad, 2017). The effect of the loss of organics from the created biocement, grout, mortar or bricks has not been investigated in detail.

Limestone remediation.Many historic structures around the world, from the Great Sphinx to old churches to the Lincoln memorial, were constructed using limestone. Unfortunately, these structures are subject to weathering, exacerbated by the generally decreasing pH of rainwater, due to increasing atmospheric CO_2 concentrations and other acidic gases in the atmosphere (Nazel, 2016; Villa et al., 2020). These carbonate-based stones and structures are vulnerable to gradual dissolution, leading to increased porosity, the accelerated entry of water, more rapid dissolution, increased freeze-thaw damage and associated decreasing mechanical integrity (Marvasi et al., 2020; Nazel, 2016; Tiano et al., 1999).

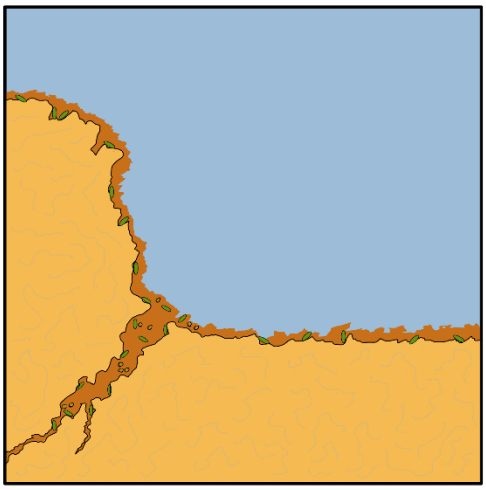

Figure 2.3: Schematic indicating the potential for biomineralization-based approaches to protect limestone structures (light orange) by filling existing cracks and cover the limestone surface with biocement (dark orange with green organisms) to minimize the entry of acidic rainwater that would lead to limestone deterioration.

Limestone remediation is often focused on preventing the entry of rain- and melt-water, the restoration of mechanical integrity and the protection of the weakened inner structure by establishing protective surface layers, filling existing pores and reducing the porosity of deteriorated limestone (Figure 2.3) (Nazel, 2016). Existing remediation methods often include the use of chemicals, such as fluorinated polymer coatings (Marvasi et al., 2020; Sadat-Shojai & Ershad-Langroudi, 2009). Biomineralization could be an ecological alternative since biomineralization mimics the natural stone formation process (Marvasi et al., 2020) and is generally based on the use of low viscosity, aqueous fluids, which can readily penetrate pores and can be applied directly onto the surfaces using low-cost approaches, such as spraying (Castanier et al., 2000; Marvasi et al., 2020; Perito et al., 2014). As outlined in Table 2.1, several biomineralization approaches result in the production of carbonate minerals and have potential

for the restoration of limestone structures. The use of alkalizing, calcium carbonate precipitating microbial cultures could also combat the development of autochthonous acidifying microbial cultures, which can locally contribute to increases in porosity and decreasing mechanical strength due to localized acidification and associated dissolution of calcium carbonates (Castanier et al., 2000).

There are still several limitations to employing biomineralization-based approaches to building restoration. The use of microorganisms can result in a certain level of skepticism in the general population. The development of stains or off-color in the precipitates due to metabolic by-products associated with the biological production of calcium carbonates is also of concern. Furthermore, the possibility of subsequent growth of other microbes (e.g. air-borne fungi) is a concern; fungi or other microorganisms, commonly referred to as 'black molds', can cause damage or defacement to building materials. Mold growth could be stimulated by decaying bacteria, added enzymes or nutrients, or metabolic by-products generated during the biomineralization treatment (Nazel, 2016). While Tiano et al. (1999) were unable to detect a color change on limestone, due to deposited biominerals, with the naked eye, it could be detected quantitatively using a chromameter (Tiano et al., 1999). The addition of pigments has been suggested, which could alleviate the potential aesthetic issue of color differences (Castanier et al., 2000; Nazel, 2016); in addition, a reduction of the amount of organics included in the treatment solutions or the use of enzymes instead of microbes could decrease potential worries regarding the use of living microbes and reduce the concern regarding subsequent growth of fungi or other microbes on the remediated surfaces. A remaining limitation is that mineral

precipitation occurs predominantly on the surface of microporous structures, on which microbes or enzymes would be deposited (De Muynck et al., 2011; Marvasi et al., 2020). The use of smaller microbes (e.g. starved bacteria or spores), which transport more readily into and through porous media (Bouwer, 2000; Cunningham et al., 2007; Gerlach, 2001) or the use of (much smaller sized) enzymes have potential to alleviate these limitations (De Muynck et al., 2011; Krajewska, 2009a).

Concrete Remediation and Self-Healing Cement.As noted above, defects, such as tiny cracks or gaps, are one of the biggest problems in cement and concrete longevity because these defects can drastically reduce the life of the structure by causing corrosion of the cement, concrete or their reinforcements. These defects can occur through quality issues during implementation, temperature fluctuations (freeze-thaw cycles), vibrations (earthquakes, traffic, construction), chemical corrosion, or other processes causing cosmetic or structural damage. Biologically induced mineral precipitation has been proposed for the remediation of cement and concrete as well as for the development of self-healing materials (Achal et al., 2015; Phillips et al., 2013a). In principle, biomineral-precipitating solutions and enzymes (or organisms) can either be applied once a defect has been discovered (remediation) or can be designed to be activated once a defect occurs (self-healing) (Figure 2.4).

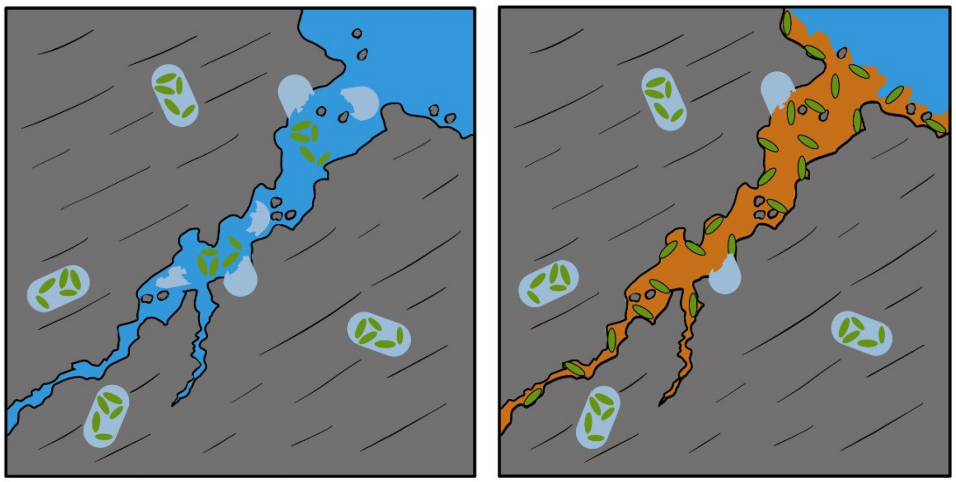

Figure 2.4: Biomineralization-driven concrete remediation and self-healing. Existing cracks can be filled with biocement (orange) or self-healing cement can be designed, which contains microbes in the form of cells or endospores as well as chemicals that promote precipitation once damage occurs. Biomineral-precipitating bacteria or enzymes are envisioned to become active once cracks occur in the cement and re-seal the developing fractures.

Establishing conditions appropriate for biomineralization to occur in cementitious materials remains a challenge. Cement, in contrast to limestone, is a very high pH environment with pH values as high as 13 combined with often low oxygen availability (Lee & Park, 2018). Both, these parameters can pose challenges for some microbes and enzymes because extreme pH values and low oxygen availability can negatively influence the survival and activity of microbes and enzymes. While the pH of water in cement generally decreases over time due to carbonation of the cement (Papadakis et al., 1989), it can remain a challenge to reliably provide pH values around 10 or lower, which are more amenable to supporting microbial growth and the activity of enzymes such as urease (Fidaleo & Lavecchia, 2003; Lauchnor et al., 2015). Some organisms have been demonstrated to have high salt and pH tolerance while being ureolytically active but

there remains a need to identify more high pH-tolerant organisms and enzymes (Skorupa et al., 2019).

Treating cracked or cracking cement materials using surface applied treatments is fairly straightforward unless cosmetics are of concern (as discussed above for many limestone remediation projects). In one laboratory study, cement specimens were immersed in suspensions containing *Bacillus sphaericus* and the resulting biomineral formation on the surface reduced subsequent water absorption by 65-90% and improved the resistance to freeze-thaw cycle damages (De Muynck et al., 2008). Biomineralization-based concrete repair approaches are suggested to be suitable for sealing cracks up to 2 mm in width (Achal et al., 2015; Wiktor & Jonkers, 2016; Wiktor & Jonkers, 2011). When crack healing was compared with control samples significant differences were observed after 100 days of immersion in water (Wiktor & Jonkers, 2011). In field trials, it was demonstrated that bacterial biomineralization systems can be used to create concrete with self-healing properties in applications such as irrigation canals and parking garages (Wiktor & Jonkers, 2016). It has also been reported that this approach could be used to potentially recycle concrete and other building materials (Wiktor & Jonkers, 2016). If post-cement damage treatment is pursued active bacterial cultures or enzymes can be used and oxygen, or other electron acceptor limitations, discussed below, are often not a concern.

The principal feasibility of using ureolysis-induced calcium carbonate precipitation by *Sporosarcina pasteurii* and other *Bacillus sp.* has been demonstrated by many researchers (see, *e.g.*, reviews by (Arias et al., 2017; Joshi et al., 2017; Krajewska, 2009b; Phillips et al., 2013a)). The feasibility of creating self-healing cements has also been demonstrated in principle (Erşan et

al., 2016b; Wang et al., 2014a; Zhang et al., 2020). In cement structures cracks occur due to changes in temperature, pressure and mechanical stresses (Jonkers et al., 2010) and most cracks start small. Thus even slow precipitation, as, *e.g.*, promoted by metabolic biomineralization might be sufficient to seal the initially small apertures and prevent them from becoming larger (Alazhari et al., 2018). However, it is less clear whether bacteria or their spores can survive long enough and resuscitate quickly enough to reliably seal cracks inside cement or concrete under the wide range of conditions expected depending on season and climate conditions (Bang et al., 2010; Mitchell et al., 2019; Sharma et al., 2017). Studies have demonstrated *B. pseudofirmus, B. subtilis*, and *B. alkalinitrilicus* are capable of self-healing cracks of <0.8 mm in concrete (Basilisk, 2020; Jonkers et al., 2010). In these and other studies, the cracks were effectively sealed in the presence of water (Sharma et al., 2017).

If self-healing of cement through biomineralization is desired for extended periods of time, the self-healing agents have to be incorporated into the cement or concrete (Wang et al., 2014b) and have to remain active, or need to be activated, inside the cement or concrete over the service life of the structure once damage occurs. It has been suggested that encapsulation of bacteria, their spores and their incorporation into cement mixtures can increase spore survival (Alazhari et al., 2018; Wang et al., 2014b). Indeed, it has been proposed that enzymes or bacteria could retain sufficient self-healing potential for years to seal cracks that might develop (Sharma et al., 2017; Van Tittelboom et al., 2010). In addition, for self-healing to occur, sufficient calcium, electron donor and acceptor are necessary, however high concentrations of material other than cement and aggregate (sand, gravel, etc.) may have detrimental effects on the

mechanical properties of the concrete (Alazhari et al., 2018). Thus, tradeoffs between the amount of additional materials to be incorporated into concrete to ensure self-healing and the required mechanical properties of concrete need to be considered.

Once resuscitation of bacteria needs to occur, electron acceptors (*e.g.*, oxygen), electron donors and a carbon source need to be available. Limitations in the availability of any one of these, can affect the rate of activation of bacteria, enzymatic activity and thus the speed of self-healing. It has been proposed to incorporate capsules into cements, containing oxygen releasing compounds, such as calcium peroxide (CaO_2), combined with electron donors, a carbon source and an additional source of calcium, such as calcium lactate. The capsules would release these compounds upon crack formation and would promote microbial resuscitation, growth, activity and ultimately $CaCO_3$ precipitation (Lee & Park, 2018).

The existence of bacterial strains capable of growth in the absence of oxygen and calcium carbonate precipitation has also been demonstrated. In laboratory studies anaerobic growth of and calcium carbonate precipitation has been observed by both, ureolytic and non-ureolytic organisms, such as fermenters, denitrifiers, sulfate reducers and iron reducers (Hamdan et al., 2017; Skorupa et al., 2019; van Paassen et al., 2010b). Until now, only nitrate reduction seems to have emerged as a possibly viable alternative to urea hydrolysis (Erşan et al., 2016a; Erşan et al., 2016b) but other methods for concrete self-repair are being developed (Zhang et al., 2020).

Basilisk, a biotechnology startup company, in the Netherlands, focuses on next generation cement additives. Basilisk produces admixtures for concrete self-repair and concrete remediation. Basilisk uses a metabolically driven biomineralization reaction, using bacterial

cultures consisting of several *Bacillus* species. Basilisk indeed uses calcium lactate as the source of calcium and encapsulates spores and calcium lactate into concrete materials for long lasting performance. The technology is protected by several patents (Jonkers, 2011; Jonkers, 2009; Jonkers & Mors, 2016; Wiktor & Jonkers, 2014) and is designed to reduce maintenance requirements, extend service life and protect concrete reinforcements. The *Bacillus sp.* spores used are estimated to survive up to 200 years as long as appropriate pH, temperature, oxygen, moisture and nutrients are provided (Jonkers et al., 2010). Basilisk's concrete repair admixtures can be mixed and applied using conventional sprayers resulting in the formation of limestone. While promising, it is unclear at this point how long the potential for self-healing will remain active.

A similar approach for self-healing was used as part of the UK's first site trial of self-healing concrete (Davies et al., 2018). In a collaboration between academic (Cardiff University) and industrial (Costain) engineers five concrete panels for a highway upgrading project were tested as part of the "Materials for Life" project. Researchers created 5 different concrete panels, one of them had bacteria in the cement mixture. When load-displacement curves were analyzed, the panel with bacteria exhibited a displacement of about 5.4 mm, while the other panels exhibited 9.2 mm displacement on average. Results after 6 months were sufficiently positive for the bacterially mediated self-healing process but longer-term assessments have to be performed to verify applicability of reducing or removing the requirement for inspection, maintenance and repair of concrete structures (Davies et al., 2018).

Stabilization Applications

Soil stabilization.Soil is a complex mixture containing minerals, liquids, gases, organic matter, and organisms that help create a dynamic environment in which many biological, chemical, or physical processes are taking place. Soils can be highly heterogeneous and inconsistent soil properties can cause structural damage or, worse, put human lives at risk. Soil stabilization is designed to provide consistent properties, and it is common practice for many construction and engineering processes including highway-, building- and airfield-construction, supporting earthen dams or embankments, irrigation networks or preventing wind and water erosion. Regardless of the application, soil stabilization involves improving the mechanical properties of the soil by either mechanical or chemical means to achieve the properties needed, *e.g.,* high strength and durability. Many different methods for soil stabilization (aka soil grouting) are available including biomineralization-based methods (Kalkan, 2020; Mujah et al., 2017; van Paassen, 2011).

Biomineralization can be applied to soils or other porous media to increase stability or enhance mechanical properties; if used for those applications, it is often referred to as biogrouting or biocementation of soils (*Note that the use of biomineralization as a potential tile grout was discussed above in the in the 'Biological Bricks, Grout and Mortar' section and was also referred to as biogrout*). As summarized in this section, biocementation has been applied at large scales and continues to be investigated as an alternative to the more traditional mechanical or chemical means of soil stabilization. Many of the current stabilization methods are reliant on mechanical means or materials with a significant energy and environmental footprint (Behnood,

2018; Mujah et al., 2017). One of the most common methods of biomineralizing soil is microbially induced calcium carbonate precipitation (MICP) treatment, which allows soil particles to be bound together by microbially precipitated calcium carbonate, providing a stable connection (or 'bridge') between the particles while maintaining sufficient permeability for water to infiltrate (Kalkan, 2020; Mujah et al., 2017) (Figure 2.5).

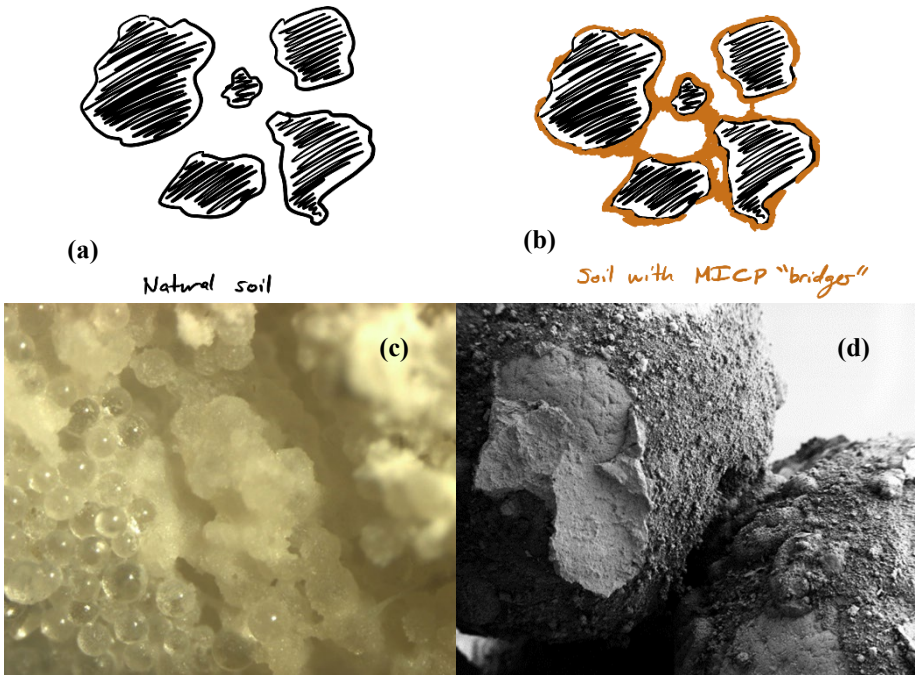

Figure 2.5: Schematic representation of biomineralization-based soil stabilization or 'biogrouting'. (a) soil particles not biomineralized represent unstable soils prone to soil liquefaction; (b) soil particles with mineral "bridges" (orange) between them. These bridging connections stabilize soils and make them less prone to liquefaction. (c) stereoscope image showing glass beads cemented together by ureolysis-induced calcium carbonate precipitates; (d) SEM image showing sand grains connected by microbial ureolysis-produced calcium carbonate precipitates (c, d: Montana State University, unpublished data).

MICP-based soil stabilization can principally be accomplished in two ways: biostimulation and bioaugmentation. Biostimulation is achieved by providing nutrients to indigenous bacteria in order to stimulate growth and precipitation, which can be beneficial in order to adapt to certain local environmental conditions such as temperature or regulatory restrictions. Bioaugmentation is the method of supplementing the soil with exogenous bacteria and has been researched more extensively for soil stabilization than biostimulation. Bioaugmentation is useful when hoping to achieve desired stabilization parameters quickly, and usually pre-cultivated organisms are used with well-known characteristics, such as *Sporosarcina pasteurii*. The ability to improve soil onsite using biocementation could significantly reduce the costs of soil improvement due to a decrease in costs associated with manufacturing and transporting materials, such as cement, bentonite or other materials, used in more traditional soil stabilization methods (Gowthaman et al., 2019; Kalkan, 2020; Mujah et al., 2017). Additional benefits might be achieved when biostimulation is utilized instead of bioaugmentation, because the materials and energy needed for pre-cultivating and transporting the bacteria are eliminated. In addition, more uniform precipitation may be achieved in the presence of native bacteria instead of injecting bacteria or enzymes into the soil and creating gradients of bacterial or enzyme concentrations, which in turn often result in non-homogeneous mineral precipitation, though this risk can be alleviated through the use of well-designed injection strategies (Barkouki et al., 2011; Ebigbo et al., 2012; Hommel et al., 2016; Hommel et al., 2015). In addition, there is a risk of ecological impacts from introducing large amounts of non-native bacteria (Gomez et al., 2019) and introducing non-native organisms might also face regulatory restrictions. Overall,

biostimulation may have the advantage of relying on organisms that have adapted to the local environment, including -but not limited to- adaptation to the prevailing dominant electron acceptor(s) but biostimulation-based implementations might be slower, at least initially, than bioaugmentation-based approaches (Gat et al., 2016; Phillips et al., 2013a).

Research by Gat et al. (2016) on the potential for biostimulation in arid and low nutrient environments, such as in coastal liquefiable sand, showed promise. This study investigated simple carbon sources (molasses and yeast-extract), which are rich in organic carbon, and found that mineralization can be achieved even when only using molasses. This could be beneficial for future research and applications aimed at achieving soil stabilization using relatively common and inexpensive carbon sources, and reducing additional costs associated with bioaugmentation. One important note from this research is the recommendation of promoting slow increases in pH when attempting biostimulation because rapid pH increases can cause significant alterations to the native soil community (Gat et al., 2016).

Dhami et al. (2017) performed a comparison between bioaugmentation and biostimulation using soil samples from the Margaret River region in Australia. In the bioaugmented treatments both, *S. pasteurii* and *Bacillus cereus,* were used for urease production and carbonic anhydrase production, respectively. Biostimulation and bioaugmentation promoting ureolysis were found to be more effective than bioaugmentation with carbonic anhydrase producers. It was also demonstrated that when high amounts of nutrients are present in the soil – either naturally occurring or through injection – both ureolytic and carbonic anhydrase augmentation were found to be effective and the carbonate crystals from MICP grew to larger

sizes than under low nutrient conditions. In addition, *S. pasteurii* and *B. cereus* were able to survive alongside indigenous organisms in high nutrient conditions, but the native bacterial populations experienced significant changes regardless of the treatment method. A key takeaway from these results were that the choice of biomineralization method may largely depend on the organic carbon content of the soil and the time available for the treatment. Biostimulation seems to be very useful in carbon rich environments, while bioaugmentation paired with supplemental nutrients may be favored in low nutrient soils (Dhami et al., 2017).

Gomez et al. (2019) compared the differences in biocementation between bioaugmentation with *S. pasteurii* and biostimulation of sandy soils using column experiments. Gradients of cementation developed throughout the columns and final calcite content between 0.5% and 5.3% by mass were observed. Near the inlet the soil was highly cemented, resulting in cone penetration resistances increasing by over 500% (up to 32.1 MPa) in the treated soils, and the shear wave velocities increased by 600% (up to 967 m/s). In addition, the biostimulated columns contained larger calcite crystals than the columns bioaugmented with *S. pasteurii* while *S. pasteurii* bioaugmented columns produced more overall crystals of smaller size (Gomez et al., 2019). Differences in amounts, distribution and crystal size of calcium carbonate could have an influence on the mechanical properties of porous media. This along with other work demonstrates strategies for achieving appropriate soil improvements depending on how soil stabilization is performed, therefore allowing customization based on the needs of the project and the regulatory framework.

Cost uncertainty is still one of the limitations of biomineralization for soil stabilization because so much of the research has been done on the laboratory scale using analytical-grade reagents. Using high purity reagents could be cost prohibitive for full-scale applications due to the amounts of urea and calcium chloride needed. Omoregie et al. (2019) compared the feasibility of using technical-grade reagents with laboratory-grade reagents along with using tap water or deionized water when preparing cementation solutions. Surface strength generally increased with increasing cementation solution concentrations, regardless of whether analytical or technical-grade chemicals and water were used. Samples treated with the highest concentrations (1.0 M) achieved surface strength values of at least 4826 kPa when measured from the top surface (the hand-held pocket penetrometer used to measure this had a maximum range of 4826 kPa). The surface strengths varied for the samples treated with 0.25 M, 0.5 M, and 0.75 M without clear relationship between surface strength and type or concentration of cementation solution. Post-treatment XRD analyses revealed nearly identical calcium carbonate content and polymorph composition with ~93% calcite and ~7% vaterite for both, the analytical grade and technical grade chemicals (Omoregie et al., 2019). These results along with the cost analysis indicate that technical-grade media may serve as a cost-effective alternative for biomineralization-based soil stabilization (Omoregie et al., 2019).

As described in Behnood (2018), one of the most common soil stabilization practices is chemical grouting. However, chemical grouting can be expensive, and it can be difficult to treat large volumes of soil due to the fairly high viscosity requiring high injection pressures and the viscosity increase over time (Mujah et al., 2017). Similar issues have been encountered with soil

biocementation; rapid precipitation and premature clogging of the injection site can occur if the bacterial suspension and the cementation solutions are injected simultaneously. Ebigbo et al. (2012) demonstrated that injection site clogging can be avoided and a much more uniform distribution of calcium carbonate can be achieved through an injection strategy, which includes rapid injection of bacteria, followed by a bacteria and urea-free rinse, a rapid injection of a calcium and urea mixture, another calcium free rinse and a rest period to allow for precipitation. Mujah et al. (2017) reported a similar strategy, during which the bacterial suspension was injected first, followed by the calcium-urea solution to achieve a more homogenous soil treatment.

Another difference between chemical methods and biomineralization are the speed of the cementation process. Depending on numerous environmental factors such as temperature, concentrations of nutrients, pH, etc. the microbes and enzymes involved in the biocementation process can exhibit varying levels of activity which can make biocementation a more complex and slower process than chemical grouting. However, biomineralization-based grouting of soils might provide a sustainable alternative to chemical grouting due to lower toxicity, lower energy requirements and tunable rates of solidification depending on bacterial (or enzyme) activity and supply of biocementation agents (Mujah et al., 2017; Reddy, 2013)

However, there are potential drawbacks with a biomineralization approach to soil stabilization. When the process involves ureolysis, the production of ammonia is a concern, especially when it has the potential to leach into groundwater. There are strategies to alleviate this potential threat through treatment of the process water and potentially utilizing the produced

ammonium as fertilizer for local agriculture (Mujah et al., 2017). The effects of adding nutrients to soil and groundwater are also not always readily predictable but may contribute to the growth of unwanted microbes (Reddy, 2013).

Fly ash, a waste product from coal combustion, has not only been repurposed for building materials (as discussed above in 'Building and Construction Materials'), it is also used in many applications including stabilization of soil and embankments. While the load bearing capacity of fly ash is generally lower than soil, ureolytic biomineralization using *S. pasteurii* stabilized fly ash and increased compressive strength by 25% to 390% (Yadav et al., 2020). In specific, fly ash samples were treated with the same number of bacteria and varying concentrations of urea and $CaCl_2$ between 0.1 M and 0.25 M. Relationships between fly ash particle size and bacteria size were determined to be important for the movement of the bacteria, with a particle size 50-400 μm being the most favorable for bacterial transport (Yadav et al., 2020). The strength of untreated fly ash was 37.19 kPa compared to 183.31 kPa for the 0.1 M urea & 0.25 M $CaCl_2$ mixture. The other concentrations resulted in strength values ranging from 46.47 kPa to 171.61 kPa. The strength increase was attributed to higher amounts of calcium carbonate and a more uniform distribution of calcite throughout the fly ash. Significant reductions in permeability (by about one order of magnitude) were observed after some of the treatments compared to the untreated fly ash (Yadav et al., 2020).

Maintaining permeability during biomineralization treatments is important, since it allows for continued injections at relatively low injection pressures and increases the treatable volume of soil, fly ash or similar (Yadav et al., 2020). van Paassen (2011) and Ebigbo et al.

(2012) specifically discussed the importance of maintaining permeability to achieve homogeneous distributions of $CaCO_3$ precipitates and how biomineralization can provide significant advantages over traditional chemical grouting techniques using resins, gels, or cement, which often drastically affect soil permeability. Ebigbo et al. (2012) developed an injection method (described in some detail above) and demonstrated experimentally and through mathematical modeling that this easily implemented method allows for a fairly homogeneous distribution of precipitated calcium carbonate. Van Paassen's work involved significant laboratory testing on sand columns and eventually a 100 m^3-scale demonstration in a testbed. It was found that approximately 43 m^3 of the sand were successfully cemented and had compressive strengths of up to 12 MPa. The cementation patterns on the 100 m^3 scale followed the patterns of the fluid flow through the soil but were unfortunately not homogenous (van Paassen, 2011; van Paassen et al., 2010a). Subsequent laboratory and field tests were performed by van Paassen et al. to demonstrate the feasibility of stabilizing gravel beds with biogrout. Borehole collapse during horizontal directional drilling is a common problem, so several laboratory experiments, a mesoscale experiment in a 3 m^3 container of gravel and a field demonstration were performed in the Netherlands. Gravel bed stabilization was successful and up to 6% of the total dry weight of field samples were described to be calcium carbonate (van Paassen, 2011).

Although biomineralization for the purpose of soil stabilization has primarily been performed using urea hydrolysis-induced calcium carbonate precipitation, there is emerging research into other microbially induced methods as well. Specifically, nitrate reduction-induced

calcium carbonate precipitation may be a promising alternative and is often referred to as MIDP (Microbially Induced Desaturation and Precipitation). Initial successes on the laboratory and field scale have been demonstrated (van Paassen et al., 2010b; Wang et al., 2020; Wang et al., 2021; Zeng et al., 2021). Nitrate reduction promotes calcium carbonate precipitation according to the reaction outlined in Table 2.1 with nitrogen gas being the major by-product. In contrast to the ammonium produced during urea hydrolysis, the nitrogen gas would not require removal and can result in desaturation of the soil, which can be desirable when trying to reduce the liquefaction potential of soils (Figure 2.6). Both, urea hydrolyzing and nitrate reducing microorganisms are ubiquitous in soils and the addition of substrates such as calcium acetate and calcium nitrate will readily stimulate growth of denitrifying microbes. As outlined in Table 2.1, the activity of denitrifiers will increase carbonate alkalinity and promote the precipitation of calcium carbonate. A potential drawback of this method can include slower than urea hydrolysis-induced calcium carbonate precipitation because denitrification is a growth-dependent process while urea hydrolysis may be growth-independent. Furthermore, the produced nitrogen gas can impact the permeability and thus the calcium carbonate distribution through MIDP treatment. In addition, nitrite, nitrous oxide, and nitric oxide are all potential unwanted by-products, which can accumulate if nitrate reduction is incomplete, and thus would also require treatment of the process water and potentially soil gases (van Paassen, 2011).

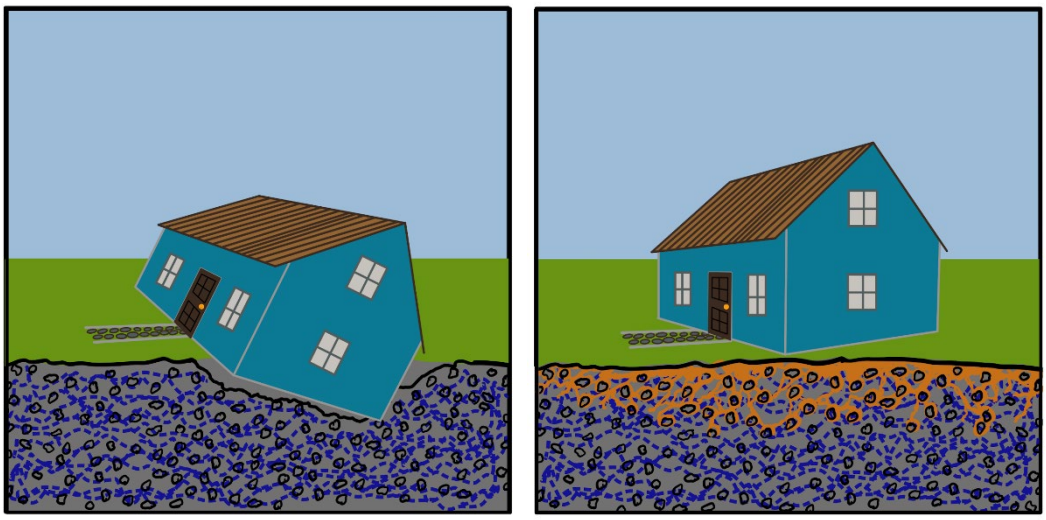

Figure 2.6: Left, untreated loose soil can cause foundations to fail and structures to be damaged. Right, soil stabilized using engineered biomineralization.

Wang et al. (2021) recently summarized the potential for nitrate reduction-induced MIDP to stabilize soils that are prone to liquefaction in an effort to reduce the risk to structures built on these types of soils. There are a number of research and development projects that have focused on the potential of using the combined desaturation of and calcium carbonate precipitation in porous media to improve soil properties (O'Donnell et al., 2017a; O'Donnell et al., 2017b; Pham et al., 2018). Media optimization demonstrated that denitrification and $CaCO_3$ precipitation rates were maximal with only small amounts of toxic by-products accumulating when the molar carbon to nitrogen ratio was 1:1.6 (Pham et al., 2018). Based on measurements of pore water pressure, volumetric strain and cyclic shear resistance behavior soils treated with MIDP were found to be at a significantly lower risk for liquefaction (He et al., 2014). Even when the saturation only decreased by 5% shear strength was significantly increased (He et al., 2014). Wang et al. (2021) reported details of work demonstrating that even a single MIDP treatment can

reduce the saturation of soils to 80%, however the saturation and mechanical properties achieved through MIDP appeared to vary depending on the type of soil and number of applications (Wang et al., 2021). In summary, biomineralization-based soil stabilization technologies are beginning to mature to full-scale applications and their potential is beginning to be recognized by contractors and customers. It is expected that full-scale applications of biomineralization-based biogrouting technologies will become common over the next decade.

Mine Tailings and Bioremediation.Remediation of mine tailings is another promising application of biomineralization. Mine tailings are often problematic because of the danger of collapse and the potential of releasing metals such as Cu, Pb, Zn, Cd, Cr, Se, and As, thus posing a risk to human and environmental health. Heavy metals can leach through rain- or snowmelt-waters. Immobilizing or otherwise shielding heavy metals from exposure to water can reduce the metal leaching rate (Reddy, 2013; Yang et al., 2016). There are a number of more traditional treatment methods that can be applied, including phytoremediation, thermal treatments, excavation, electro reclamation and capping (Reddy, 2013; Yang et al., 2016). Biomineralization of soils or mine tailings loaded with heavy metals, as demonstrated by Yang et al. (2016), has been proposed as a treatment considering how stable MICP precipitates can be in multiple geological settings (Figure 2.7)**.**

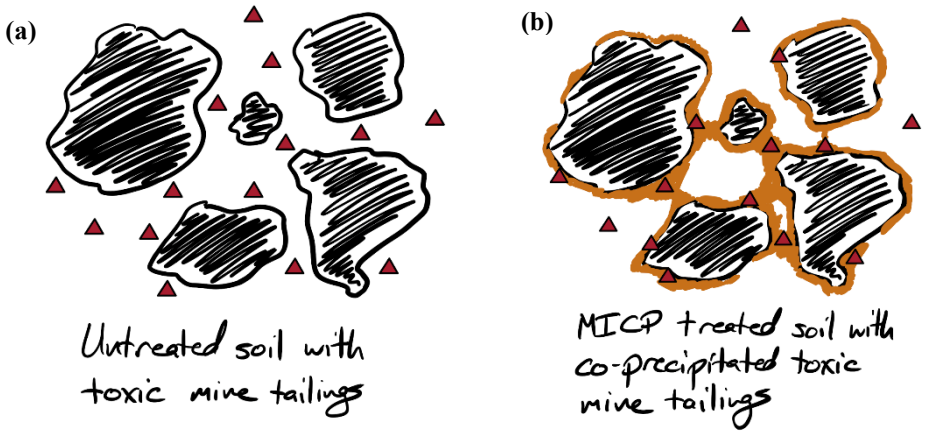

Figure 2.7: (a) Untreated soil in the presence of toxic metals (red triangles) from mine tailings, (b) the biomineralization process can co-precipitate toxic metals initially present in the solution while also providing additional surface area for sorption.

Yang et al. (2016) isolated the urease-producing bacterium, *Bacillus firmus*, from acidic copper mine tailings at the Xinjiang Copper Industry Co. Ltd in China. *B. firmus* XP8 exhibited high urease activity and resistance to high metal concentrations. XP8 cells were grown overnight and exposed to the contaminated soil for 7 days; uninoculated control samples maintained a pH of 5.6 while the pH of inoculated mine tailings rose from 5.6 to 7.7 within 7 days. The original soil had a pH of 2.7 because it had not yet been amended with the nutrient media. Soil pH is an important factor when considering this method of metal immobilization because higher pH encourages precipitation by affecting the solubility of metal hydroxides, carbonates, and phosphates (Yang et al., 2016). Because the bioavailability of a metal can influence its resulting toxicity, sample analysis was performed for five different fractions of metals (soluble-exchangeable, carbonate-bound, Fe/Mn oxide-bound, organic/sulfide-bound, and 'residual fraction') to estimate bioavailability. The metal content of each fraction was divided by the total

amount of that specific metal found in the mine tailing soil; this ratio was termed the distribution coefficient. Carbonate-bound metals increased after MICP treatment while the soluble-exchangeable fractions decreased (Yang et al., 2016) demonstrating the ability of biomineralization-based technologies to reduce the bioavailability and mobility of toxic metals.

Zhao et al. (2017) found significant potential for MICP to be a sustainable and efficient method for treating water contaminated with heavy metals. Zhao et al. (2017) observed a cadmium removal efficiency of ~53% (10 to 4.7 mg/L) after 3 hours, and 61% after 48 hours using MICP promoted by a *Bacillus* sp. isolated from mine soil. Mugwar and Harbottle (2016) investigated the MICP-based remediation potential for cadmium, zinc, lead and copper using *S. pasteurii*. They observed that, when the medium was amended with urea, microbial activity continued even in the presence of metal concentrations that were higher than previously determined minimum inhibitory concentrations (MICs). Their research suggests that even though microbial activity might be inhibited in the presence of heavy metals, with urea present there is sufficient ureolytic activity to promote the co-precipitation of heavy metals using MICP. As the metals co-precipitate, the toxicity of the solution is reduced and enables increased hydrolysis and precipitation. These results indicate that MICP remediation is possible even at metal concentrations significantly higher than estimated based on toxicity data as long as a large enough proportion of the initial microbial population survives, commences urea hydrolysis and induces calcium carbonate precipitation. Li et al. (2013) performed a similar study and found that a strain of *S. pasteurii* was able to achieve greater than 90% removal of cadmium, zinc, copper, and lead within two hours. Results of control treatments were not reported by Li et al. (2013),

thus differences in the rates and extent of metal removal compared to other studies could be due to abiotic processes (Li et al., 2013; Mugwar & Harbottle, 2016).

Kumari et al. (2014) compared the ability of the ureolytic bacterium *Exiguobacterium undae* to remove cadmium from soils at 10°C and 25°C. After the original sample of soil was air-dried and autoclaved, 100 mg of $CdSO_4$ were added per 1 kg of soil followed by addition of an overnight culture of *E. undae*. Forty-five % of Cd^{2+} were immobilized within one hour at both temperatures, and after five hours the immobilized Cd^{2+} reached 79% and 84% for 10°C and 25°C, respectively. After two weeks, the more bioavailable, soluble-exchangeable fractions of cadmium had been reduced by about 97% relative to untreated controls at both temperatures. Over the same two-week period the more stable, carbonate-bound form of cadmium in the soil increased approximately three-fold to 71.4 mg kg^{-1} and 67.8 mg kg^{-1} for the 25°C and 10°C MICP treatments relative to untreated controls (Kumari et al., 2014).

As mentioned at the beginning of this section, the stabilization of mine tailings is also important. Gowthaman et al. (2019) evaluated the effectiveness of stabilizing soil slopes in cold subarctic regions by isolating *Lysinibacillus xylanilyticus*, an indigenous, ureolytic bacterium from soil samples taken from Onuma, Hokkaido, Japan. The bacterium was tested for growth and urease activity at temperatures ranging from -10°C to 50°C to address the potential of MICP for the treatment of mine waste tailings in colder regions. Most work, so far has only been performed within the temperature range of 25°C to 60°C (Gowthaman et al., 2019; Kumari et al., 2014). Little growth of *L. xylanilyticus* was observed above 40°C and urease activity appeared to be insignificant below 5°C and above 25°C, but relatively stable between these temperatures

(Gowthaman et al., 2019). Soil stabilization experiments were performed with three types of sand with average particle sizes (D_{50}) of 1.6 mm, 0.87 mm, and 0.2 mm as well as with soil samples; the sand fraction of the soil had an average particle size (D_{50}) of 0.23 mm. In column experiments the MICP-treated sand was found to have a UCS (uniaxial compressive strength, estimated using a needle penetrometer) about 3.75 times higher than untreated sands. The authors concluded that the fine particles present in the slope soil -about 12% of this soil consisted of particles with a grain size of less than 125 μm- were beneficial in providing support for the calcium carbonate bridging between larger sand grains. It was also noted by Gowthaman et al. (2019) that very fine particles may have limited permeability that could limit infiltration of bacteria and cementation solutions into the soil; a challenge discussed above in the context of fly ash stabilization in the 'Soil Stabilization' section. Recognizing that fine particles can aid in stabilization but can become problematic at higher percentages within the soil should be an important consideration in future biomineralization technology scale-up.

Gowthaman et al. (2019) also tested samples modeled as a physical slope instead of a column (Figure 2.8). More than 80% of the soil was successfully stabilized with a 3-4 cm layer of cemented soil at the surface, while the soil below that layer was not successfully stabilized. The UCS of the slope surface was determined to be between 2 to 8 MPa with the higher strength values being obtained from the lower areas of the slope. This difference was attributed to the injection method, which likely caused the bacteria being transported preferentially toward the bottom of the slope sample.

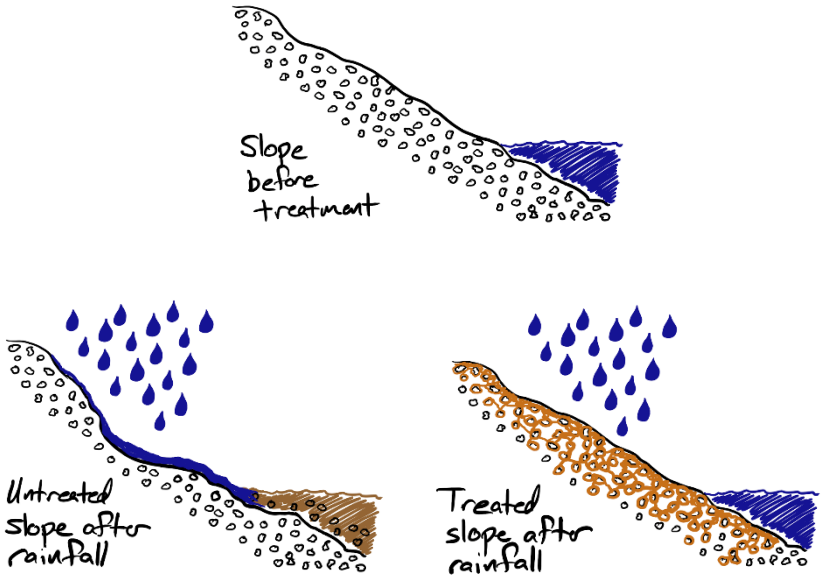

Figure 2.8: Biomineralization treatments can stabilize slopes reducing erosion during runoff, snowmelt, etc.

Dust Suppression.Another problem being addressed by utilizing biomineralization is dust suppression and erosion control. Among other contributors to erosion, wildfires are becoming more frequent and the altered chemical and biological makeup of burned soil can lead to problems with erosion, water quality, flood control and general ecosystem health (Hodges & Lingwall, 2020). Current technologies have not been able to provide a cost-effective method for treating large areas affected by forest fires in order to prevent erosion (Hodges & Lingwall, 2020). Hodges and Lingwall (2020) explored the effects of wind and water on burned soils that were treated using MICP; both, bio-stimulation and bio-augmentation were evaluated. *S. pasteurii* and different concentrations of biomineralization solutions, which consisted of urea, nutrient broth, ammonium chloride and $CaCl_2$, were applied to soil samples (Figure 2.9). In

addition, some soil samples were treated with only the urea-broth solution with bacteria and no added calcium or with only the urea and Ca^{2+} solutions but no added bacteria to compare potential benefits of bioaugmentation vs. biostimulation. Erosion tests were performed at 10, 20, and 30 mph simulated wind speed on burned and unburned soils subjected to the above treatments (Hodges & Lingwall, 2020). Successful treatments created a water-permeable crust that stabilized the soils through an increase in soil strength by 25-50 kPa. These MICP treatment methods were generally not effective against mass loss at higher wind speeds, but even a single application resulted in some stabilization and a thin crust layer which could play an important role in protecting the soil for long enough to allow new plant growth to develop and further stabilize the soil. At lower wind speeds, these biomineralization methods were more successful and proved effective for dust control for both burned and unburned soil. Similar to the smaller particles discussed above in the 'Mine Tailings and Bioremediation' section, ash particles could be improving the stabilization of the soils by promoting calcium carbonate bridging between larger sand grains. In addition, it was found that there were beneficial effects through treatment with only urea solutions, only calcium solutions or without the addition of bacteria. The reasons for these improvements have not been explored in depth and further tests are being performed (Hodges & Lingwall, 2020).

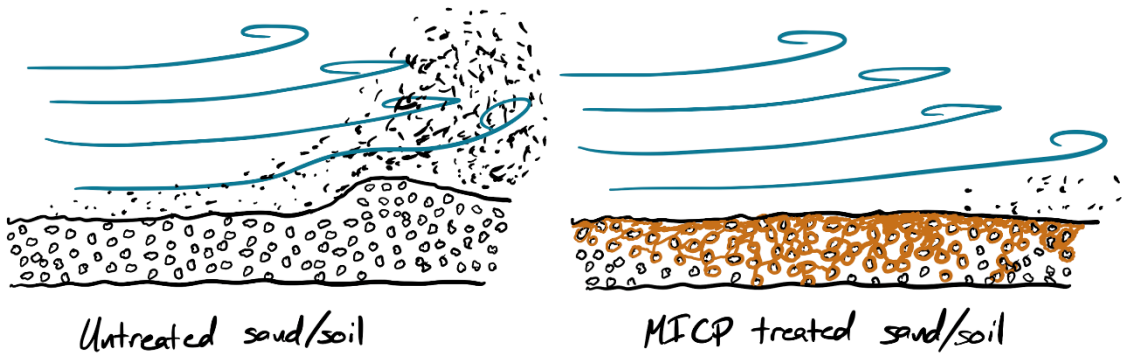

Figure 2.9: Schematic representation of dust suppression using engineered biomineralization treatments. Microbially produced mineral precipitates cement together fine particles that would otherwise be eroded as dust during wind and weather events.

Similar to burned soils, sandy soils can also contribute to dust pollution and many regions could benefit from dust suppression. Almajed et al. (2020) explored the use of enzymatically induced calcium carbonate precipitation (EICP) treatment to manage wind-caused erosion of desert sand. Multiple concentrations and combinations of urea, calcium chloride, sodium alginate (SA, a biopolymer) and powdered milk were applied to sand samples; EICP was promoted using jack bean urease. Multiple treatments were evaluated, including different molar urea to calcium chloride ratios (1:0.67 and 1:1.25), SA solutions of 0.5%, 1.0%, and 2.0%, treatments with only $CaCl_2$, along with samples treated with only water or untreated samples (Almajed et al., 2020). All treatments, except the untreated controls and water only treatments, formed a crust and the resistance to wind erosion increased after curing the samples for seven days. The erosion resistance remained effective after 28 days with erosion rates (percent of mass loss), staying below 0.01% for all treated samples. This represented a significant improvement over the erosion

rate of the control and water treated samples which were around 97% and 94%, respectively (Almajed et al., 2020). Similar to previous studies, the points of contact between soil particles were stabilized by the presence of calcium carbonate, which contributed to erosion resistance. An additional factor contributing to the wind resistance in the SA treated soils was the formation of alginate hydrogels created as divalent calcium ions replaced sodium ions within the sodium alginate. While the developed hydrogel increased the soils' ability to resist erosion and retain water, it also reduced the permeability of the soil making it more difficult for EICP treatment solutions to penetrate deeper into the soil; as a result, thinner crusts were observed in the SA-treated soils (Almajed et al., 2020).

Research and development are continuing with the goal of increasing the effectiveness and usefulness of biomineralization for multiple stabilization applications, including soil stabilization, stabilization and immobilization of metals in mine tailings and other bioremediation applications, as well as in dust suppression. The use of microorganisms and enzymes to promote mineral precipitation offers potential benefits, including being more environmentally friendly, reducing costs and energy usage. However, there is still limited use of this technology on the larger scale, and further research and development is needed.

Subsurface Applications

The earth's subsurface contains many important resources, such as water, minerals, oil and gas. The subsurface is also used for the storage of natural gas and other compounds, such as wastes, wastewater and CO_2 (Baines & Worden, 2004; Bauer et al., 2013; Ferguson, 2015). In addition, the subsurface is used for the purification of useful products, such as drinking water. A

concern exists that contaminants from natural or anthropogenic sources can enter the subsurface where they can pose a risk to human and environmental health. Technologies exist to inject or extract compounds into or out of the subsurface, and engineering applications, such as oil production, deep subsurface mining, groundwater management and subsurface remediation are common (Montana Emergent Technologies, 2020; National Research Council, 2005; Yudhowijoyo et al., 2018).

Leakage pathways around wells or in their vicinity can be problematic for any subsurface application since they can lead to loss of injected or stored fluids as well as result in inefficient recovery. However, safe injection into, storage in and recovery from the subsurface are essential, and ensuring wellbore integrity is in turn essential for environmental and economic reasons. Wellbore integrity can be defined as the "application of technical, operational and organizational solutions to reduce risk of uncontrolled release of formation fluids throughout the life cycle of a well" and wellbore integrity concerns are often related to the development of leakage pathways (NORSOK Standard, 2013). Leakage pathways can often be sealed using cement injections ('cement squeezes') with Portland cement remaining the most commonly used wellbore integrity remediation agent (Kirkland et al., 2020; Yudhowijoyo et al., 2018). Unfortunately, in some cases leakage pathways consist of very small aperture fractures or delaminations that can be difficult to seal because the low injectivity of these small aperture leakage pathways might require injection pressures higher than permissible during wellbore remediation, due to concerns regarding damage to the well or the formation. Thus, cement squeezing might be ineffective or even impossible because the fairly large cement particles simply might be too big to effectively

enter and seal small apertures (Phillips et al., 2018). An advantage of biomineralization-based methods is that the minerals are formed *in situ* by microbes from aqueous solutions. Microbes are only a few micrometers in size and can therefore access areas inaccessible to regular cement (Cunningham et al., 2011; Kirkland et al., 2019; Phillips et al., 2013a; Phillips et al., 2018).

Enhanced oil recovery, wellbore-sealing and secure subsurface CO_2 storage are some of the applications, which have been demonstrated on the field-scale using engineered biomineralization technology (Cunningham et al., 2011; Hommel et al., 2020; Mitchell et al., 2010; Montana Emergent Technologies, 2020; Phillips et al., 2013b).

Finite Resource Recovery.Enhanced oil recovery (EOR) operations are designed to increase the recovery of finite oil and gas resources from existing reservoirs (Alvarado & Manrique, 2010). Enhanced oil recovery is generally achieved through a process called ‘sweeping’, during which fluids are injected into oil-bearing formations to push remaining oil out of the formation. Often water is injected into one well to ‘push’ oil towards another well, which is pumping (‘pulling’) the oil out of the ground (Thomas, 2008). The process becomes challenging if high permeability zones exist, through which the injected water escapes. These zones are often referred to as ‘thief zones’ and transport injected fluids at rates faster than the oil-bearing formation therefore reducing the net recovery of resources (Kirkland et al., 2020; Sen, 2008). Even though having higher permeability, these thief zones still consist of formations with fairly small pores or fractures (Figure 2.10). It can be challenging to reduce the permeability of these zones reliably using cement injection since cement cures over a finite amount of time and it is necessary to control where cementing occurs.

Biocementation fluids have viscosities similar to water and can be transported with the injection water into thief zones where the enzymes or bacteria adhere to the pore or fracture surfaces. Subsequent injection of biocementation fluids (*e.g.*, urea and calcium containing solutions) promotes precipitation of minerals (*e.g.*, calcium carbonate) in the areas where bacteria or enzymes are present, which reduces permeability (Ebigbo et al., 2012; Kirkland et al., 2020; Sen, 2008). When permeability is reduced sufficiently in the thief zone, injected sweeping fluids will travel through oil-bearing zones for additional resource recovery as demonstrated by Kirkland et al. (2020).

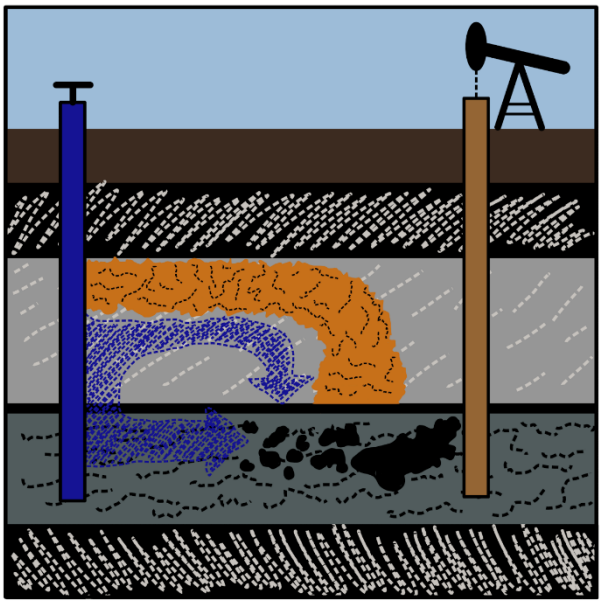

Figure 2.10: Enhanced oil recovery enabled through microbial mineral formation. Biominerals (orange) block fractures or high permeability thief-zones, thus directing the flow of sweeping fluids such as water or CO_2 (blue) through resource-rich zones, enhancing the recovery of oil (black).

Hydraulically fractured horizontal oil & gas wells in unconventional formations accounted for <5% of wells drilled in 2006 but >75% by 2016; these wells are now responsible for approximately 50% of US oil & gas production (EIA, 2016; EIA, 2020). However, these unconventional wells can exhibit rapid decline in production (as much as 60-80% after the first year) (Thomas, 2008). Currently, wells drilled and hydraulically fractured to extract oil and gas may recover only 10% of the fossil fuels present in the formation because only the oil and gas close to a fracture can be extracted reliably due to the very limited fluid mobility in shale rocks (Thomas, 2008). Thus, significant amounts of producible (but not accessed) reserves remain in the reservoir. One way to recover more oil and gas from these wells is by blocking old fractures with diverting agents and re-fracturing the formation to open new fractures in the reservoir. Existing diverting agents are difficult to control in wells that may be several miles deep but biomineralization may represent a new diverting agent technology that could be used to improve the success of re-fracturing to enhance the recovery of oil and gas from declining wells. However, additional research including expanding the temperature range where biomineralization could be used and demonstrations at the reservoir scale are needed to assess the actual feasibility in the subsurface.

Wellbore Integrity.Oil and gas wells have been drilled for more than a century and there are about 2.3 million abandoned and more than 900,000 active wells in the US alone (EIA, 2020; Townsend-Small et al., 2016). Many wells develop leaks, especially as they age (Boothroyd et al., 2016; Dusseault et al., 2000). Wells develop leaks because subsurface pressures and

temperatures vary, resulting in contractions and expansions, shrinkage or cracking in the cement over time, and through ground movement from earthquakes or the drilling of nearby wells. Leaking wells are a problem for the oil and gas industry in several ways. First, the lost hydrocarbons represent lost revenue. Second, lost hydrocarbons are a source of air and water pollution in the vicinity of leaking wells and may even pose acute risks to human life in the case of dangerous gas buildup (Boothroyd et al., 2016; McKenzie et al., 2012). Third, even perceived pollution in the vicinity of an oil or gas well can cause negative public perception that is difficult to overcome and can cause financial harm. Repairing leaky wells potentially thousands of feet below surface can be expensive and is often unsuccessful (Bagal et al., 2016; Montana Emergent Technologies, 2020).

Phillips et al. (2018), described the use of biomineralization to remediate a leakage pathway (channel) 310 m below ground located in the well cement at a well in Alabama. It was observed that MICP treatment using conventional oil field subsurface fluid delivery technologies (packer, tubing string, and a slickline deployed bailer) was successful in sealing the compromised wellbore cement. The authors injected urea-calcium solutions and microbial suspensions (*Sporosarcina pasteurii*). Injectivity decreased with the number of MICP treatments. A decrease in the pressure decay after shut-in, a measure of improved wellbore integrity, was also observed. The authors also observed a substantial deposition of precipitated solids in the original flow channel when comparing the pre- and post-MICP-treatment cement bond logs suggesting the biomineralization treatment sealed the channel and could be used to remediate leakage pathways in oil and gas wells (Figure 2.11).

Montana Emergent Technologies (MET) has trademarked a process called BioSqueeze®, which uses ureolysis-induced calcium carbonate precipitation to seal difficult to seal wells (Montana Emergent Technologies, 2020). Much of the required R&D was conducted in collaboration with Montana State University and has been published in various peer reviewed journals (Kirkland et al., 2021b; Kirkland et al., 2019; Kirkland et al., 2020; Phillips et al., 2018). So far, MET has successfully completed more than 30 commercial scale BioSqueeeze® treatments often resulting in residual annular pressures of less than 1 psi.

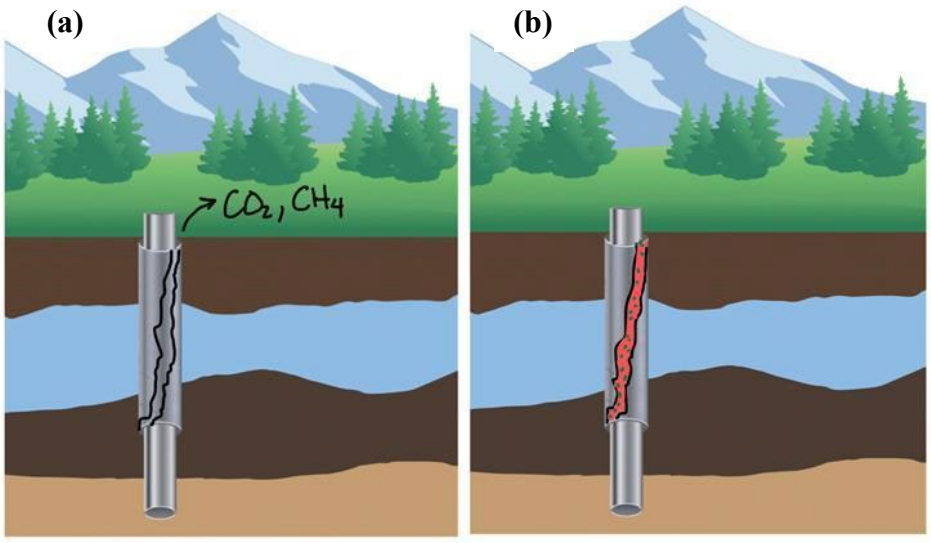

Figure 2.11: (a) When wellbore integrity is disturbed, gas can leak through small apertures such as delaminations or fractures. (b) Microbial biomineralization has been demonstrated to be capable of sealing these small apertures and preventing the leakage of gases.

Other envisioned applications are related to geologic carbon sequestration (GCS) and geothermal well drilling and operation. Concerns over global warming have stimulated a concerted effort to limit CO_2 emissions (IPCC, 2014; IPCC, 2018). Geologic carbon

sequestration (GCS) has been proposed as one part ('wedge') in the battle to tackle the reduction of CO_2 emissions (Pacala & Socolow, 2004). Carbon capture is suitable for large point sources, such as large fossil powerplants and cement plants. CO_2 can be captured at the source and injected into the deep subsurface. One challenge with GCS is storage security, meaning the injected CO_2 must remain safely underground for at least decades, if not centuries (IPCC, 2014; Kudryavtsev et al., 2012). Wellbore and caprock integrity are crucial to the success of GCS and methods to seal potential leakage pathways around wells in aquifers containing CO_2 using ureolysis-induced calcium carbonate precipitation are under development (Kirkland et al., 2021a; Phillips et al., 2013b). Recently, (Kirkland et al., 2021a) performed a biomineralization treatment of a compromised wellbore cement 300 m below ground under conditions that simulated the low pH that might be found in carbon sequestration storage environments. It was observed that biomineralization treatment reduced injectivity by 94% and that mineralization could be promoted in CO_2-affected brines. However, the authors concluded that additional research is required to assess the long-term seal integrity and ensure storage of CO_2 in GCS (Kirkland et al., 2021a).

Geothermal energy is gaining popularity since it represents a low carbon emission source for heat and electricity generation. The drilling of geothermal wells is expensive, and a major cause of non-productive drilling time is the loss of drilling fluids, aka lost circulation (Alsaba et al., 2014; Denninger et al., 2015; Mansour et al., 2019; Marbun, 2013). The loss of drilling fluids occurs when fractures or other high permeability zones are encountered during drilling. If circulation is lost, lost circulation materials (LCMs), such as sawdust, mica, graphite, calcium

carbonate, nylon fibers, mylar or walnut shells, are often injected at high rates to stop losses of drilling fluids (Boukadi et al., 2004; Nayberg, 1987). Existing LCMs are not readily immobilized in the formation or can degrade or erode over time, potentially requiring continuous addition throughout the drilling process. Biomineralization of LCMs could result in immobilization and create a more durable seal against the loss of drilling fluids. The use of biomineralization to enhance LCM performance is in the early stages of technology development and to the authors knowledge no field demonstrations have been performed yet.

Other potential applications of biomineralization

Biomineralization has also been demonstrated to be useful in areas such as art. Limestone and rock have long been used in the creation of sculptures. Recently, a group of interdisciplinary engineering and art undergraduate students at Montana State University used ureolysis-induced calcium carbonate biomineralization to design and sculpt an approximately 0.9 m x 0.3 m x 0.3 m large replica of the Bridger Mountain range as well as an approximately 1 cm x 5 cm x 7 cm replica of the MSU mascot, the Bobcat, using biomineralization approaches (Figure 2.12) (Troyer et al., 2017). The Bridger Mountain range is located just outside of Bozeman (MT, USA) and served as the inspiration for the biomineralized replica. As described in Troyer et al. (2017), the project was supported through a design contest, “Engineers Make a World of Difference”, sponsored by the Norm Asbjornson College of Engineering at Montana State University to promote the spirit of discovery and imagination for the engineering students. Loose sand was treated with microbes and urea-calcium solutions until a solid cohesive block was formed roughly representing the outline of part of the Bridger Mountain range. Subsequent carving and

sculpting of the relief resulted in a replica of the Bridger mountains. In the development of the Bobcat mascot replica, ureolytic biomineralization techniques were used to biocement loose sand inside a Bobcat shaped cookie cutter, which was subsequently painted in Montana State University colors.

Figure 2.12: (Left) 0.9 m x 0.3 m x 0.3 m Biomineralized replica of the Bridger Mountain Range. (Right) Biomineralized replica of the Montana State University mascot, the Bobcat.

Conclusions and Outlook

Biomineralization is a natural process with significant potential for engineering applications. While this book focused on various minerals and various processes related to the precipitation and dissolution of minerals through microbial activity, this chapter focused on developed and currently developing applications. This chapter focused on the review of parameters that influence biomineralization for engineering applications associated with development of novel construction materials, soil stabilization to mitigate hazards to public health and subsurface applications such as improving wellbore integrity. By far, the most frequently utilized mineral is calcium carbonate and urea hydrolysis is the most frequently researched microbial metabolism to initiate mineral precipitation. Applications in construction, soil stabilization and the sealing of leaky wells have advanced the furthest, and some of them

have been commercialized. Other technologies are on the verge to full-scale application and thus commercialization. Much research and development work remains to be performed in this field, and additional applications for biomineralization will be developed in the construction, environmental, biotechnology and medical fields.

These research and development activities will contribute to the development of environmentally friendly methods and products as well as economic competitiveness. Biological manufacturing methods, such as engineered mineral precipitation, can significantly reduce energy-intensive cement manufacturing activities and contribute to resource and climate conservation. The world is expected to add more than two trillion square feet of new building space by 2060 which is equivalent of adding another New York City every month for the next 40 years (UN environment, 2017). Microbially induced calcium carbonate precipitation has the potential to reduce the net carbon footprint of building and construction materials, but work remains to develop this technology for the wide range of applications that cement currently dominates (Davies et al., 2018). In addition, biomineralization has been demonstrated to be useful in areas such as art. There are also applications where biomineralization does not directly compete with traditional cement, including the co-precipitation of certain groundwater contaminants such as strontium (Lauchnor et al., 2013; Mitchell & Ferris, 2006a) and restoring the integrity of wells with ultrafine leaks. Engineered microbial mineral formation has grown from a theory and proof-of-principle vision to a technology being applied in the marketplace.

Acknowledgements

This work was supported by National Science Foundation (NSF) (Award #2036867) FMSG: Biologically Assembled and Recycled Construction and Structural Materials (BRICS) and a Montana State University (MSU) Research Expansion Funds (REF) Award from the MSU Office of Research, Economic Development and Graduate Education (REDGE).

CHAPTER THREE

TEMPERATURE-DEPENDENT INACTIVATION AND CATALYSIS RATES OF PLANT-BASED UREASES FOR ENGINEERED BIOMINERALIZATION

Contribution of Authors and Co-Authors

Manuscript in Chapter 3

Author: Marnie J. Feder

Contributions: Conceptualization; data curation; methodology; writing-original draft; writing-review and editing.

Co-Author: Arda Akyel

Contributions: Data curation; formal analysis; methodology; validation; writing-review. Co-wrote and revised manuscript.

Co-Author: Vincent J. Morasko

Contributions: Data curation; formal analysis; methodology; writing-original draft; writing-review and editing.

Co-Author: Robin Gerlach

Contributions: Conceptualization; data curation; formal analysis; funding acquisition; methodology; writing-original draft; writing-review and editing.

Co-Author: Adrienne J. Phillips

Contributions: Conceptualization; data curation; formal analysis; funding acquisition; methodology; writing-original draft; writing-review and editing.

Manuscript Information

Marnie J. Feder, Arda Akyel, Vincent J. Morasko, Robin Gerlach, Adrienne J. Phillips

Engineering Reports

Status of Manuscript:
____ Prepared for submission to a peer-reviewed journal
____ Officially submitted to a peer-reviewed journal
____ Accepted by a peer-reviewed journal
_X_ Published in a peer-reviewed journal

Wiley
Volume 3, Issue 2
DOI: 10.1002/eng2.12299

Abstract

Engineered (bio)mineralization uses the enzyme urease to catalyze the hydrolysis of urea to promote carbonate mineral precipitation. The current study investigates the influence of temperature on ureolysis rate and degree of inactivation of plant-sourced ureases over a range of environmentally relevant temperatures. Batch experiments at 30°C demonstrated that jack bean meal (JBM) has a 1.7-56 times higher activity (844 μmol urea hydrolyzed g^{-1} JBM min^{-1}) than the other tested plant-sourced ureases (soybean, pigeon pea, and cottonseed). Hence, ureolysis and enzyme inactivation rates were evaluated for JBM at temperatures between 20 and 80°C. A combined first-order urea hydrolysis and first-order enzyme inactivation model described the inactivation of urease over the investigated range of temperatures. The temperature-dependent rate coefficients (k_{urea}) increased with temperature and ranged from 0.0018 at 20°C to 0.0249 L g^{-1} JBM min^{-1} at 80°C; JBM urease became ≥ 50% inactivated in as little as 5.2 min at 80°C and in as long as 2,238 min at 50°C. The combined urea hydrolysis kinetics and enzyme inactivation model provides a mathematical relationship useful for the design of biomineralization technologies and can be incorporated into reactive transport models.

Introduction

Engineered (bio)mineralization or ureolysis-induced calcium carbonate precipitation (UICP) techniques (Eq. 3.1) have been an increasingly popular area of research for use in ground improvement, construction materials, remediation, and subsurface applications (De Muynck et al., 2010; DeJong et al., 2011; El Mountassir et al., 2018; Heveran et al., 2020; Krajewska, 2018;

Mitchell et al., 2019; Phillips et al., 2013a; Rahman & Singh, 2020). In fact, ground improvement with mineralization strategies has been studied extensively resulting in a new field of study described as bio-mediated geotechnics (DeJong & Kavazanjian, 2019; DeJong et al., 2011; Gomez et al., 2015; Hamdan et al., 2016; Martinez et al., 2013; Peng & Liu, 2019). In the subsurface, where temperatures increase with increasing depth, engineered mineralization has the potential to be utilized in place of traditional cement or grout for remediating wellbore integrity, sealing fractures in concrete and rock formations utilized for fluid storage (e.g. CO_2, natural gas, or H_2), controlling flow paths for oil and gas recovery, or creating subsurface barriers for water pollution control (Cuthbert et al., 2013; Fujita et al., 2008; Lauchnor et al., 2013; Mitchell et al., 2010; Phillips et al., 2016; Phillips et al., 2018).

UICP is a process that can be catalyzed by the enzyme urease (from bacteria, plants, or fungi), during which urea is hydrolyzed, which in the presence of calcium ions can induce calcium carbonate precipitation (Equation 3.1) (Hamdan & Jr, 2016; Phillips, 2013; Stocks-Fischer et al., 1999).

$$(NH_2)_2CO + 2H_2O + Ca^{2+} \rightarrow 2NH_4^+ + CaCO_3 \qquad \text{Equation 3.1}$$

UICP, utilizing the ureolytic bacterium *Sporosarcina pasteurii* or plant-based sources of urease, has been researched and used extensively in practice (Cunningham et al., 2014; DeJong et al., 2006; Hamdan et al., 2016; Handley-Sidhu et al., 2013; Krajewska, 2009b; Mitchell & Ferris, 2006b; Nemati & Voordouw, 2003; Phillips et al., 2016; Stocks-Fischer et al., 1999; Tobler et al., 2012; Whiffin et al., 2007). The focus of this investigation were plant-based sources of the enzyme, because of the potential limitations in using bacteria, such as *S. pasteurii*,

in higher temperature applications, since *S. pasteurii* has been shown to not grow above 40°C (Skorupa et al., 2019).

One challenge in successfully promoting UICP with urease is that the enzyme is subject to increasingly fast inactivation at elevated temperatures. Thus, accounting for changes in rates of ureolysis-induced mineral precipitation due to different temperatures is important for achieving optimal mineral formation in a desired time frame. Hence, the motivation for this work was to develop simple mathematical relationships describing the kinetics of ureolysis and the inactivation rate of urease over a range of temperatures relevant for UICP applications. These mathematical relationships will be useful for the development of reactive transport models targeting the optimization of UICP-based technologies, for example by designing strategies to increase reagent temperatures to increase rates of ureolysis, or in the case of deeper subsurface applications, developing strategies to protect urease from rapid inactivation at higher temperatures. We have demonstrated previously that such reactive transport models can be essential in the design of successful field-scale applications of the UICP technology (Cunningham et al., 2019).

Urease is abundant in leguminous seeds, with soybeans (*Glycine max*) reportedly containing 0.012% urease/dry mass, jack beans (*Canavalia ensiformis*) containing 0.07–0.14% urease/dry mass (Krajewska, 2009a) and bacterial cells of *Sporosarcina pasteurii* containing up to 1% of urease/dry mass (Bachmeier et al., 2002). Enzymes are commonly characterized in terms of (enzyme) units, with one ‘unit’ generally referring to the amount of enzyme needed to convert a certain mass of substrate per time interval. For urease, one unit is often defined as 1

μmol of urea hydrolyzed per minute although sometimes 1 μmol of ammonium being liberated per minute is also used; note that these two definitions are related to each other by a factor 2 (*cf*. Eq. 3.1). The activity of different enzyme sources is then generally reported as units per mg (or g) of enzyme source. Observed enzyme activity can thus vary depending on the purity of the enzyme source as well as depending on the reaction conditions including temperature, pH, substrate concentrations, etc.

Ureolysis rates have been determined for many sources of urease, including but not limited to jack beans, soybeans, cottonseeds (*Gossypium hirsutum*), pigeon peas (*Cajanus cajan)* and microbial cells including *S. pasteurii*, the most commonly used bacterium for promoting UICP (Ferris et al., 2004; Lauchnor et al., 2015; Mateer & Marshall, 1916; Phillips et al., 2013a; Sujoy & Aparna, 2013; Tobler et al., 2011). The activity of purified urease has been reported to be in the range of 2700–3500 units per mg of enzyme from jack bean, 650-800 units per mg of enzyme for soybean, 3120 units per mg of enzyme for pigeon pea, and 14.5 units per mg of enzyme for cottonseed preparations, and 2500 units per mg of enzyme for *S. pasteurii* (as summarized in (Krajewska, 2009a) Table 3.2 and references therein). Thermal and chemical inactivation for a variety of enzymes has been described for a range of pH, temperature, pressure and experimental conditions and possible inactivation mechanisms have been examined using activity-time profiles and mathematical relationships ranging from first-order to higher order biphasic models (Aymard & Belarbi, 2000; Illeova et al., 2020; Krajewska, 2016; Krajewska et al., 2012; Polakovič & Vrábel, 1996; Polakovic et al., 1998; Sadana, 1988).

After confirming that JBM had the highest urease activity per mass unit relative to ground cottonseed, pigeon pea and soybean meals, a model was developed for JBM mathematically describing urea hydrolysis kinetics during simultaneous inactivation of urease for temperatures between 20 and 80°C, which correspond to subsurface depths of up to approximately 2400 m (Harrison, 1986). A simple combined first order inactivation and first order kinetic model described the experimental data well, and the work presented here will contribute towards the improved design of full-scale applications of the UICP technology for well-sealing, soil stabilization and other applications using plant-based enzyme sources.

Materials & Methods

Materials

Jack bean meal (JBM) with an activity specified as ≥ 750 units/gram (μmol urea hydrolyzed per minute) at pH 7 and 25°C (J0125, Sigma-Aldrich, St. Louis, MO) was utilized as a source of urease in these experiments. Soybean flour (SB) (S9633, Sigma-Aldrich, St. Louis, MO), cottonseed flour (CS) (C4898, Sigma-Aldrich, St. Louis, MO) and pigeon peas (PP) (North Bay Trading Co. Brule, WI, ground to a flour using a household coffee grinder) were used as alternative plant-based sources of urease. No reported urease activity was included in the specification sheets associated with the plant sources other than for the JBM.

All plant-based urease sources were prepared by adding 5 g L^{-1} of the ground plant powder into water in a flask on a stir-plate which was mixed at 300 rpm for approximately 16 hours. ACS certified urea (Fisher Scientific, Fair Lawn, NJ) was prepared as a 40 g L^{-1} solution

in water which was mixed until the urea pellets were dissolved. All urea and plant-based urease solutions were made with deionized water (DI) and filtered through sterile 0.2 μm disposable Nalgene bottle top filters (ThermoFisher, Rochester, New York) prior to use to remove non-dissolvable meal constituents. Glassware was autoclaved prior to use.

Batch Kinetic Experiments

Batch experiments were carried out in digital shaking water baths operating at the desired experimental temperature (20-80°C) at 70 rpm. The initial heating period to reach each temperature was determined by measuring the temperature over time with an Omega CDS107 temperature probe. Time to reach 95% of the target temperature was determined to be less than 3.5 minutes for each treatment. Experiments were carried out in 30 mL glass bottles that contained 10 mL of 5 g L^{-1} plant-based urease (JBM, SB, CS, or PP) to which 10 mL of 40 g L^{-1} urea solution were added pre-heated to the desired experimental temperature. This created urease-urea mixtures with final concentrations of 2.5 g L^{-1} JBM, SB, CS or PP and 20 g L^{-1} urea.

Batch experiments were run in triplicate for durations of two to eight hours, depending on temperature. Samples (60 μL) were collected for urea analysis every 1 to 15 minutes for up to two hours and then every 30 minutes for up to eight hours. Urea concentrations were determined using a modified Jung assay (Jung et al. 1975) as detailed in (Phillips, 2013). Briefly, the modified Jung assay was performed by measuring absorbance at 505 nm in 96 well plates using either appropriately diluted samples or acidified standards to assess urea concentrations. Samples were diluted in 0.5 M H_2SO_4 to stop enzyme activity and obtain urea concentrations that fell within the linear range of the calibration curve (0 and 2 g/L) (Jung et al., 1975; Phillips, 2013). In

all batch experiments, less than 10% of the total experimental volume was removed for sampling. A urease-free control with 20 g L^{-1} urea was also run to assess abiotic hydrolysis within the experimental time; abiotic hydrolysis of urea was not observed at the tested temperatures up to 80°C. The solutions were purposefully not buffered to simulate more closely what would happen during UICP applications, during which the pH would increase initially before calcium carbonate precipitation would occur. The buffer capacity of the JBM solution was measured as described in the SI.

Inactivation Experiments

Enzyme inactivation was determined by exposing 10 mL of 5 g L^{-1} JBM suspensions to temperatures between 50 and 80°C for 0.04 hours (2.5 min) to 168 hours. Exposed JBM suspensions were cooled down rapidly on ice at pre-determined times and stored at 4°C until utilized in batch experiments to determine the remaining enzyme activity (A). To determine A, each 10 mL sample of thermally-exposed JBM urease suspension was warmed to 30°C and mixed with 10 mL of a 40 g L^{-1} urea solution at 30°C. Samples were collected over 2 hours and appropriately diluted in 0.5 M H_2SO_4 prior to urea measurement using the modified Jung Assay. Activity (A) was estimated by determining the average urea hydrolysis rate based on the difference in the initial and residual urea concentrations after 2 hours (Equation 3.2). Here, U_0 and $U_{\Delta t}$ are the urea concentrations initially and after two hours (120 minutes), respectively, and Δt is the time of the kinetic experiment (2 hours).

$$A = \frac{[U_0 - U_{\Delta t}]}{\Delta t} \qquad \text{Equation 3.2}$$

Modeling Methods

For comparison with other studies, an apparent first-order rate coefficient (k_a) was determined (Equation 3.3); these initial comparisons did not explicitly account for enzyme inactivation

$$\frac{dU}{dt} = -k_a[U] \qquad \text{Equation 3.3}$$

where dU is the differential change in urea concentration, dt is the differential change in time, and k_a is the apparent first order reaction rate coefficient (min^{-1}).

Ureases can become inactivated at elevated temperatures above 50°C. Hence, the model was modified to include both changes in urea concentration (U) and concentration of enzyme source (E) (Equation 3.4); k_{urea} is the temperature-dependent first order ureolysis rate coefficient and E is temperature- and time-dependent.

$$\frac{dU}{dt} = -k_{urea}[U][E] \qquad \text{Equation 3.4}$$

Here, the reaction equation is second order overall, first-order with respect to U and first-order with respect to E. The inactivation of the urease enzyme at elevated temperatures was modeled using the normalized activity term (a) (Equation 3.5), a function of temperature and time within this study (Equations 3.6, 3.7 and 3.8):

$$a = \frac{E}{E_0} = \frac{A}{A_0} \qquad \text{Equation 3.5}$$

where E_0 represents the initial concentration of the active enzyme, E represents the concentration of the active enzyme at a given time.

To predict changes in (a) over time at different temperatures three inactivation models of differing complexity were considered, one single-step and two multi-step inactivation models (graphically represented in Table 3.1) (Henley & Sadana, 1984; Sadana, 1991; Sadana, 1988). All k values in these models are temperature-dependent and detailed explanations of the higher order inactivation mechanisms in the Supplemental Information. The derivations and inactivation models are described thoroughly by Sadana (1991).

Table 3.1. Representation of inactivation models and their corresponding theoretical inactivation pathway(s) investigated within this study. Here E represents the native form of the enzyme, E_1 represents an isomerized form of the enzyme with a different activity than E, and E_d represents the inactivated form of the enzyme without any catalytic activity.

Model	Mechanism
First order	$E \overset{k_d}{\rightarrow} E_d$
Series-parallel	$E \overset{k_1}{\rightarrow} E_1$, $E \overset{k_3}{\searrow} E_d$, $E_1 \overset{k_2}{\swarrow} E_d$
Series-type	$E \overset{k_1}{\rightarrow} E_1 \overset{k_2}{\rightarrow} E_d$

Single Step Inactivation Model

The single step inactivation model was the most-simple model investigated within this study; in Equation 3.6, a is the normalized activity after exposure to temperature (T) for time t and k_d is the first-order thermal inactivation rate coefficient at a given T.

$$a = e^{-k_d \cdot t} \qquad \text{Equation 3.6}$$

The normalized activity (a) over time for a given exposure temperature (50-80°C), for exposure times up to 168 hrs, was determined by taking samples and determining the remaining

activity using batch ureolysis tests which were conducted at 30°C. The inactivation rate coefficients (k_d) for each temperature (50 and 80°C) were then determined by linearly regressing the residual activity versus time on a semi-natural log plot, with the slope being k_d.

The natural logarithm of k_d was then plotted against $1/T$ and linear regression was used to obtain a relationship for the temperature-dependency of the inactivation coefficient ($k_{d(T)}$). Since enzyme inactivation below 50°C was slow (k_d values were very small), experiments would have required exposures of 168 hours (7 days) or longer to observe significant reduction in enzyme activity, which might have introduced artifacts due to non-temperature exposure-related degradation of the enzyme; hence, the residual enzyme activities (A) for temperatures below 50°C were calculated from the Arrhenius-type equation developed in this work.

Multiple Step Inactivation Models

The higher-order models investigated included a series type and series-parallel type model which include multiple inactivation pathways (Henley & Sadana, 1984; Sadana, 1991; Sadana, 1988). In a series-parallel model (Table 3.1 and Equation 3.7), the native enzyme follows one of two paths towards the inactivated form, (1) a two-step series path that assumes the inactivation of the native enzyme (E) to the completely inactivated form E_d via a partially inactivated isozyme (E_1) and (2) a single step path toward complete inactivation (E_d) (Sadana, 1991). The series-type inactivation model (Table 3.1 and Equation 3.8) follows a two-step inactivation pathway through a partially inactivated isozyme (E_1) to a completely inactivated form (E_d) (Sadana, 1991). In each of these higher order models, kinetic coefficients k_1, k_2 and k_3 are the inactivation coefficients from the native form (E) to the isozyme form (E_1) to the inactive

form (E_d). An additional parameter included in these biphasic models is a β term which represents the activity ratio of E_1 and E.

$$a = \left[\left[\left(1 + \frac{\beta k_1}{k_1 - k_2 - k_3}\right) e^{-(k_1+k_3)t}\right] - \left[\left(\frac{\beta k_1}{k_2 - k_1 - k_3}\right) e^{-k_2 t}\right]\right] \quad \text{Equation 3.7}$$

$$a = \left[\left(1 + \frac{\beta k_1}{k_2 - k_1}\right) e^{-k_1 t} - \frac{k_1 \beta}{k_2 - k_1} e^{-k_2 t}\right] \quad \text{Equation 3.8}$$

The parameters associated with the series-parallel and series inactivation models (β, k_1, k_2, and k_3) were estimated using 'fmincon', a nonlinear regression code within MATLAB®, which minimizes the difference (sum of the squared residuals) between experimental and predicted data. Constraints were added that would only evaluate a specific range of numerical values, for example, reversibility of the reactions was not permitted (i.e., no negative k_1, k_2, or k_3 values).

Results & Discussion

Ureolysis Rates of Different Plant-Sourced Ureases

The rates of ureolysis of the four plant sources (JBM, SB, PP and CS) were initially compared at 30°C and 60°C using batch experiments containing the same mass of meal without further purification. This initial comparison occurred based on the apparent first-order rate coefficient (k_a) for each enzyme source, i.e. not explicitly accounting for inactivation (*cf.* Equation 3.3, Figure 3.1). JBM exhibited an approximately 1.7 times higher ureolysis rate at 30°C and 3.3 times higher ureolysis rates at 60°C than SB, the second-most active source; urease

activity decreased in the order JBM > SB > PP > CS. The reaction progress curves, used to calculate the k_a values presented in Figure 3.1, are presented in the Supplemental Information (Figure 3.S1). Since the urease content of each meal is unknown, no comparison of the specific (i.e. per urease molecule) activity for the different plant sources can be provided. At 30°C JBM was the most active with 844 units per gram (μmol of urea hydrolyzed per minute per gram of meal), SB with 504, PP with 201 and CS with 15 units per gram of meal. At 60°C JBM was the most active again with 2,252 units per gram of meal, SB with 676, PP with 206, and CS with 27 units per gram of meal. The urease activities observed for JBM (844 and 2,252 units per g of JBM at 30°C and 60°C, respectively) are in agreement with the manufacturer's information that states >750 μmol of urea hydrolyzed per minute per g of JBM at 25°C and pH 7 (Sigma-Aldrich Product Specification). These results also agree with the order of plant urease activities as summarized and reported in Krajewska et al. (2009a) with the exception that PP was reported to have a higher activity than SB and CS. JBM was chosen over the other plant-based urease sources or purified enzymes for further study, because its high activity and reasonable cost indicate its potential for successful use in engineering applications.

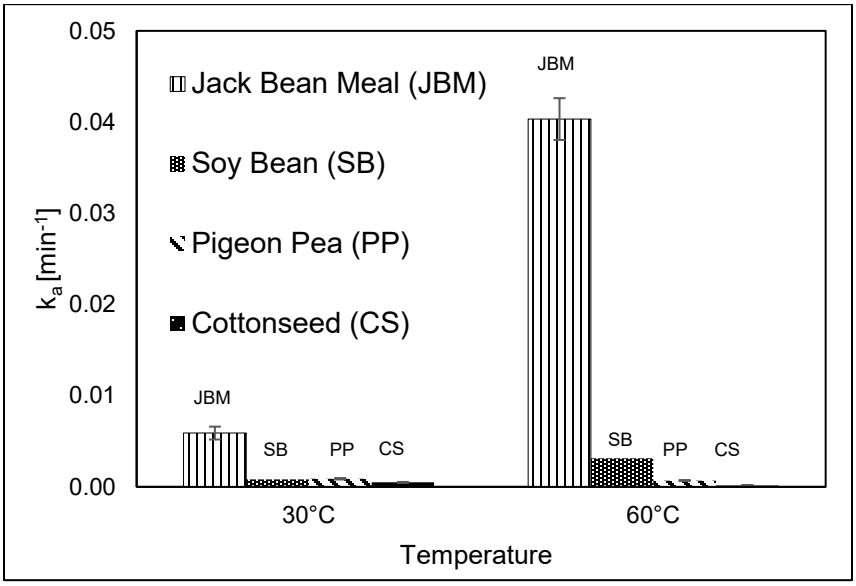

Figure 3.1. Apparent first-order rate coefficients [min^{-1}] determined by linear regression and fitting an overall first-order rate expression to experimental data. Apparent rate coefficients for JBM, SB, PP and CS are plotted for 30°C and 60°C (the rate coefficients plotted here are referred to as apparent first order rate coefficients because temperature-dependent inactivation is not accounted for specifically in this analysis). The errors represent the standard deviation of triplicate results; error bars are very small if not easily visible.

Temperature-Dependent Kinetics of Urea Hydrolysis by Jack Bean Meal

Apparent, Temperature-Dependent Urea Hydrolysis Rates from Batch Kinetic Experiments.

Results from batch experiments containing JBM performed at temperatures between 20 and 80°C are shown as the change in urea concentration over time (Figure 3.2). In all treatments, the pH increased to around 9.3 very quickly, i.e. after approximately 1% of the added urea (i.e. 0.2 g/L of the 20 g/L) had been hydrolyzed; the pH remained around 9.3 for the remainder of the experiment. At 30°C, JBM was observed to hydrolyze 60% +/- 5% (average +/- standard deviation, n=3) of urea within two hours. Urea hydrolysis rates increased with increasing temperatures to an optimum around 60°C where complete hydrolysis of 20 g L^{-1} urea

was achieved within 60 minutes at 60°C. For temperatures < 60°C, urea hydrolysis occurred at slower rates; for temperatures > 60°C, ureolysis was faster initially (e.g. during the first 30 minutes) but slowed down rapidly afterward, presumably due to the inactivation of urease at elevated temperatures. For instance, urea hydrolysis occurred quickly at temperatures above 70°C but ceased after approximately 30 minutes at 75°C and 20 minutes at 80°C, with approximately 40% and 68% of urea remaining, respectively, and no statistically significant decrease being observed, suggesting that JBM urease had been completely inactivated.

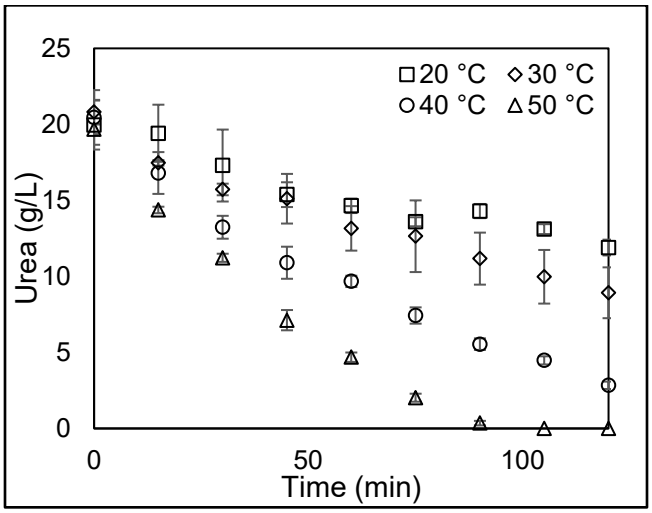

Figure 3.2. Urea concentrations (g L^{-1}) over time (minutes) in the presence of 2.5 g L^{-1} JBM. Temperatures ranged from 20 to 50°C in top panel, 55 to 65°C in the middle panel and 70 to 80°C in the bottom panel.

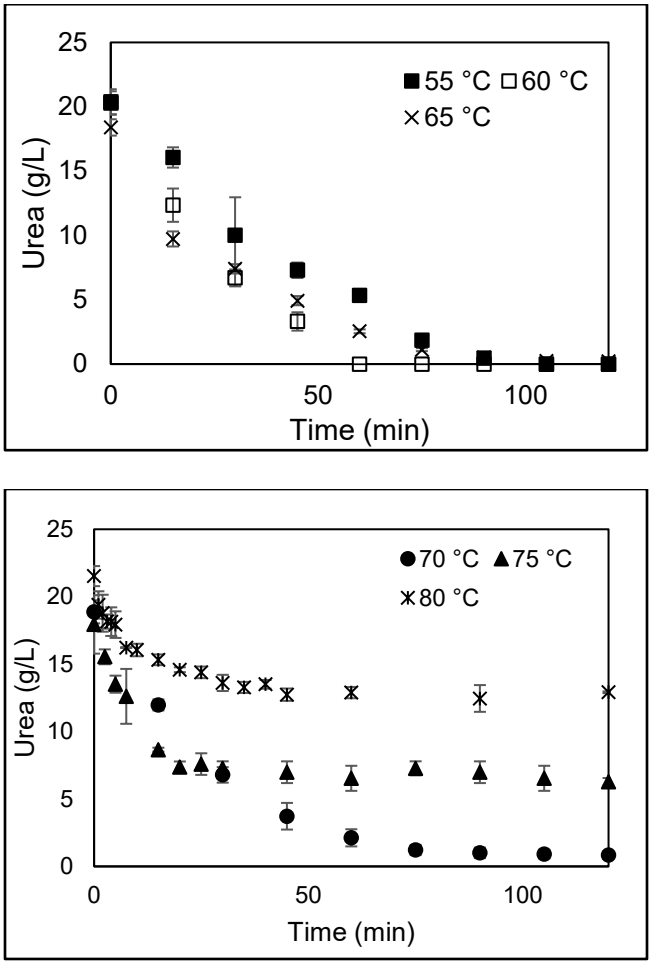

Figure 3.2. Continued.

Temperature-Dependent Inactivation of JBM Urease.Since inactivation of urease was observed at elevated temperatures, the temperature-dependent rate of inactivation was evaluated separately in batch experiments. JBM was exposed to temperatures between 50 and 80°C for various times and at pre-determined times the remaining enzyme activity was determined. JBM urease showed more than 50% inactivation after 2,238 min (37.5 h) during exposure at 50°C, 835 min (13.9 h) at 55°C, 317 min (5.3 h) at 60°C, 125 min (2.1 h) at 65°C, 62 min (1 h) at

70°C, 26 min (0.4 h) at 75°C and 5 min (0.1 h) at 80°C (Figure 3.3). Illeová et al. (2003) noted that urease lost 50% of its activity after 3000 min (50 h) at 55°C and suffered complete loss of activity in less than 60 min (1h) at 87.5°C. In a more recent study, Illeová et al. (2020), noted that that the urease lost 50% of activity after 360 min (6 h) at 65°C and 3 min (0.05 h) at 85°C (Illeova et al., 2020). In the Illeová et al. (2003, 2020) studies the jack bean enzyme had been purified and suspended in either a 0.1 M or 0.05 M phosphate buffer at pH 7.0, respectively, which could explain the differences observed in the study presented here.

Results of the first-order inactivation model (Equation 3.6) for urease inactivation between 50 and 80°C were plotted using an Arrhenius-type plot. The resulting ln(k_d) values as plotted versus 1/T are shown in Figure 3.4 along with the resulting Arrhenius-type equation also listed in Table 3.2, $R^2 = 0.99$). The coefficients obtained from each model for temperatures between 20 and 80°C are summarized in the Supplementary Information (Table 3.S2) along with the correlation coefficients for their respective fits.

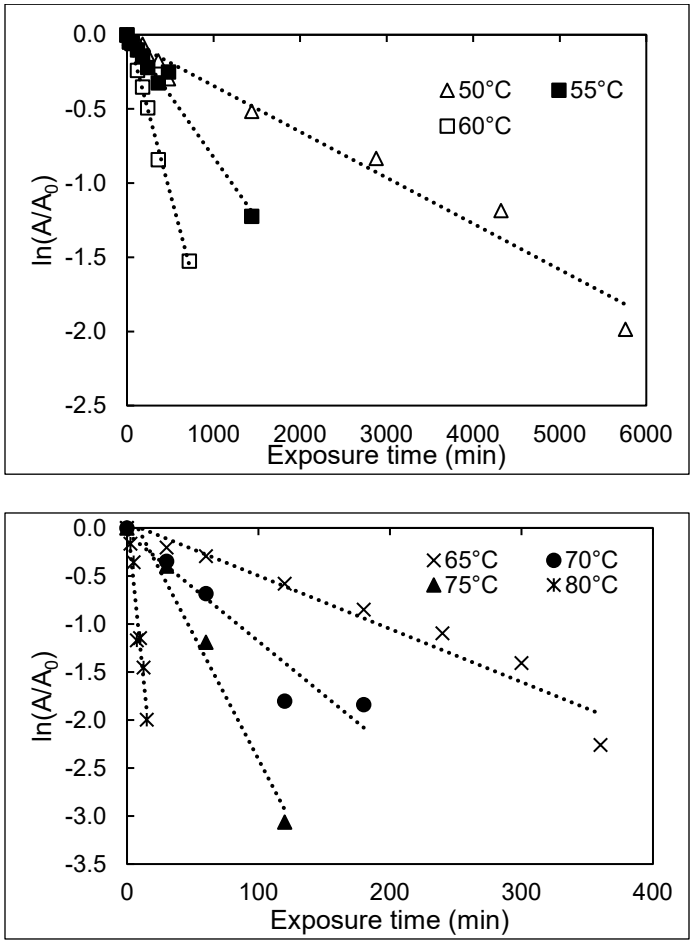

Figure 3.3. Residual ureolytic activity ($\ln[A/A_0]$) of jack bean meal exposed to various temperatures for different amounts of time (up to 5760 minutes [96 hours]); top panel: 50-60°C, bottom panel: 65-80°C.

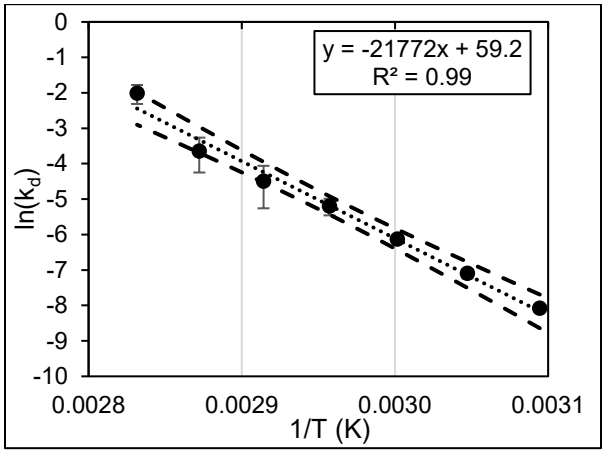

Figure 3.4. Temperature-dependency of inactivation coefficients ln(k_d) (k_d in min^{-1}; T in K). Data from enzyme inactivation experiments were fitted to a first-order inactivation model across the temperature range of 50-80°C (323-353K). Confidence intervals (Lower Confidence Level (LCL), Upper Confidence Level (UCL), 95%) of the rate estimates were determined from different exposure periods. UCL and LCL values were natural log transformed and error bars were generated. Also, confidence bands (CB, 95%), represented by the dashed lines, were generated around the regression for the mean response (ln(k_d)), represented by the dotted line, as a function of 1/T for temperatures between (50-80°C).

Table 3.2. Arrhenius-type equations and correlation coefficients (R^2) for the temperature-dependency of rate coefficients obtained from mathematical modeling using first order, series-parallel and series-type models (units for k [min^{-1}], T [K]).

	First- order		Series-parallel		Series-type	
	Equation	R^2	Equation	R^2	Equation	R^2
ln k_d	-21772 (1/T) + 59.2	0.99	-	-	-	-
ln k_1	-	-	-12705 (1/T) + 26.8	0.56	-19021 (1/T) + 51.0	0.99
ln k_2	-	-	-1617 (1/T) + 0.2	0.03	2760 (1/T) - 9.0	0.64
ln k_3	-	-	-18876 (1/T) + 50.5	0.98	-	-

Temperature-Dependent Inactivation and Urea Hydrolysis Kinetic Modeling. The combined inactivation and urea hydrolysis models (summarized in Table 3.1) predicted the temperature-dependent urea hydrolysis results well over the temperature range from 20-80°C. Each model predicts the urea hydrolysis data well with correlation coefficients (R^2 values) of 0.93 or greater except for the 75°C estimates ($R^2 < 0.81$, refer to detailed discussion in SI below Figure 3.S9; the fit results are summarized in Table 3.S2). The comparison of the model results and experimental data are plotted at three temperatures (30°C, 60°C, and 80°C) for easy comparison (Figure 3.5). It becomes obvious that the three different models are not easily distinguished from each other for any of the temperatures, indicating that each model is adequate for predicting urea hydrolysis rates at temperatures between 20 and 80 °C. A discussion about the k_{urea} values can be found in the SI and the k_{urea} values are plotted in Figure 3.S10. In addition, the urea hydrolysis data and first order model results for all temperatures between 20 and 80°C are shown in Figure 3.S9.

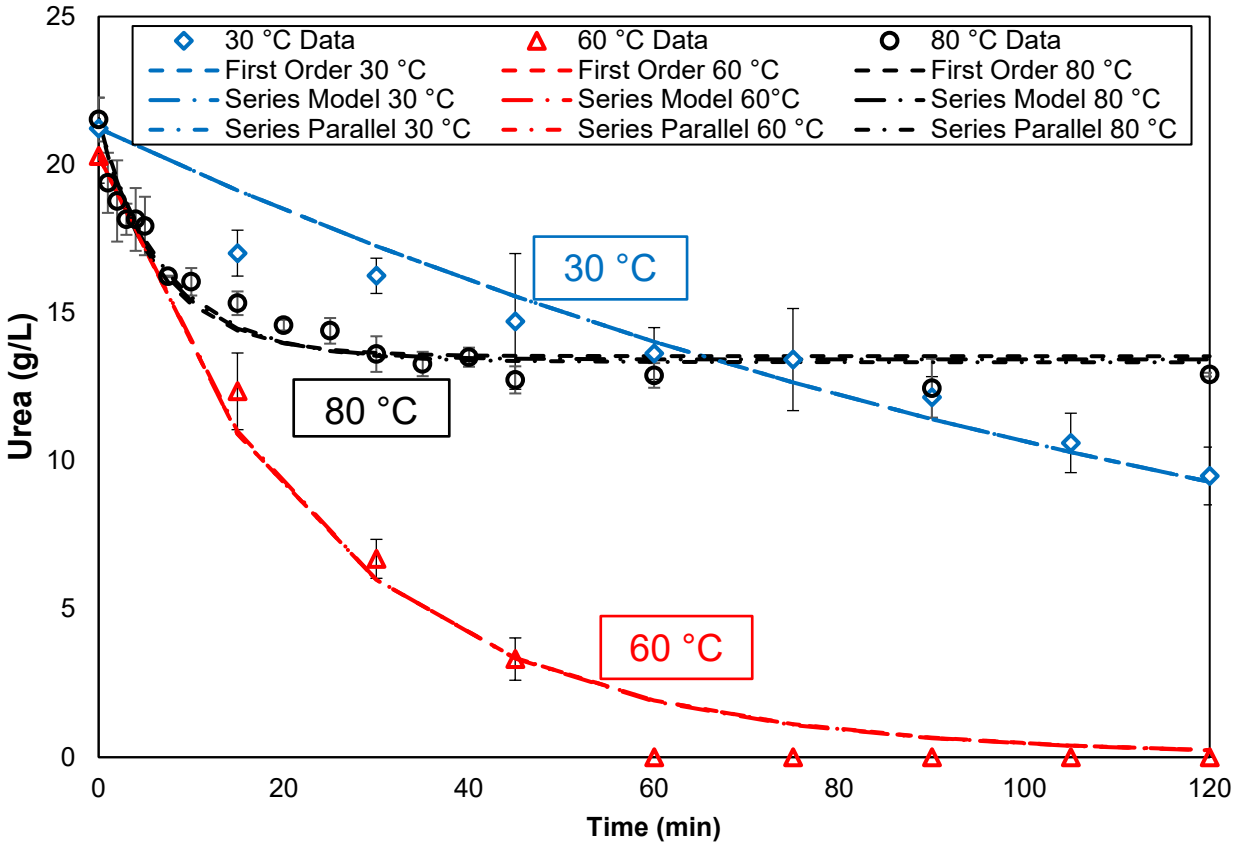

Figure 3.5. Comparison of predicted urea concentration from series-type (dash-dot-dot), series-parallel (dash-dot) and first-order (dashes) models and experimental ureolysis data for 30°C (diamonds, blue), 60°C (triangles, red), and 80°C (circles, black). The model fits for each temperature overlap almost perfectly, hence, the lines are not easily distinguishable.

It has been suggested that enzyme inactivation kinetics can be described using a first-order inactivation model, which describes a one-step irreversible inactivation of the enzyme from its native form to an inactivated form (Anthon & Barrett, 2002; Aymard & Belarbi, 2000; Henley & Sadana, 1984; Illeova et al., 2003). In other cases, higher order or more complex inactivation models, including series-parallel and series type models, might better describe the pathway (Sadana, 1991). For purified urease, Illeová et al. (2003) proposed a thermal inactivation model

between the temperatures of 55 and 87.5°C using a biexponential model, with at least three different reaction steps, including reversibility (Illeova et al., 2003). It can be difficult to fully determine the mechanisms responsible for inactivation which may follow a hexamer to monomer transformation with a possible active trimer intermediate depending on the solution chemistries and experimental conditions (Grancic et al., 2012; Henley & Sadana, 1984; Illeova et al., 2003; Polakovič & Vrábel, 1996; Sadana, 1988). First-order models have therefore been used to adequately describe inactivation kinetics for enzymes under broad temperature ranges (Sadana, 1991; Sadana, 1988) and first order models seem sufficient to describe the combined process of urea hydrolysis and urease inactivation for subsurface applications.

To further analyze the appropriateness of the three models, the resulting natural log of the kinetic coefficient(s) were plotted as a function of $1/T$, comparing the fit of the trendlines (Figures 3.S2-3.S8), and the temperature dependent equations and their correlation coefficients are summarized in Table 3.2. Our objective was to have an acceptable fit of the experimental data, while minimizing model complexity. The developed kinetic relationships are to be added to an existing reactive transport model (Cunningham et al., 2019; Ebigbo et al., 2012; Hommel et al., 2020; Hommel et al., 2016; Hommel et al., 2015), and since there is no strong justification from the fitted data for a more complex model, the first order model is proposed. The rate coefficients, k_1, k_2 and k_3 would be expected to increase as temperature increases if they had a significant influence on the model behavior as seen with k_d (Figure 3.S2-3.S8) (Sadana, 1991). However, temperature dependencies were only clearly observable for the rate-controlling

coefficients (k_3 in the series parallel and k_1 in the series-type model, discussed in more detail below).

The estimates for the activity ratio (β) determined within MATLAB® decreased as temperature increased (Figure 3.S5, 3.S8); the literature suggests that for urease, $\beta = 1$ at lower temperatures (25°C), and that β may be greater than or less than one for a range of temperatures (Sadana, 1991). However, β also did not significantly influence the fit of the models; for the series-type inactivation model k_2 was found to be greater than k_1 meaning the isozyme form of the enzyme was rapidly degraded; for the series-parallel model, k_2 *and* k_3 were found to be greater than k_1, hence the inactivation of both the native and isozyme form of the enzyme occurs so rapidly that the value of β does not significantly affect the fit of the model.

Indeed a more in-depth analysis of the rate-controlling parameters for the models revealed that for the series-parallel model, the estimated k_1 values (rate constant describing the transformation of the native enzyme to the isozyme) were approximately two orders of magnitude smaller than the values for k_3 (rate constant describing the transformation of the native form to the completely inactivated form), indicating that the series inactivation pathway proceeded more slowly than the direct inactivation pathway. This suggests that the series-parallel model behaved similarly to the direct inactivation first-order model. Within the series model, the first inactivation step from the native enzyme to the isozyme form was rate controlling, while the second step could be considered instantaneous relative to the first step because the estimates for k_2 for all temperatures were always higher than for k_1 (Table 3.S2 and Figures 3.S2, 3.S3). The two rate-controlling coefficients (k_3 in the series-parallel model and k_1 in the series model),

representative of the steps mentioned in the rate limiting analysis, are the same magnitude and exhibit a similar temperature-dependency, indeed resembling the first-order model and its rate controlling coefficient k_d (*cf*. Table 3.2, which shows that similar equations describe the temperature dependency of k_d for the first-order inactivation model, k_3 for series-parallel, and k_1 for the series-type model).

Conclusions

This work investigated urea hydrolysis kinetics of various plant-based ureases over a range of temperatures (20-80°C) using experimental and modeling approaches. Jack bean meal (JBM) exhibited the highest activity among the urease sources investigated at both low (30°C) and higher temperatures (60°C) (i.e. 844 and 2,252 μmol urea hydrolyzed min^{-1} g^{-1} of meal, respectively). At 30°C, JBM had an approximately 1.7x greater activity than soybeans (SB), 4.2x greater activity than pigeon peas (PP) and 56x greater activity than cotton seeds (CS); at 60°C JBM exhibited an approximately 3.3x greater activity than SB, 11x greater activity than PP and 83x greater activity than CS. JBM was chosen for an in-depth analysis to determine the rates of ureolysis across a temperature range of 20 to 80°C as well as inactivation rates for temperatures >50°C. The highest ureolysis rates in this study were observed at 60°C with 20 g L^{-1} urea hydrolyzed by 2.5 g L^{-1} JBM in less than one hour. Greater initial ureolysis rates were observed at temperatures greater than 60°C, but due to the inactivation of the enzyme (see Table 3.S2 for representative enzyme half-lives at elevated temperatures) urea was hydrolyzed less efficiently

than in the 60°C case. More than 50% inactivation of the urease enzyme was observed as quickly as 5.2 mins at 80°C and as slowly as 2,238 min at 50°C.

Three enzyme inactivation schemes were fitted to the experimental data, and a simple first-order inactivation model, in which the native form of the enzyme is inactivated through a single-step, adequately described the urease inactivation data across the temperature range of 20 to 80°C. While enzyme inactivation might occur through a multi-step process, the outcome of the biphasic models was dominated by one rate-limiting step explaining why a simple first-order inactivation model was sufficient for predicting the progress of ureolysis at temperatures up to 80°C. The first-order model, would be less computationally expensive to implement into reactive transport models, such as the ones developed by us and others (DeJong et al., 2011; Ebigbo et al., 2012; Hommel et al., 2015). Control and prediction of urea hydrolysis and urease inactivation rates have important implications for the deeper terrestrial subsurface where temperature generally increases with increasing depth and for which more temperature-tolerant strategies may need to be developed.

The current study investigated the rates of enzyme-mediated ureolysis that can contribute to the precipitation of calcium carbonate, recognizing that the presence of calcium was not investigated in this study. Future work should focus on the thermal stability of microbially produced ureases, kinetics of the reactions under different chemical conditions such as at different pH values, in the presence of divalent cations or CO_2-affected brine, and the kinetics of thermally induced urea hydrolysis since thermochemical urea hydrolysis could represent a possible alternative to microbially or enzyme-induced urea hydrolysis for UICP.

Nomenclature

k_a – apparent first order ureolysis rate coefficient (min^{-1})

k_{urea} – first order ureolysis rate coefficient (L g^{-1} JBM min^{-1})

k_d – inactivation rate coefficient (first order model) (min^{-1})

k_1 – coefficient of isomerization (min^{-1})

k_2 – coefficient of inactivation of isomerized form (min^{-1})

k_3 – coefficient for direct inactivation in series-parallel model (min^{-1})

β – ratio of specific enzyme activities in series-parallel and series-type models

U – concentration of urea (g L^{-1})

U_0 – initial concentration of urea (g L^{-1})

$U_{\Delta t}$ – concentration of urea after a given time (Δt) (g L^{-1})

a – normalized activity of enzyme (unitless)

A – activity of urease (g L^{-1} min^{-1})

A_0 – initial activity of urease (g L^{-1} min^{-1})

T – temperature (°C, K, specified, which unit is used)

t – time (min)

E – concentration of initial native form of enzyme (g L^{-1})

E_1 – isomerized form of enzyme

E_d – inactivated form of enzyme

Acknowledgements

This work was supported by the Department of Energy under funding DE-FE0026513 Wellbore Leakage Mitigation Using Advanced Mineral Precipitation Strategies. Any opinions, findings, conclusions or recommendations expressed herein are those of the authors and do not necessarily reflect the views of the Department of Energy (DOE). The authors acknowledge Al Parker at the Center for Biofilm Engineering, Montana State University for his assistance in the statistical analysis. Authors declare no conflict of interest relevant to this article.

Supplemental Information

Estimation of buffer capacity of JBM solutions

JBM solutions were prepared as described in the Materials and Methods section and diluted to final concentrations of 5 g L^{-1} JBM using deionized water. A (0.01 M) NaOH solution was added dropwise to 10 mL of the JBM solution and the pH was monitored. The pH increased to 9.3 after approximately 0.033 mmol of NaOH had been added, which is equivalent to approximately 1% of the added urea (i.e. 200 mg/L of 20 g/L) having been hydrolyzed.

More Detailed Description of Enzyme Inactivation Models

Series-parallel model.The series-parallel inactivation scheme is described with a biexponential model (Equation 3.S1), following one of two paths towards the irreversibly denatured enzyme, E_d. Inactivation can occur either through the immediate inactivation of the native enzyme E or through a series-type inactivation, with an intermediate isomer E_1 (See Table 3.1 for more information). The kinetic coefficient k_1 represents the inactivation coefficient of isomerization from the native form E to the active intermediate E_1. While k_2 represents the coefficient of inactivation of E_1 to the denatured enzyme E_d with an activity of zero. The kinetic coefficient k_3 represents the most direct path of inactivation where the native enzyme E is directly inactivated to E_d. Finally, the coefficient β represents the ratio of specific activities of E_1/E_0 (Sadana, 1991)

$$A = A_o\left[\left[\left(1+\frac{\beta_1 k_1}{k_1-k_2-k_3}\right)e^{-(k_1+k_3)t}\right]-\left[\left(\frac{\beta_1 k_1}{k_2-k_1-k_3}\right)e^{-k_2 t}\right]\right] \qquad \text{Equation 3.S1}$$

At 20°C, $\beta = 1$, which implies no, or only a minor rearrangement of the enzyme results in E_1 with the same specific activity as E (Sadana, 1991). It may be that the unfolding of the structure of urease would present an intermediate form of the enzyme with increasingly less activity as the enzyme denatures at higher temperatures.

Series-type model. This series-type inactivation scheme is a simplified version of the series-parallel inactivation scheme. It contains the same active intermediate pathway but does not include the direct inactivation pathway. (Equation 3.S2) (See Table 3.1 for more information).

$$A = A_o \left[\left(1 + \frac{\beta_1 k_1}{k_2 - k_1} \right) e^{-k_1 t} - \frac{k_1 \beta_1}{k_2 - k_1} e^{-k_2 t} \right] \qquad \text{Equation 3.S2}$$

Reaction Progress Curves

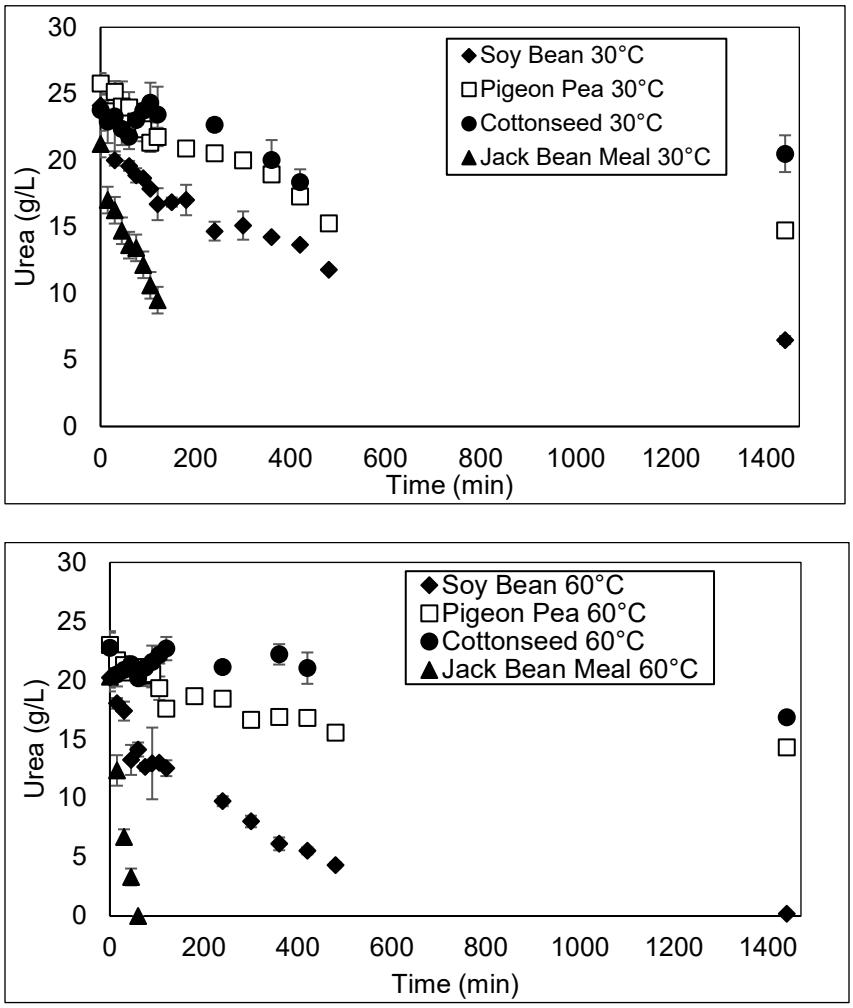

Figure 3.S1. Urea concentrations (g L^{-1}) over time (minutes) in the presence of 2.5 g L^{-1} JBM, SB, PP, CS. Temperatures are 30°C in top panel, and 60°C in the bottom panel.

Table 3.S1. Summary of enzyme activities for plant-based sources of urease that were not previously heat-treated (JBM, SB, PP, CS) between 20 and 80°C.

Source of ground urease	**Temperature (°C)**	**Activity (µmol urea hydrolyzed (g ground plant-based urease source*min)$^{-1}$)**
JBM	20	590
JBM	30	844
SB	30	504
PP	30	201
CS[#]	30	15
JBM	40	1197
JBM	50	1664
JBM	55	1670
JBM	60	2252
SB	60	676
PP	60	206
CS[#]	60	27
JBM	65	1759
JBM	70	1860
JBM	75	1267
JBM	80	959

[#]Because of the lower activity of cottonseed compared to the other sources, instead of a 60-minute reference time frame, 24 hours was used to calculate this activity

Temperature dependency of first-order inactivation coefficients and β.

Table 3.S2. Regression fitting (along with R^2 values) to estimate the inactivation coefficients for each temperature and each model (first order, series-type and series-parallel). In the first order inactivation model, half-life represents the time in minutes for half of the enzyme to become inactivated at the respective temperature. Kinetic model coefficients were obtained for series-type and series-parallel models. Their correlation coefficients from the urea consumption data [min^{-1}] are also presented. Values for β were shown for the series-type and series parallel models but their influence on the model fits was negligible (see discussion in Results and Discussion section 'Temperature-Dependent Kinetics of Urea Hydrolysis by Jack Bean Meal' in main text).

First Order					
T (°C)	T (K)	k_d (min^{-1})	Half-life (min)	k_{urea} (L g^{-1} min^{-1})	R^2
20	293.15	2.88E-07*	2,408,094*	1.76E-03	0.97
30	303.15	3.34E-06*	207,825*	2.77E-03	0.93
40	313.15	3.30E-05*	20,974*	6.15E-03	0.97
50	323.15	3.10E-04	2238	9.99E-03	0.97
55	328.15	8.30E-04	835	1.03E-02	0.97
60	333.15	2.19E-03	317	1.68E-02	0.98
65	338.15	5.53E-03	125	1.54E-02	0.99
70	343.15	1.12E-02	62	1.75E-02	0.98
75	348.15	2.63E-02	26	1.50E-02	0.81
80	353.15	1.34E-01	5	2.49E-02	0.95

*Predicted using experimental k_d for temperatures for than 50°C

Table 3.S2. Continued

Series Model Coefficients Summary						
T (°C)	T (K)	k_{urea} (L g^{-1} JBM min^{-1})	k_1 (min^{-1})	k_2 (min^{-1})	β	R^2
20	293.15	1.76E-03	1.33E-06	1.24E+00	1.4756	0.99
30	303.15	2.77E-03	8.32E-06	9.53E-01	1.2346	0.93
40	313.15	6.15E-03	5.21E-05	7.35E-01	0.9936	0.97
50	323.15	1.00E-02	3.30E-04	4.79E-01	0.7002	0.97
55	328.15	1.03E-02	8.75E-04	5.11E-01	0.6782	0.97
60	333.15	1.69E-02	2.13E-03	2.75E-01	0.5738	0.99
65	338.15	1.52E-02	5.00E-03	6.16E-01	0.3448	0.99
70	343.15	1.83E-02	1.30E-02	4.47E-01	0.199	0.98
75	348.15	1.30E-02	1.85E-02	4.80E-01	0.226	0.68
80	353.15	3.48E-02	1.24E-01	1.25E-01	0.0003	0.95

Table 3.S2. Continued

Series-Parallel Model Summary							
T (°C)	T (K)	k_{urea} (L g^{-1} JBM min^{-1})	k_1 (min^{-1})	k_2 (min^{-1})	k_3 (min^{-1})	β	R^2
20	293.15	1.76E-03	4.72E-08	3.39E-03	1.36E-06	0.9192	0.97
30	303.15	2.77E-03	1.60E-07	4.66E-03	8.46E-06	0.8002	0.93
40	313.15	6.15E-03	5.42E-07	6.40E-03	5.25E-05	0.6812	0.97
50	323.15	9.99E-03	4.52E-05	6.52E-02	2.85E-04	0.4994	0.97
55	328.15	1.03E-02	4.52E-05	6.52E-02	2.85E-04	0.4994	0.97
60	333.15	1.68E-02	1.22E-05	3.18E-03	2.14E-03	0.488	0.98
65	338.15	1.51E-02	6.97E-05	3.12E-04	4.74E-03	0.5164	0.99
70	343.15	1.82E-02	3.40E-07	5.87E-03	1.29E-02	0.3536	0.98
75	348.15	1.28E-02	1.70E-05	1.92E-02	1.89E-02	0.2485	0.71
80	353.15	2.20E-02	1.04E-03	4.10E-02	1.14E-01	0.1588	0.96

Detailed tabulation and graphs of different coefficients and their temperature dependency for the three inactivation models**.**

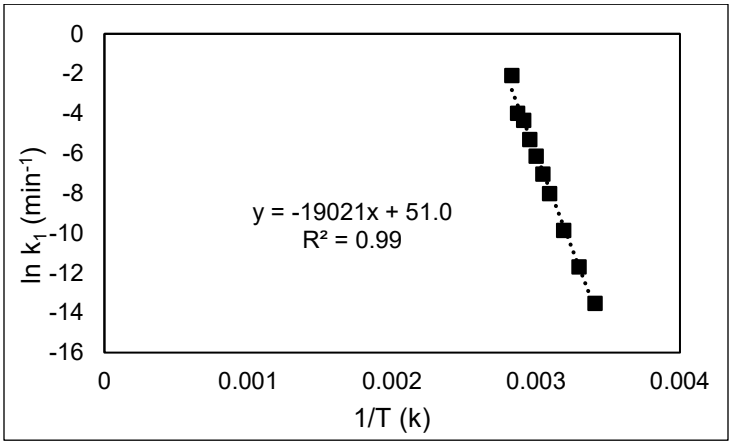

Figure 3.S2. Temperature-dependent inactivation coefficient for series-type model determined by plotting the natural log of k_1 values obtained from inactivation experiments across the temperature range of 50-80°C(323-353K).

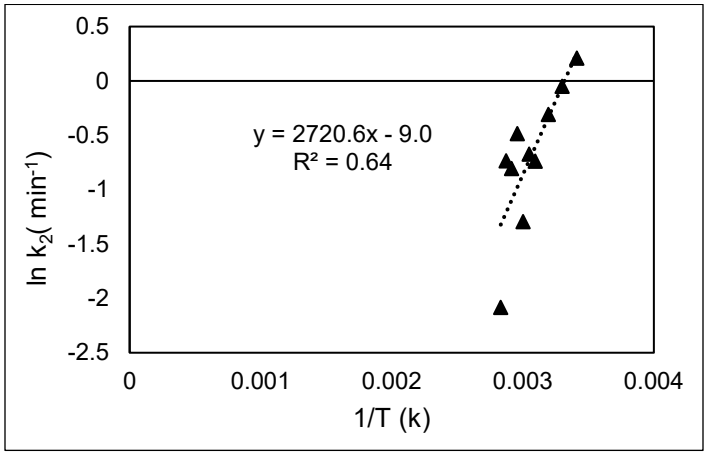

Figure 3.S3. Temperature-dependent inactivation coefficient for series-type model determined by plotting the natural log of k_2 values obtained from inactivation experiments across the temperature range of 50-80°C(323-353K). Within the series model, the first inactivation step from the native enzyme to the isozyme form was rate controlling, while the second step could be considered instantaneous relative to the first step because the estimates for k_2 for all temperatures were always higher than for k_1 (Table 3.S2 and Figures 3.S2, 3.S3). In the series-type inactivation model, k_2 was found to be greater than k_1 meaning that the isozyme form of the enzyme was rapidly degraded and the activity ratio (β) of the E_1 to E form of the enzyme did not influence the fit of the model. In addition, the k_2 data had a poor fit ($R^2 = 0.62$) when plotted on the Arrhenius type plot.

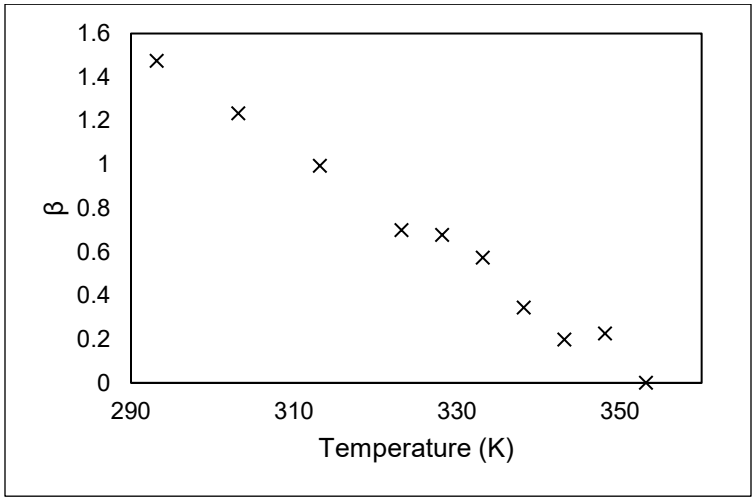

Figure 3.S4. Temperature dependence of relative activity ratio of activity coefficient for series-type model determined by plotting β values (unitless) obtained from inactivation experiments across the temperature range of 50-80°C(323-353K).

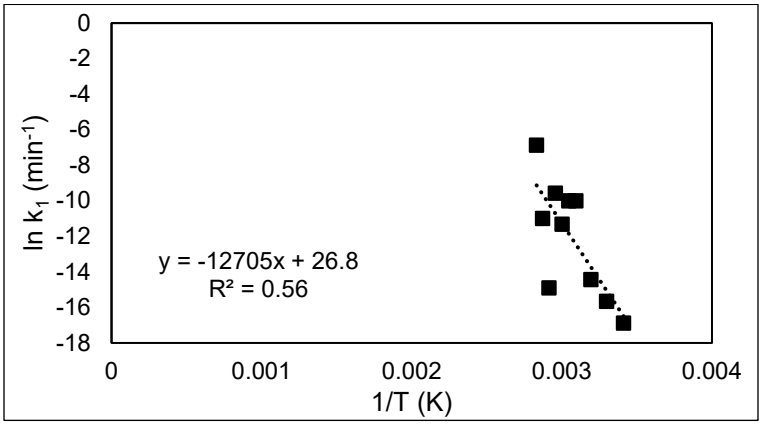

Figure 3.S5. Temperature dependent inactivation coefficient for series-parallel model determined by plotting the natural log of k_1 values obtained from inactivation experiments across the temperature range of 50-80°C (323-353K). In the series-parallel model, the estimated k_1 values (rate constant to transform from native form to isozyme form) were approximately two orders of magnitude smaller than the values for k_3 (rate constant to transform the native form to the completely inactivated form), indicating that the series inactivation pathway proceeded more slowly than the direct inactivation pathway. This suggests that the series-parallel model behaved similarly to the direct inactivation first-order model. In addition, the k_1 and k_2 data had a poor fit (0.56 and 0.034 R^2) when plotted on the Arrhenius type plot.

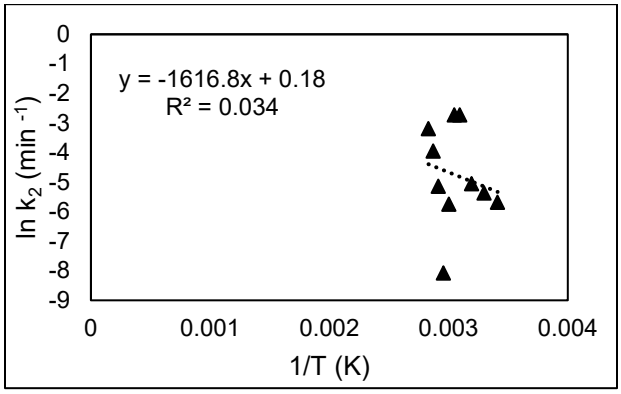

Figure 3.S6. Temperature dependent inactivation coefficient for series-parallel model determined by plotting the natural log of k_2 values obtained from inactivation experiments across the temperature range of 50-80°C (323-353K).The two rate controlling coefficients (k_3 in the series-parallel model and k_1 in the series model), representative of the steps mentioned in the rate limiting analysis, are the same magnitude and exhibit a similar temperature dependency, indeed resembling the first-order model (*cf.* Table 3.2, which shows that similar equations describe the temperature dependency of k_d for the first-order inactivation model, k_3 for series-parallel, and k_1 for the series-type model).

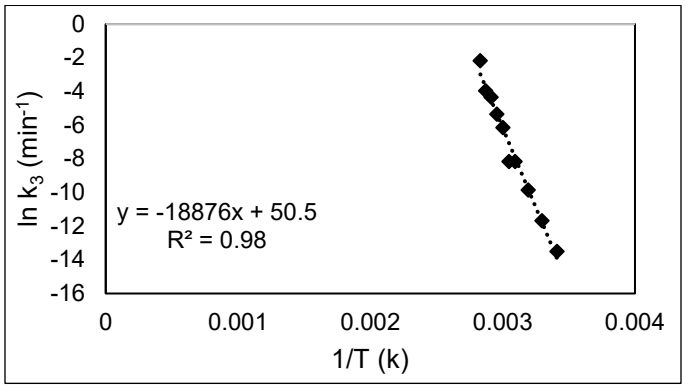

Figure 3.S7. Temperature dependent inactivation coefficient for series-parallel model determined by plotting k_3 values obtained from inactivation experiments across the temperature range of 50-80°C(323-353K).

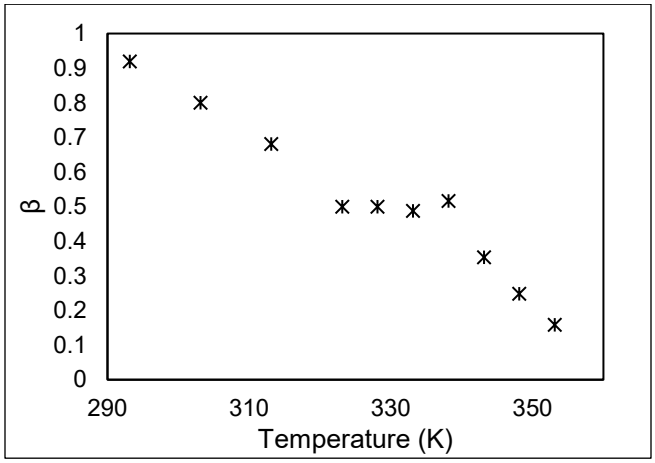

Figure 3.S8. Temperature dependence of relative activity ratio of activity coefficient for series-parallel model determined by plotting β values (unitless) obtained from inactivation experiments across the temperature range of 50-80°C(323-353K).

Detailed Fitting Results of Overall First Order Enzyme Inactivation Model for Different Temperatures.Figure 3.S9 presents an expansion of Figure 3.5 in the main text of the manuscript and provides a comparison of the overall model using the k_d and k_{urea} values estimated during this work with the reaction progress curves presented in Figure 3.2 for the first order enzyme inactivation case. As described in the main manuscript, the overall model, accounting for temperature-dependent urea hydrolysis kinetics and urease inactivation, fits the experimental data well, with correlation coefficients (R^2 values) of 0.93 or greater except for the 75°C estimates (R^2 = 0.81, for the first order model).

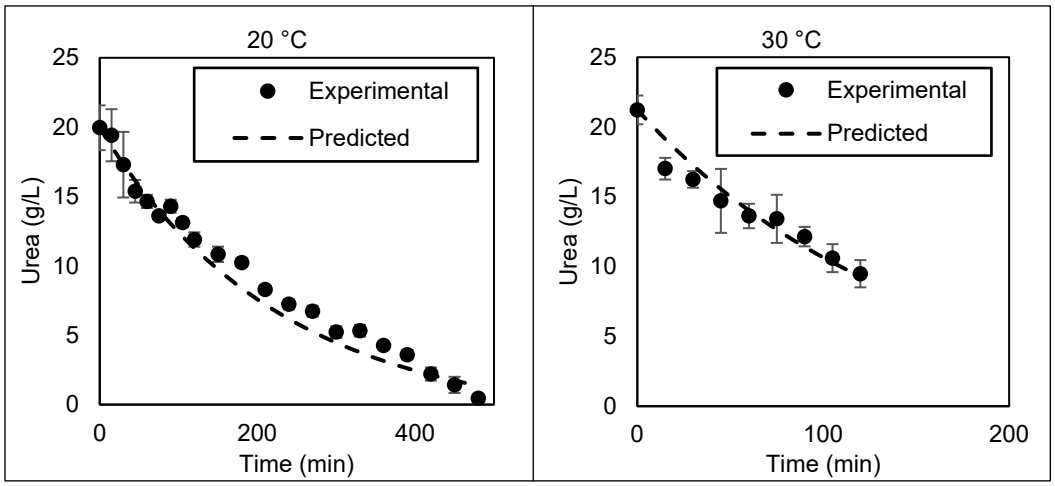

Figure 3.S9: Experimental and first-order predicted urea concentrations between 20-80 °C were plotted over time.

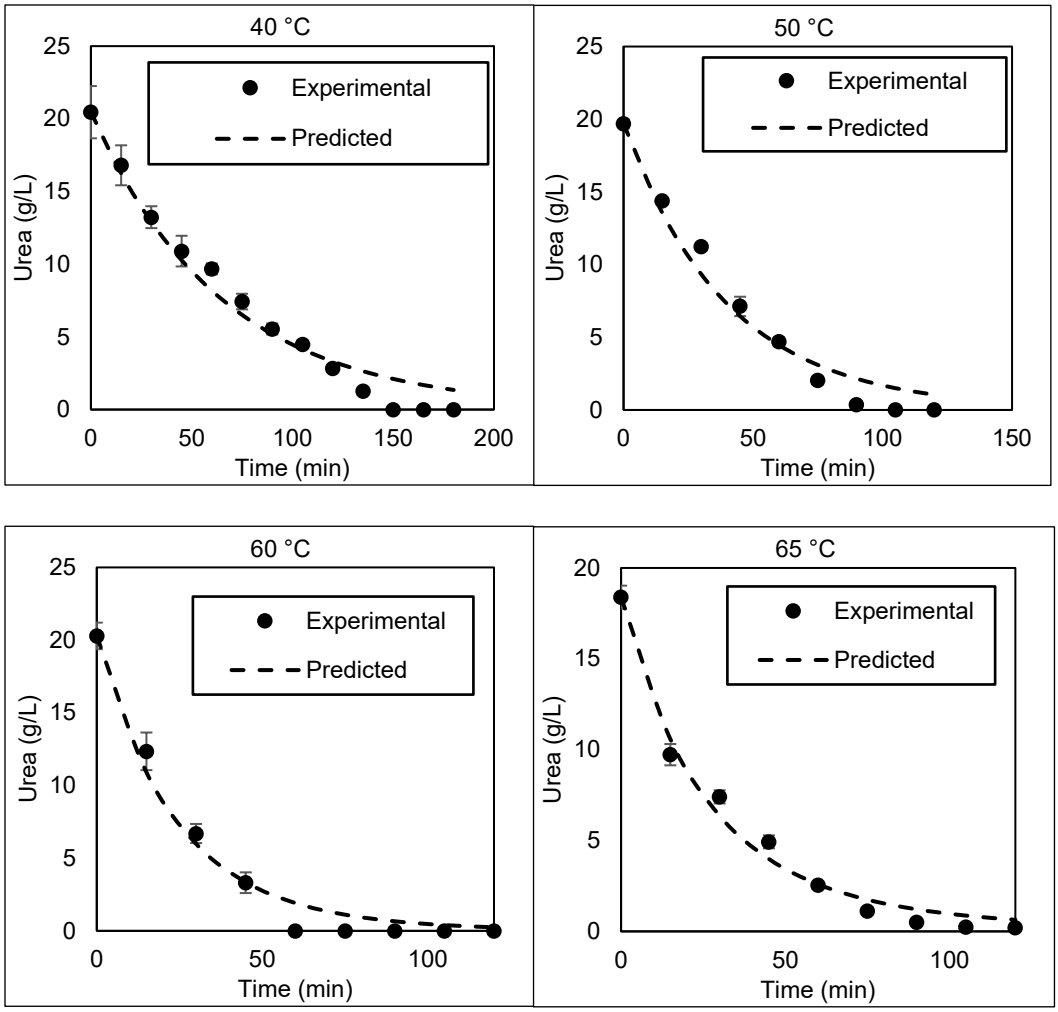

Figure 3.S9: Continued

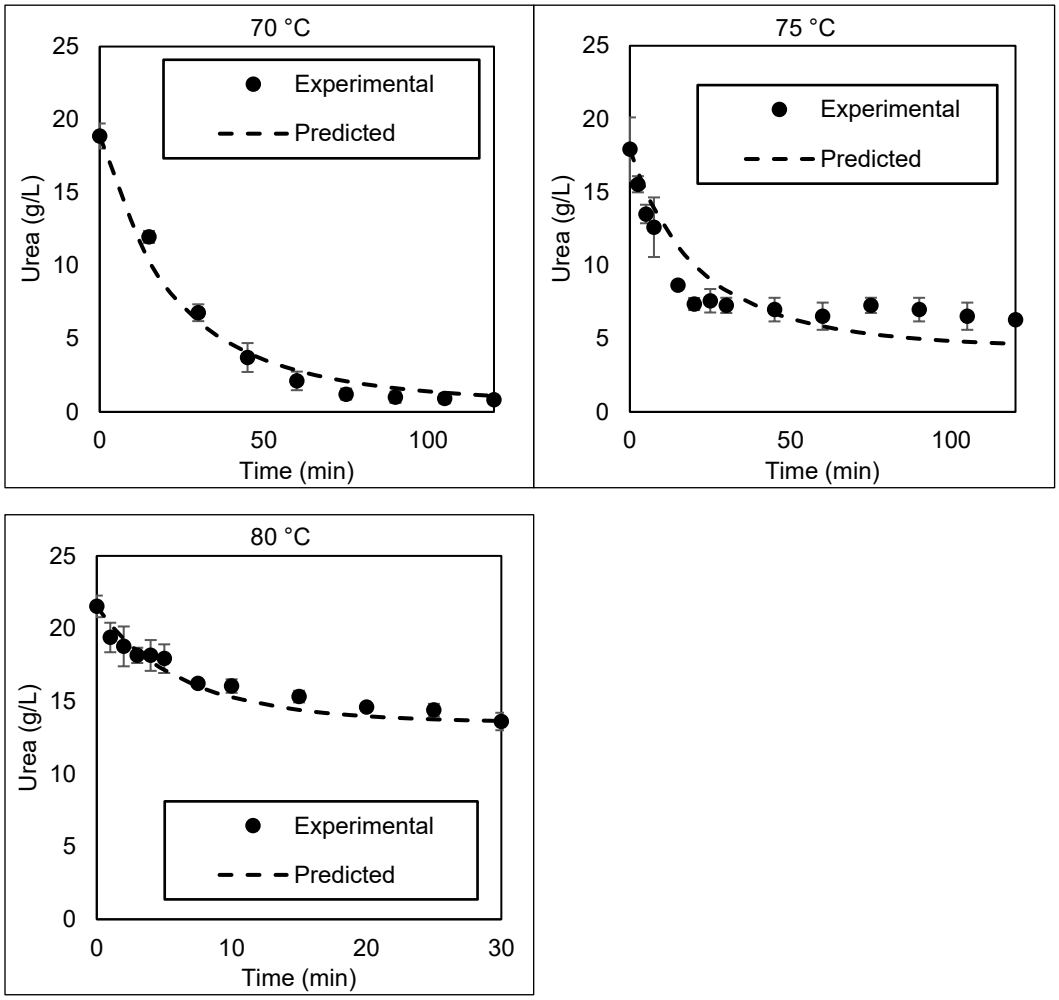

Figure 3.S9: Continued

The lower regression coefficient for the 75°C is likely the result of challenges in reliably measuring the inactivation of urease and decreases in urea concentrations at the rapid timescales necessary for the higher temperature treatments. As evident from Figures 3.4 and 3.S10, there are large differences in k_d and k_{urea} values between the 70, 75 and 80°C treatments based on the Arrhenius-type models describing their temperature dependencies. Hence, even small differences in temperature from the expected value, which might occur if a vial is being kept out of the 75°C

shaking water bath just slightly longer than usual, as well as a few seconds difference in taking a sample and adding it to H_2SO_4 to stop the enzyme can result in significant uncertainties in the k_d and k_{urea} estimates. The fact that this work was conducted at 5°C steps for temperatures between 50 and 80°C compensates partially for such uncertainties and hence the lower R^2 for the 75°C case does, based on our statistical assessment, not significantly affect the model validity, as e.g. demonstrated in Figure 3.4, where the k_d values at 75°C still fall with in the 95% confidence bands.

The second lowest regression coefficient ($R^2 = 0.93$) was observed for the 30°C model. This lower regression coefficient seems to be related to the second data point (at 15 min), which is significantly lower than the model prediction. There are two possible reasons for this divergence: (1) there is a possible error related to the measurements (which could not be confirmed), or (2) the uncertainty associated with extrapolating the k_d values used for model fits for temperatures < 50°C where changes in k_d are very small based on the Arrhenius-type (i.e. exponential) dependence of k_d on temperature (Figure 3.4). As discussed in the main manuscript, experiments attempting to determine the k_d for temperatures below 50°C would have required long experimental times (longer 7 days), which might have introduced artifacts due to non-temperature exposure-related enzyme degradation.

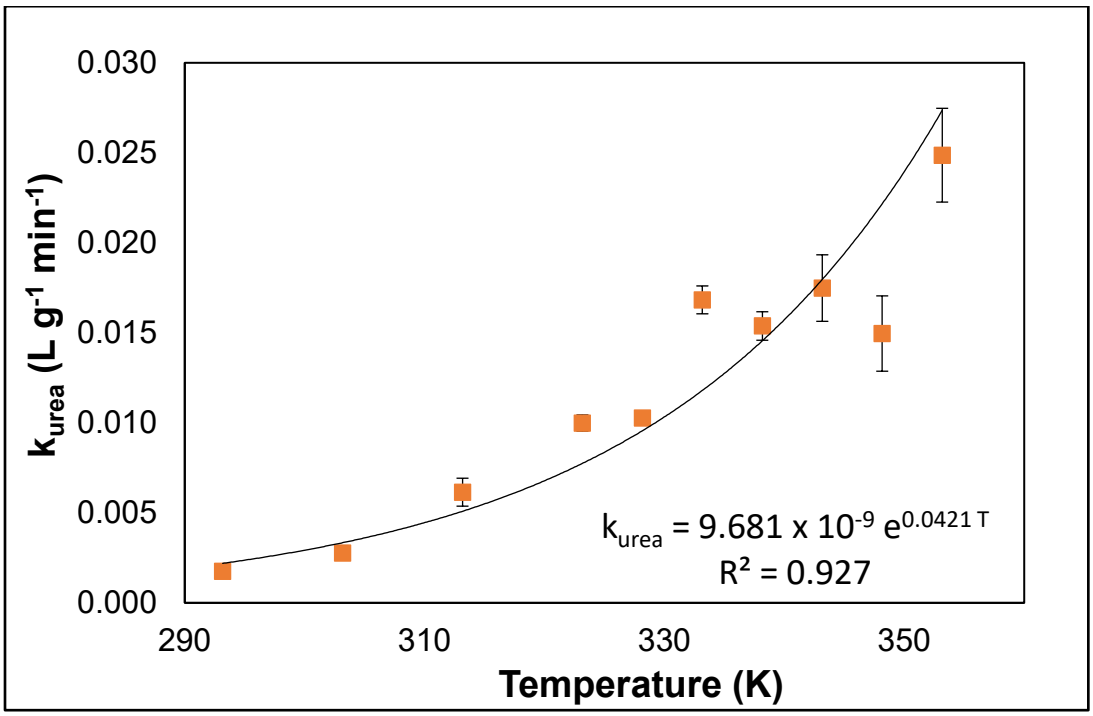

Figure 3.S10: Arrhenius-type plot of experimentally determined k_{urea}-dependency on temperature

CHAPTER FOUR

SPOROSARCINA PASTEURII UREASE AS AN ALTERNATIVE TO JACK BEAN MEAL UREASE

Contribution of Authors and Co-Authors

Manuscript in Chapter 4

Author: Arda Akyel

Contributions: Designed and performed experimental work and analyzed data. Wrote and revised the manuscript.

Co-Author: Adrienne J. Phillips

Contributions: Contributed to experimental design and the manuscript's revision with comments and feedback.

Co-Author: Robin Gerlach

Contributions: Contributed to experimental design and the manuscript's revision with comments and feedback.

Manuscript Information

Arda Akyel, Adrienne J. Phillips, Robin Gerlach

Status of Manuscript:
_X_ Prepared for submission to a peer-reviewed journal
____ Officially submitted to a peer-reviewed journal
____ Accepted by a peer-reviewed journal
_ _ Published in a peer-reviewed journal

Abstract

Microbially induced calcite precipitation (MICP) has the potential to solve engineering challenges such as sealing leaky oil and gas wells by plugging narrow fractures that cannot be sealed with traditional cement. MICP produces a biocement from water-like solutions with the help of an enzyme called urease, which is most commonly sourced from Jack Beans. The current study evaluates urease, produced by *Sporosarcina pasteurii*, as an alternative to plant-based ureases. *S. pasteurii* urease was characterized regarding its durability and usability under elevated temperature conditions, which are often encountered in the deeper subsurface. Using a simple *S. pasteurii* enzyme extract work here demonstrated that the first-order urea hydrolysis rate coefficients (k_{urea}) and thermal inactivation coefficients (k_d) increased with increasing temperatures over the tested temperature range of 20-80 °C. k_{urea} values ranged from 0.0089 L/g *S. pasteurii*/min at 20 °C to 0.2093 L/g *S. pasteurii*/min at 80°C. The half-life of urease decreased with increasing temperatures, residing at 461 minutes at 60 °C and falling to 2 minutes at 80°C. Results here show that 60 °C is the optimal temperature for urea hydrolysis, with 20 g/L of urea hydrolyzed within 60 min at this temperature. In contrast, at 80 °C only 63% of the urea present was hydrolyzed across the same time frame, and at 20 °C, it took eight times longer for complete urea hydrolysis to occur. The determined kinetic parameters were also compared to a plant-based urease, and normalized first-order ureolysis rate coefficients (k'_{urea}) were found to be similar (from 20-80 °C). The estimated cost per gram of urease produced from *S. pasteurii* was 20-60% lower than for urease produced from jack bean meal. Even though *S. pasteurii* cannot

grow at elevated temperatures, urease extracted from it were able perform ureolysis with increasing reaction rates with higher temperatures.

Introduction

Ureolysis-induced calcite precipitation (UICP)-based technologies (*e.g.*, microbially induced calcite precipitation, MICP or enzymatically induced calcite precipitation, EICP) enable a wide range of engineering applications, including the sealing of leaky wells, applications in hydraulic fracturing, enhanced oil recovery, dust suppression, carbon dioxide sequestration, and groundwater remediation (Achal et al., 2015; Cunningham et al., 2019; Krajewska, 2018; Mujah et al., 2017; Phillips et al., 2013a). UICP can reduce permeability and porosity, increase particle aggregation, and facilitate the precipitation of environmental contaminants (Akyel et al., 2022; El Mountassir et al., 2018; Hommel et al., 2020). The major advantage of UICP relative to traditional Portland cement is that the cementation fluids have a low, water-like viscosity and are solely comprised of microscopic particles, *i.e.*, bacterial cells with an approximate size of 2 μm or enzymes that are of even smaller size (Cunningham et al., 2019; Phillips et al., 2013b; Skorupa et al., 2019). These low-viscosity solutions can be delivered more easily into small pore spaces or apertures than viscous cement suspensions containing larger particles (>15 μm) (Almajed et al., 2020; Cunningham et al., 2019; Phillips et al., 2013a). The utility of UICP to seal leakage pathways around wellbores down to a depth of ~600 m (~2000 ft) has been demonstrated (Kirkland et al., 2021a; Kirkland et al., 2020; Phillips et al., 2016; Phillips et al., 2018).

UICP is driven by the activity of the enzyme urease, which can be obtained from several species of plants (*e.g.*, Soy Bean, Jack Bean) and bacteria (*e.g.*, *Sporosarcina pasteurii*) (Feder et al., 2020; Illeova et al., 2020; Phillips et al., 2013a; Tepe et al., 2019). Urease hydrolyzes urea and produces ammonia (NH_3) and carbonic acid (H_2CO_3) (Eq. 4.1-4.2) (Krajewska, 2018; Phillips et al., 2013a). Ammonia functions as a Brønsted-Lowry base, increasing the pH and turning the dissolved carbonic acid into carbonate ions (CO_3^{2-}) (Eq. 4.3-4.5). In the presence of calcium (Ca^{2+}), calcium carbonate ($CaCO_3$) precipitation can occur (Eq. 4.6).

Urea hydrolysis

$$CO(NH_2)_2 \text{ (urea)} + H_2O \xrightarrow{\text{Urease}} NH_2COOH + NH_3 \qquad \text{Equation 4.1}$$

Spontaneous reactions

$$NH_2COOH + H_2O \rightarrow NH_3 + H_2CO_3 \qquad \text{Equation 4.2}$$

$$2NH_3 + H_2O + H_2CO_3 \leftrightarrow 2NH_4^+ + OH^- + HCO_3^- \qquad \text{Equation 4.3}$$

Carbonic acid dissociation

$$H_2CO_3 + OH^- \leftrightarrow HCO_3^- + H_2O \qquad \text{Equation 4.4}$$

$$HCO_3^- + OH^- \leftrightarrow CO_3^{2-} + H_2O \qquad \text{Equation 4.5}$$

Mineralization Reaction

$$Ca^{2+} + CO_3^{2-} \rightarrow CaCO_3 \text{ (Biocement)} \qquad \text{Equation 4.6}$$

It is common to encounter temperatures well above ambient temperature in deep subsurface applications (DeJong et al., 2011; Kirkland et al., 2021a). Unfortunately, *S. pasteurii* is not capable of growing at temperatures above ~40 °C (Skorupa et al., 2019), and thus MICP implementations at higher temperatures might not be easily possible. However, urease, the enzyme responsible for UICP, can withstand elevated temperatures for certain periods of time

and hydrolyze urea at elevated temperatures (Feder et al., 2020; Hommel et al., 2020; Illeova et al., 2003; Illeova et al., 2020).

Previous works have primarily used Jack Bean Meal (JBM) as the urease source in UICP tests; however, urease can also be successfully extracted from *S. pasteurii* using sonication (Stocks-Fischer et al., 1999). *S. pasteurii* can be grown at scale using bioreactors, thus avoiding direct competition with food production. Furthermore, bioreactor-based urease production directly adjacent to the subsurface application site would minimize the need for enzyme stabilization the enzyme and long-distance transport.

The work presented here aimed to produce urease using bacterial cells and compare the activity of extracted *S. pasteurii* urease to JBM urease. This study provides data regarding the reaction and inactivation kinetics of urease extracted from *S. pasteurii* cells at temperatures between 20 and 80 °C, thus contributing to reliable implementations of UICP-based technologies in higher temperature environments like those encountered in the deep subsurface. Thermal inactivation and reaction rate coefficients for *S. pasteurii* urease were compared with urease from JBM, and collectively, the findings allow for the improved design of UICP-based engineering applications.

Materials & Methods

Bacterial strain, growth media, and growth conditions

S. pasteurii (ATCC® 11859™) cells were grown in filter-sterilized (0.2 μm bottle top filter, Rapid-Flow™, Nalgene, NY) Brain Heart Infusion (BHI) broth at a concentration of 37

g/L (BD BBL™, NJ) amended with 20 g/L (0.33 M) urea (Fisher Scientific, NH). For solid media preparation, 15 g/L granulated agar (BD Difco™, NJ) was added and autoclaved. BHI growth medium was inoculated with 10% (v/v) *S. pasteurii* and incubated on a horizontal shaker at 120 rpm and 30 °C for 16 hours.

Urea analysis

Urea concentrations were determined using a modified "Jung Urea Assay," a colorimetric assay run in 96-well plates (Jung et al., 1975; Phillips, 2013). Samples were acidified and diluted in sulfuric acid (H_2SO_4) to stop enzyme activity, final concentration of 0.5 M H_2SO_4.

Urease extraction from bacterial cells

Urease was extracted from whole cells using sonication, similar to the protocol described in Stocks-Fischer et al. (1999). *S. pasteurii* cells were grown for 16 hours, and the optical density (OD) was adjusted to 0.85 (OD_{600nm} 200 µL in a flat-bottom 96-well plate). A crude urease preparation was obtained from *S. pasteurii* cells (200 mL) by harvesting the bacterial biomass via centrifugation at 5,000 x *g* for 10 minutes at 4 °C (Sorvall, Legend XTR, Thermo Scientific, MA). Approximately 160 mL (80%) of the supernatant was removed and transferred into a 50 mL conical tube. The centrifugation process was repeated with the same relative centrifugal force, the supernatant was decanted, and the cell pellet was resuspended in 40 mL of a buffer solution containing 0.1 M of sodium phosphate (pH 7), 1 mM EDTA, and 5 mM 2-mercaptoethanol. The resuspended culture was placed in an ice bath to cool the samples during the sonication application. The cell suspensions were sonicated for 2-6 minutes with a sonication

probe (XL-2000, QSonica, CT) at 15 W before being cooled down on the ice for 2 minutes; the sonication and cooling process was repeated 5 times. The suspension was then centrifuged at 13,000 x *g* for 10 minutes at 4 °C, and the supernatant was filtered through a sterile 0.2 µm bottle top filter to remove cell debris as well as any remaining viable cells. This filtered supernatant will hereafter be referred to as the extracted enzyme solution (EES).

Batch kinetic studies

To track urea hydrolysis over time, batch experiments were performed in 30 mL glass vials at temperatures between 20 and 80 °C in 10 °C increments. For each trial, 10 mL of EES (diluted 3:10, 3 mL of EES mixed with 7 mL of enzyme buffer) was mixed with 10 mL of a 40 g/L urea solution to a final urea concentration (U_0) of 20 g/L.

The urea solutions were pre-heated to the desired temperature before being transferred to vials containing EES; subsequently, each treatment took less than 3.5 minutes to reach 95% of the desired temperature. Samples for urea analysis were collected immediately after mixing the EES and urea solutions.

Urease thermal inactivation experiments

The thermal inactivation of urease was evaluated at temperatures between 50 and 80 ºC in 5 °C increments by exposing batches of 10 mL of EES solution to the desired experimental temperatures in a water bath for 0 to 168 hours, depending on the temperature. It should be noted that, for example, at 50 °C the EES vials were exposed for 168 hours to reach sufficient thermal inactivation, while at 80 °C only 2 hours (120 minutes) were required. These differences stem

from the speed of urease inactivation at higher temperatures (*cf.*, Table 4.S3). The EES was removed from the water bath over time and cooled down rapidly in an ice bath to stop urease thermal inactivation. The samples were stored at 4 °C for up to 24 hours and then reheated to 30 °C, then batch experiments were conducted for two hours, and inactivation coefficients were estimated as described below (Eq. 4.9 & 4.10).

Urease activity and thermal inactivation modeling

Initially, apparent first-order reaction rate coefficients (k_a) were calculated separately from triplicate batch kinetic experiments according to Eq. 4.7.

$$\frac{dU}{dt} = -k_a[U] \qquad \text{Equation 4.7}$$

where U is the urea concentration. k_a calculated by plotting urea concentrations in a natural log scale over time (min) and the slope equal to $-k_a$ (1/min).

While at lower temperatures, the effect of thermal inactivation of urease is negligible, at elevated temperatures thermal inactivation of urease occurs at timescales similar to the duration of the batch experiments. k_a does not account for thermal inactivation. The thermal inactivation of urease can significantly affect reaction rates, and while multi-step inactivation models have been used (Sadana (1988), Henley and Sadana (1984); in Feder et al. (2020) an accurate first-order inactivation model that described adequately the thermal inactivation of JBM urease for temperatures up to 80 °C.

As Feder et al. (2020) outlined (Eq. 4.8), the reaction equation becomes second-order overall with respect to urea concentration (U) and enzyme concentration (E). When enzyme inactivation is considered, enzyme concentration (E) decreases over the time of temperature

exposure. Enzyme concentrations (E) are estimated in terms of enzyme concentration and described by (Eq. 4.9). k_{urea} represents the temperature-dependent first-order ureolysis rate coefficient.

$$\frac{dU}{dt} = -k_{urea}[U][E] \quad \text{Equation 4.8}$$

$$A = A_0 e^{-k_d \cdot t} \text{ or } a = e^{-k_d \cdot t} \text{ where } a = \frac{E}{E_0} = \frac{A}{A_0} \quad \text{Equation 4.9}$$

As detailed in Feder et al. (2020), a temperature-dependent first-order thermal inactivation coefficient (k_d) can be obtained using the urease thermal inactivation experiments described above in combination with Eq. 4.9. The initial enzyme activity is A_0, and the enzyme activity after exposure to a specific temperature for a defined period is A (Eq. 4.9-4.10). The exposure periods tested in this study are presented in Table 4.S1. Multiple A values were obtained by exposing urease to temperature conditions for different periods, and k_d was calculated. The natural log of k_d values ($\ln(k_d)$) was plotted (Figure 4.2) against 1/Temperature (K).

$$A = \frac{[U_O - U_{\Delta t}]}{\Delta t} \quad \text{Equation 4.10}$$

Nomenclature
k_a – apparent first-order ureolysis rate coefficient (1/min)
k_{urea} – first-order ureolysis rate coefficient (L/g *S. pasteurii*/min)
k'_{urea} – normalized first-order ureolysis rate coefficient (L/g urease/min)
k_d – thermal inactivation rate coefficient (1/min)
U_0 – initial concentration of urea (g/L)
$U_{\Delta t}$ – concentration of urea after a given time (g/L)
E – concentration of enzyme source (g *S. pasteurii*/L) or (g JBM/L)
A_0 – the initial activity of urease (prior to heat inactivation) (g/(L*min))
A – activity of urease after heat inactivation (g/(L*min))
t – time (min)

a – normalized activity of an enzyme (A/A_0) (unitless)
T – temperature (°C or K)

Results and Discussion

Bacterial growth and separating urease from whole cells

S. pasteurii did not grow at 45 °C, the lowest temperature tested here, which agrees with the findings by Skorupa et al. (2019), who did not observe any growth of *S. pasteurii* above 40 °C (Figure 4.S1). However, the urease produced by *S. pasteurii* remained active for close to 6 hours at 60 °C (Figure 4.S1), and therefore, *S. pasteurii* was deemed to be an alternative source of urease. However, only approximately 2% of the total urease produced by *S. pasteurii* was estimated to be present extracellularly in the supernatant (*cf.* Supplemental Information (SI), "*Growth media supernatant urease content*" section), which agrees with previous work (Forsberg & Rogers, 1971; Rice & Bayles, 2008) indicating that extracellular urease activity might be caused by autolysis of bacterial cells. Hence, in this work, a crude urease extract was prepared through lysis of *S. pasteurii* cells by sonication. Urease extraction optimization studies were performed and are presented in the SI, "*Sonication method and optimization*" section.

Temperature-dependent urea hydrolysis and inactivation rates of *S. pasteurii* urease

The EES urease, obtained from *S. pasteurii* cells, facilitated ureolysis at various temperatures (20-80 °C). Ureolysis and urease inactivation rates increased with increasing temperatures resulting in the urea concentration profiles displayed in Figure 4.1. At temperatures between 30 °C and 60 °C, all the urea present (20 g/L) was hydrolyzed. At 20 °C, the urea

hydrolysis rate was not sufficiently high to completely hydrolyze the added urea in 8 hours (480 min) though it is likely that urea would have been hydrolyzed entirely shortly thereafter. At 70 °C and 80 °C, complete urea was also not observed, even though initial urea hydrolysis rates were higher than in the lower temperature treatments. Approximately 10% and 66% of urea remained in the 70 °C and 80 °C treatment conditions, respectively (Figure 4.1); and no statistically significant decrease in urea levels were observed after 1 hour, suggesting that the *S. pasteurii*-derived urease had been completely inactivated. Apparent first-order urea hydrolysis rate coefficients (k_a) of *S. pasteurii*-extracted urease as a function of temperature are tabulated in Table 4.S2 and plotted in Figure 4.S6. The k_a increases initially with increasing temperatures, reaching a peak at around 60 °C, then decreases again with increasing temperature. These observations agree with the findings by Feder et al. (2020) and Krajewska (2016) of urea hydrolysis and urease inactivation rates increasing with increasing temperatures for JBM urease.

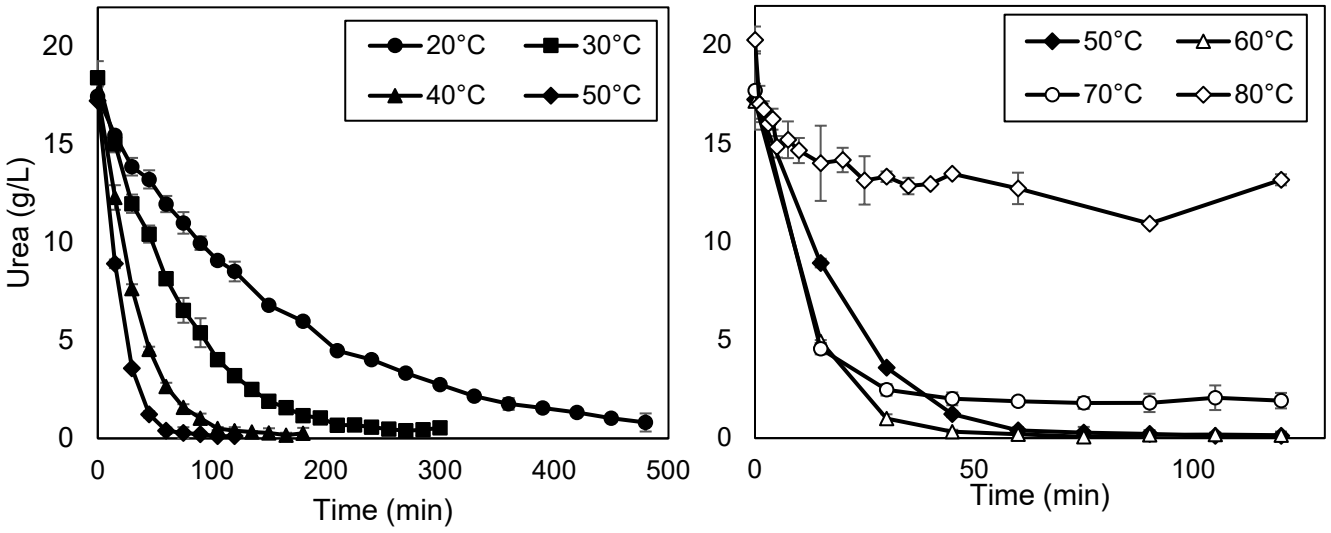

Figure 4.1: *S. pasteurii* urease activity was tracked over time at temperatures between 20 °C and 80 °C. The figure on the left presents conditions between 20-50 °C, figure on the right conditions between 50-80 °C.

To assess the rate of temperature-induced inactivation, EES was exposed to elevated temperatures for various durations. First-order inactivation rate coefficients (k_d) were calculated based on Eq. 4.9 for temperatures between 50 °C and 80 °C (Figure 4.2), results of A/A_0 are presented in Table 4.S1. Increasing inactivation of urease was observed with increasing temperatures; the resulting half-lives (estimated as $t_{1/2} = ln(2)/k_d$) of urease were estimated to be 2182, 461, 17, and 2 minutes at 50, 60, 70, and 80 °C, respectively (Table 4.1).

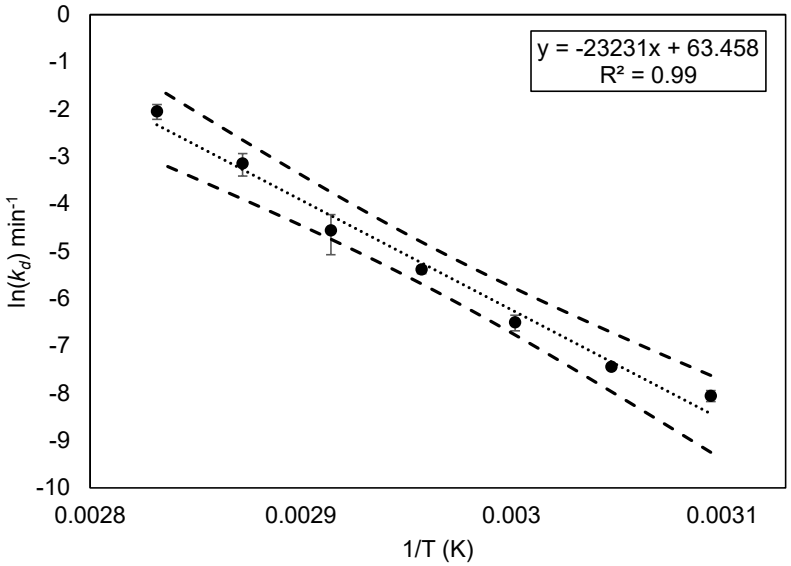

Figure 4.2: Temperature-dependency of inactivation coefficients (k_d) (k_d in 1/min; T in K) for *S. pasteurii*-extracted urease estimated directly from inactivations experiments. Data from *S. pasteurii* urease extract inactivation experiments were fitted to the first-order inactivation model in Equation 4.9 across the temperature range from 50 °C to 80 °C (323-353 K) and plotted on a natural logarithm (ln) over 1/T scale. Confidence intervals (Lower Confidence Level [LCL], Upper Confidence Level [UCL], 95%) of the rate estimates were determined from different exposure periods. UCL and LCL values were natural log-transformed, and error bars were generated. Also, confidence bands (CB, 95%), represented by the dashed lines, were generated around the regression for the mean response (ln(k_d)), represented by the dotted line, as a function of 1/T for temperatures between 50-80 °C.

Based on these k_d values, temperature-dependent first-order urea hydrolysis coefficients (k_{urea}) were calculated using Eq. 4.8 and used to account for thermally induced urease inactivation. Due to k_d values being of the same order of magnitude as the k_{urea} values, the mathematical model (Equation 4.8) systematically overpredicted the extent of urea hydrolysis for the 70 °C and 80 °C treatments (Figure 4.S7, bottom graphs). We hypothesized that experimental k_d values under-estimated the actual inactivation as a result of the time required to reach the experimental temperature (up to 3.5 min. at 70 °C and 80 °C). This hypothesis is supported by the systematic trend of the residuals from the regression analysis in Figure 4.2.

As a result of these initial findings, the k_{urea} values were re-estimated for the 70 °C and 80 °C treatments (listed in Table 4.1 marked by a double-asterisk (**)). First, k_d values were re-estimated for the 70 °C and 80 °C treatments using an extrapolation of the Arrhenius-type relationship presented above. After k_d values were predicted, k_{urea} values were re-calculated again to fit the reaction rate model to the experimental data from 70 °C and 80 °C studies (Figure 4.S7, bottom graphs). This re-analysis allowed for the generation of Arrhenius-type plots for both the first-order ureolysis rate coefficients (k_{urea}) and first-order urease inactivation coefficients (k_d), which results in k_{urea} and k_d exhibiting exponential increases with increasing temperatures (Figure 4.3 and 4.2). The estimated values for the 70 °C and 80 °C systems are listed in Table 4.1. The inactivation model was then used to predict k_d values below 50 °C (Anthon & Barrett, 2002; Feder et al., 2020; Hommel et al., 2020).

Table 4.1: First-order inactivation rate coefficients (k_d), half-lives ($t_{1/2}$), and first-order urea hydrolysis coefficients (k_{urea}) for *S. pasteurii*-urease (current study) and Jack Bean Meal (JBM)-urease (from Feder et al. (2020)) initially determined and re-estimated after accounting for non-instantaneous temperature increases and inactivation kinetics on the same time scale as urea hydrolysis kinetics.

	***S. pasteurii*-urease (Current study)**			**Jack Bean Meal-urease Feder et al. (2020)**		
T (°C)	**k_d (1/min)**	**$t_{1/2}$ (min)**	**k_{urea} (L/g *S. pasteurii*/ min)**	**k_d (1/min)**	**$t_{1/2}$ (min)**	**k_{urea} (L/g JBM/min)**
20	1.39E-07*	4,992,308*	8.90E-03	2.88E-07*	2,408,094*	1.76E-03
30	1.90E-06*	365,590*	2.02E-02	3.34E-06*	207,825*	2.77E-03
40	2.19E-05*	31,637*	4.20E-02	3.30E-05*	20,974*	6.15E-03
50	3.18E-04	2,182	7.25E-02	3.10E-04	2,238	9.99E-03
60	1.50-03	461	1.25E-01	2.19E-03	317	1.68E-02
70	1.05E-02 (4.12E-02)**	66 (17)**	1.23E-01 (1.60E-01)**	1.12E-02 (1.72E-02)**	62 (40)**	1.75E-02 (2.00E-02)**
80	1.29E-01 (4.19E-01)**	5 (2)**	1.32E-01 (2.09E-01)**	1.34E-01 (1.58E-01)**	5 (4)**	2.49E-02 (2.84E-02)**

*k_d values for temperatures less than 50°C were predicted using experimental data from 50-80 °C, using the Arrhenius plot (Figure 4.2).
**k_d & k_{urea} values were re-estimated by refitting the model between 20-60°C

Comparing the urease k_d and k_{urea} kinetic parameters for *S. pasteurii* and JBM urease (Feder et al. 2020), reveals that both urease sources exhibit a similar temperature-dependency. Inactivation rates (k_d) for urease increased with increasing temperatures (resulting in a decrease in $t_{1/2}$) and were generally similar for *S. pasteurii* and JBM urease (Table 4.1). However, the k_{urea} values differed significantly; for instance, at 60°C, k_{urea} was 0.125 L/g *S. pasteurii*/min for the *S.*

pasteurii derived EES, while k_{urea} for JBM was roughly one order of magnitude lower (0.0168 L/g JBM/min). This drastic difference can be explained by the differences in urease content between these two sources. The reported urease content of *S. pasteurii* is 1% (by weight) (Bachmeier et al., 2002), while it is 0.14% (by weight) for JBM (Krajewska, 2009a). This results in a close to 10-fold difference, which explains the roughly one order of magnitude difference in k_{urea} values between *S. pasteurii* EES and JBM. Hence, once k_{urea} is normalized to the estimated amount of urease in each enzyme preparation (*S. pasteurii* EES and JBM) (*i.e.*, expressed in L/g urease/min), k'_{urea} (normalized k_{urea} with respect to urease content) values become almost identical between *S. pasteurii* and JBM urease values reported in Feder et al. (2020) (Figure 4.3).

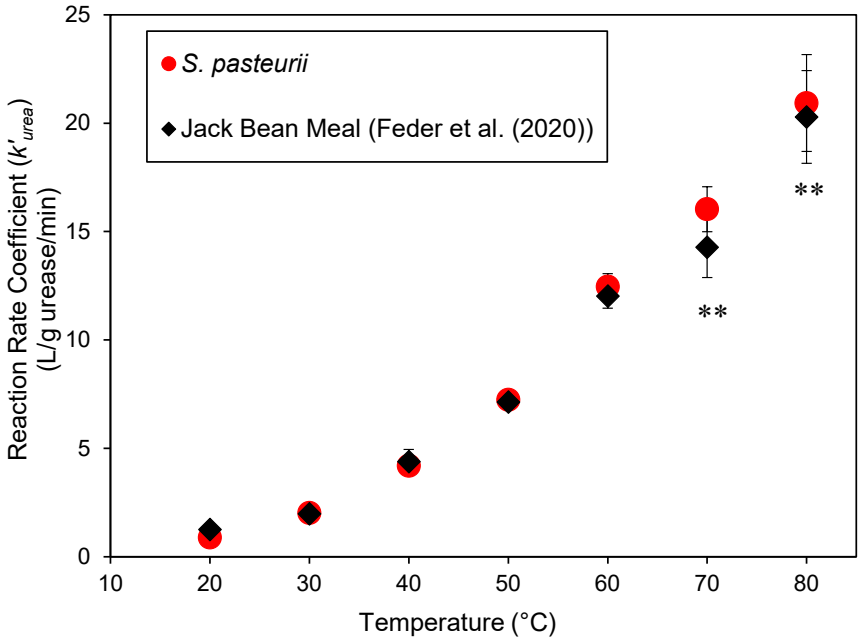

**k_d & k_{urea} values were estimated by refitting the model between 20-60°C

Figure 4.3: Arrhenius-type plot of estimated k'_{urea} values (L/g urease/min) as a function of temperature for the *S. pasteurii* (current study, red circles) and JBM urease (Feder et al. (2020), black diamonds). The urease content of *S. pasteurii* and JBM are vastly different, resulting in a significant difference in k_{urea} (L/g dry enzyme source/min) values (Table 4.1). Urease content

was estimated using the assumption of 1% and 0.14% urease per gram of *S. pasteurii* (Bachmeier et al., 2002) and JBM (Krajewska, 2009a), respectively. k_{urea} is normalized (k'_{urea}) to the estimated amount of urease rather than the urease source dry weight and reported as (L/g dry urease/min); the raw data are presented in Table 4.S4.

The bacterial urease in the EES exhibited urea hydrolysis and enzyme inactivation characteristics similar to those observed previously for JBM preparations over the temperature range tested (50-80 °C, Table 4.1). *S. pasteurii* urease can hydrolyze urea up to 80 °C; even though its cells cannot grow, though urease inactivation does become more rapid with increasing temperature, with urease inactivation dominating at temperatures of and above 70 °C. The findings at >70 °C suggest urea not being completely hydrolyzed before *S. pasteurii*-urease becomes inactivated (Figure 4.1). At 80 °C, the half-life ($t_{1/2}$) of *S. pasteurii* urease was as low as 2 minutes, while at 50 °C, the $t_{1/2}$ is estimated to be greater than 36 hours; below 40 °C the estimated half-live was 21 days and longer for even lower temperatures (Table 4.1).

Reducing application costs is essential if UICP-based technologies are to establish themselves as an economical alternative to existing cement-based construction technologies. Cultivating bacteria at ambient temperature requires relatively inexpensive infrastructure investment and has been demonstrated by us and others to be feasible in the field, *e.g.*, at application sites for well sealing (Phillips et al., 2016; Phillips et al., 2018; Zeng et al., 2021). The growth of *S. pasteurii* requires growth media components, such as nutrient broth, yeast extract, or brain heart infusion (BHI) media, which will incur costs in the range of $136 to $208 per kg nutrient at concentrations of 3 g/L, 15.5 g/L, and 37 g/L, respectively (cost estimates obtained from Neogen (MI) in April 2022). Depending on the choice of nutrient source, the cost

per liter of growth medium will be roughly as follows: Nutrient broth $0.62/L, yeast extract $2.53/L, BHI $5.00/L. BHI media was used during this study, and a bacterial cell density of approximately 0.93 g/L was achieved after 16 hours of cultivation. The cost of one gram of *S. pasteurii* using BHI media is estimated to be $5.4. If the same biomass yield were achieved with nutrient broth and yeast extract, the cost of a gram of *S. pasteurii* would be $0.67 and $2.73, respectively. In comparison, JBM is currently being sold for $345 (>250 units/L, MPbio, CA) to $934 (>750 units/L, Sigma-Aldrich, MO) per kg. One gram of JBM (Sigma-Aldrich) is therefore estimated to cost $0.93. *S. pasteurii* contains 1% (g urease/g cell) (Bachmeier et al., 2002) urease and JBM contains 0.14% (g urease/g JBM) (Krajewska, 2009a). The cost per gram of JBM urease would be $664/g urease, while *S. pasteurii* urease using BHI medium would be $540/g urease; BHI media is a rich and an expensive medium compared to alternatives. Using less expensive microbiological media, such as nutrient broth or yeast extract, can further decrease the manufacturing cost of *S. pasteurii* urease. For instance, if a media concentration of 15.5 g/L using yeast extract were assumed to result in the same biomass concentration of *S. pasteurii*, the cost of producing one gram of urease would decrease to $273/g urease.

Investigating the temperature stability of bacterial ureases is essential for a reliable biomineralization reaction. For some engineering applications, such as the deep subsurface, high *in situ* increasing temperatures are likely to occur with increasing depth. Knowing the activity and stability of urease is essential for predicting the outcomes of UICP field applications.

Conclusions

This work demonstrates the possibility of producing significant amounts of urease within 24-hours using liquid cultures of the easily culturable *Sporosarcina pasteurii*, a common soil bacterium with no known pathogenic potential. This study includes the characterization of the ureolytic properties of *S. pasteurii* with respect to activity and temperature stability and also quantifies the cost-effective nature of *S. pasteurii* urease applications.

Previous work has suggested that the optimal temperature range for urease is between 45-65 °C (Krajewska, 2016; Krajewska et al., 2012), with reaction rates only investigated between 10-35 °C to avoid thermal inactivation of urease (Krajewska, 2016; Peng & Liu, 2019). The existing literature has described significant inactivation at temperatures above 55 °C (Illeova et al., 2003; Illeova et al., 2020). Findings from this study, such as kinetic parameters (k_{urea} & k_d) of *S. pasteurii* urease, can contribute to modeling ureolysis in field conditions, especially at temperatures above the ambient temperature.

A significant advantage of using *S. pasteurii* is the multi-fold higher urease content than jack beans. Bacterial ureases can be produced readily and on-demand at prospective application sites, *e.g.*, at well pads (Akyel et al., 2022; Kirkland et al., 2021a). The cost comparison in the results and discussion section is partially complete at this point because it does not include capital investments such as bioreactors, urease extraction, farming equipment, etc., nor labor costs for bioreactor and agricultural activities, etc. and time to produce a certain amount of urease.

Cost analysis aside, there are advantages to JBM as a urease source. JBM does not require microbial growth and activity and might therefore be suitable for applications that might be limited by regulations or other concerns relating to the use of living organisms. This concern, however, can be reduced (and possibly eliminated through) the demonstrated process of extracting urease from the bacterial host. Bioreactor cultivation may have a higher energy demand (reactor heating, mixing, etc.), while JBM may compete with food production and requires farming equipment. Further improvements and cost reductions can potentially be achieved by developing more effective crude urease preparation. This work utilized sonication as the cell disruption method, which is not easily scalable for high throughput enzyme preparations. Other methods for the generation of crude enzyme extracts should be evaluated (Gagné, 2014; Mortensen et al., 2011; Stocks-Fischer et al., 1999; Yudkin, 1937).

Another improvement worth considering is that increasing the extracted enzyme's stabilization for storage could further decrease the cost and increase the application range. The crude enzyme preparations could be dried using, *e.g.*, by using vacuum or freeze dryers, fluidized bed, spray or rotary dryers, etc., which would increase the ability to store and ship bacterially produced urease to the site of application.

Ureolysis reaction rates were shown the increase with increased temperatures (20-80 °C); however, at temperatures above 70 °C, urease can be inactivated too quickly that not all the present urea (20 g/L) can be utilized. The kinetic parameters presented in this research can be used for designing and executing biomineralization applications in the field. On the other hand, it should be noted that UICP rates can differ from ureolysis rates due to the presence of calcium

ions. In future studies, the enzyme stability and reaction rates should be investigated in the presence of calcium since entrapment and this inactivation of urease in precipitated calcium carbonate is possible (Cuthbert et al., 2012).

Acknowledgments

Funding: This work was supported by the U.S. Department of Energy (DOE) and the National Energy Technology Laboratory under funding Award Number DE-FE0026513 Wellbore Leakage Mitigation Using Advanced Mineral Precipitation Strategies. Any opinions, findings, conclusions or recommendations expressed herein are those of the authors and do not necessarily reflect the views of the DOE. Additional support was provided by Montana State University's Center for Biofilm Engineering, Thermal Biology Institute, Norm Asbjornson College of Engineering, and Vice President for Research, Graduate Education, and Economic Development, as well as through the National Science Foundation (NSF) (Award #2036867) FMSG: Biologically Assembled and Recycled Construction and Structural Materials (BRICS).

Supplemental Information

Methods for bacterial cell density and viable cell determination

Biomass density was measured using optical density information at a 600-nanometer wavelength ($OD_{600\ nm}$) (Connolly, 2015). 200 µL of cell culture were transferred into a well of a 96-well flat-bottom plate (Greiner Bio-One, NC) in triplicate, and absorbances were measured with a spectrophotometer (Biotek Synergy HT, VT). The drop plate count technique was used for the determination of the number of colony-forming units per mL (CFU/mL) (Herigstad et al., 2001) on BHI solid media after appropriate dilution in phosphate-buffered saline (PBS).

Bacterial growth at various temperature conditions

Microbial growth ($OD_{600\ nm}$) and urea concentrations were tracked for 24 hours in *S. pasteurii* cultures. While *S. pasteurii* grew well at 30 °C, little growth was observed at 45 °C, and no growth of *S. pasteurii* was observed at 50 and 60 °C. The $OD_{600\ nm}$ changed from 0.08 to 0.96 over 24 hours at 30 °C and from 0.08 to 0.13 at 45 °C, but no increase in $OD_{600\ nm}$ was observed at 50 and 60 °C (Figure 4.S1).

However, *S. pasteurii* cultures hydrolyzed 18 g/L urea at temperatures between 30 °C and 50 °C. Even at 60 °C, 85% of the urea (15.3 g/L) was hydrolyzed within six hours despite no microbial growth being observed, indicating that the urease present was active for almost 6 hours at 60 °C. Negative (no bacteria) controls were run at each temperature condition, and no reduction in urease concentration nor increase in optical density was observed.

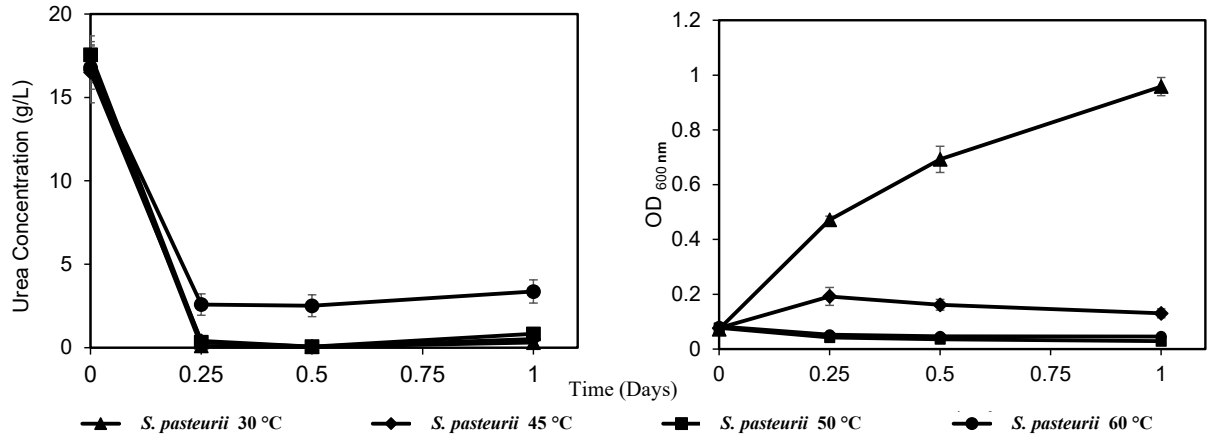

Figure 4.S1: (Left figure) Urea concentrations and (Right figure) microbial growth (as $OD_{600\ nm}$) over time in *S. pasteurii* cultures at various temperatures between 30 °C and 60 °C. *S. pasteurii* did not show significant growth at 50 and 60 °C, but significant urea hydrolysis was observed at all temperatures.

Growth media supernatant urease content

To determine how much *S. pasteurii* urease was present extracellularly in the growth medium, an overnight culture (grown in BHI at 22 °C, 120 rpm) was filtered through a 0.2 µm bottle top filter. The overnight grown culture was filtered, and a urea stock solution was added to estimate the ureolytic activity in the supernatant of the culture. Urea concentrations in the filtered supernatant decreased from 15 g/L to 5.9 g/L after 6 days and to 4.1 g/L after 11 days. On the other hand, whole-cell (*i.e.*, unfiltered) *S. pasteurii* suspensions completely hydrolyzed 20 g/L urea in approximately 6 hours at 30 °C. Extracellular urease hydrolyzed 0.063 g/L/hr urea while whole cells hydrolyzed 3.33 g/L/hr urea, indicating ~2% of the ureolytic activity was present in the supernatant.

Sonication method and optimization

Effectiveness of Sonication. Sonication was used for cell lysis to release urease from the bacterial cells. The effect of sonication on urease activity was evaluated to minimize possible damage and thus inactivation of urease by the sonication process. Cell viabilities were investigated before and after each sonication treatment. To determine the effectiveness of the sonication method, initially concentrated 5 times using centrifuging at 5,000 g, 4 °C. *S. pasteurii* cultures were sonicated on an ice bath twice for 200 seconds at 15 W sonication power to lyze the cells. The number of viable cells was reduced by 96% during the sonication process. Urea hydrolysis was tracked with extracted urease and negative control treatments (no enzyme). The obtained filtered crude enzyme preparation was capable of hydrolyzing 10 g/L of urea in 135 min; enzyme-free controls did not exhibit significant urea hydrolysis (Figure 4.S2).

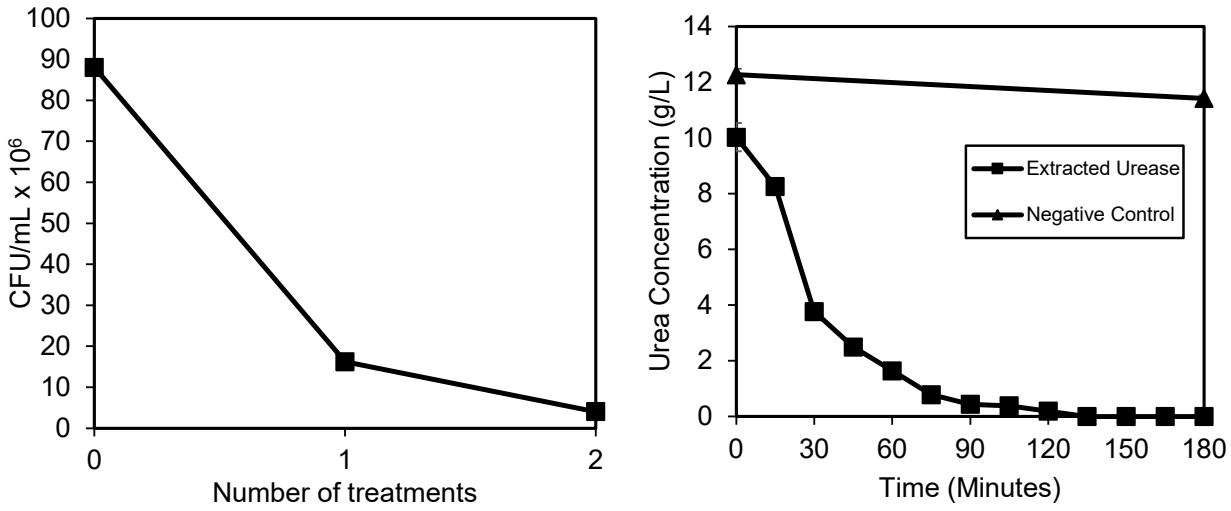

Figure 4.S2: (Left figure) Change in viable cell numbers of *S. pasteurii* after two successive sonication applications; viable cell counts decreased by 95.5%. The drop plate count technique (Herigstad et al., 2001) was used for cell counts. (Right figure) The cell-free (sonicated and filtered) extracted enzyme solution (EES) hydrolyzed 10 g/L urea in two hours at 30 °C.

Determination of urease stability in *S. pasteurii* over time. Twelve hundred mL of *S. pasteurii* culture were incubated, culturable cell (CFU/mL) and urease unit concentrations for the same culture were measured over four days. Two hundred milliliters of culture were removed daily from day 1 to day 4 for culturable cell counts (colony forming units, CFU) and enzyme extraction. The maximum concentration of the culturable number of cells (CFU/mL) was observed on Day 1 and decreased throughout the experiment (four days). Significant enzyme activity was observed starting on Day 1, and no significant change in ureolytic activity was observed through the remainder of the experiment (Figure 4.S3).

Enzymes are typically quantified in terms of "enzyme units," where one "unit" refers to the amount of enzyme that exhibits a particular activity (*e.g.*, converts a certain amount of substrate per time unit). Commonly for urease, one unit is defined as 1 μmol of urea hydrolyzed per minute. It should be noted that differences in reaction conditions (*e.g.*, temperature, pH, salinity, etc.) can result in differences in enzyme kinetics.

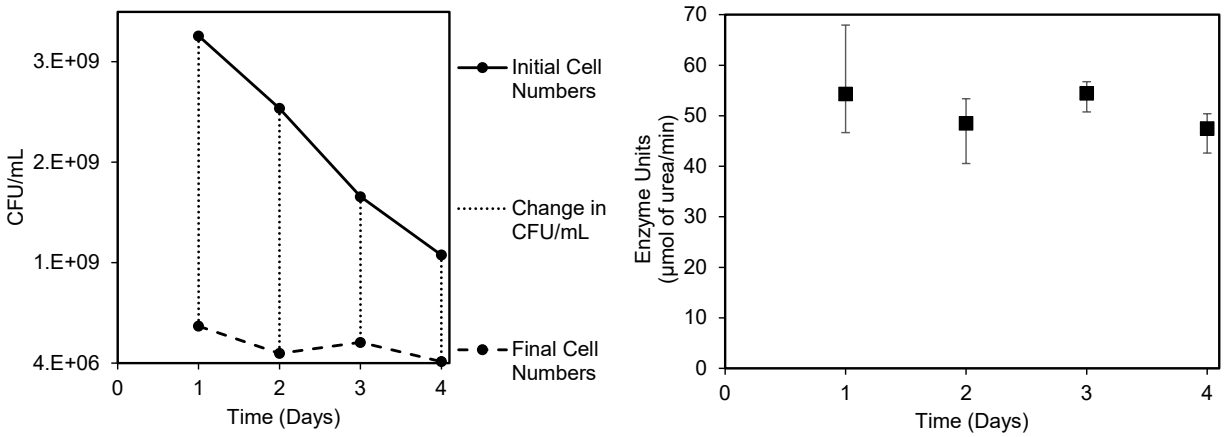

Figure 4.S3: (Left figure) Viable cell numbers of *S. pasteurii* before and after sonication on four subsequent days. The drop plate count technique (Herigstad et al., 2001) was used for cell counts. (Right figure) Urease activity in the filtered crude enzyme preparation from cultures

harvested on four subsequent days. Ureolytic activity of EES was determined at 30°C and shaking at 115 rpm.

Sonication Optimization. Extracted *S. pasteurii* urease after filtration was exposed to sonication treatment for 2, 4, and 6 minutes with intermittent cooling in an ice bath; each additional sonication treatment was performed 5 times on each sample after a 2-minute cooling period. The reduction in enzyme units would demonstrate sonication inhibition while the urease extraction process. The rate of ureolysis in these treatments did not decrease with increasing sonication times (Figure 4.S4). Hence, five repeat cycles of 6-minute sonication treatment using 2-minute intermittent cooling in an ice bath were deemed appropriate for increased extraction of urease from 40 mL suspensions using the 15 W probe sonicator used in this work. This indicates that 30-minute sonication is likely sufficient for the exhaustive release of urease from *S. pasteurii* cells.

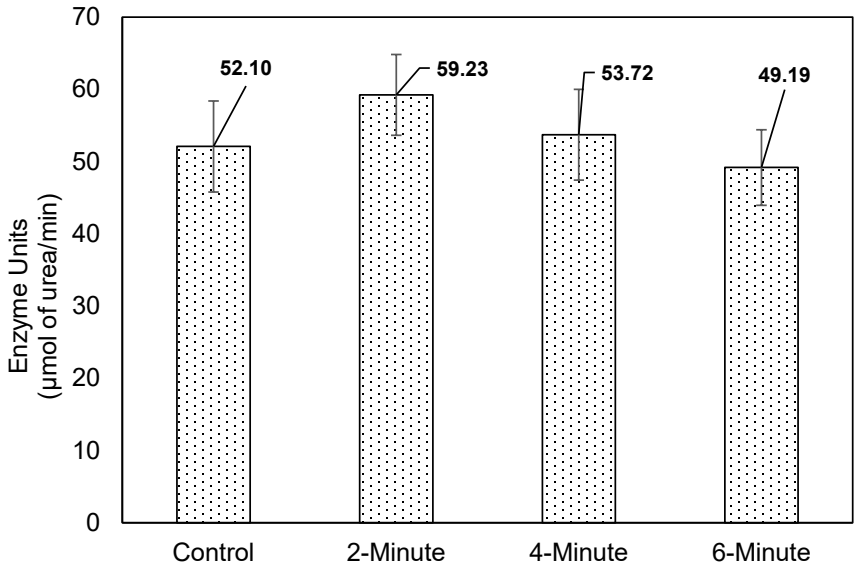

Figure 4.S4: Urease enzyme extraction optimization study from *S. pasteurii* at 30°C. The urea hydrolysis rate catalyzed by the cell extracted urease enzyme was determined after varying

durations of sonication applications, times on x-axis. It was observed that the urease was not inhibited by sonication compared to the control as the sonication duration increased.

Ureolytic activity change over time during cold storage (4 °C)

The EES was stored at 4 °C and used within 24 hours for subsequent experiments. Minor decreases over 24 hours are expected because the ureolytic activity of the EES decreased by 19% after 5 days, 20% after 10 days, and 37% after 15 days (Figure 4.S5).

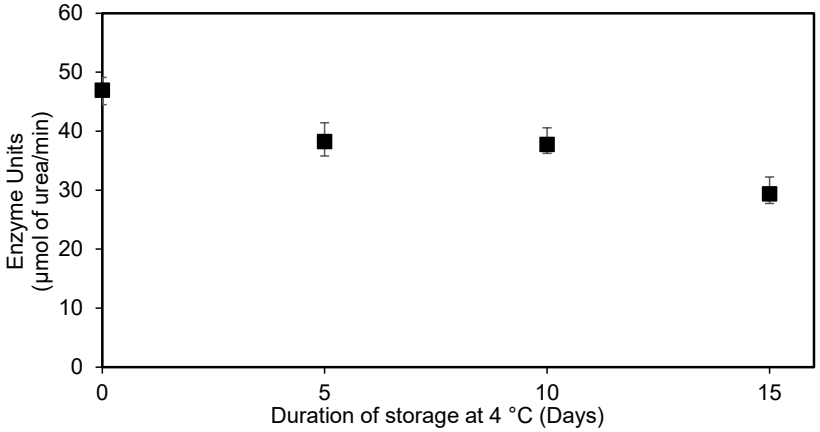

Figure 4.S5: Enzyme units were determined by running batch kinetic studies (30 °C, 115 rpm) after storing urease for 15 days; samples were collected every 5 days. Reduction in enzyme units was presented over 15 days.

Urease kinetic parameters

Table 4.S1: A/A_0 was presented for temperatures between 50-80 °C below. A_0 represents the activity without temperature exposure, while A represents activity after exposure to indicated temperature conditions for indicated periods (min.). Change in activity used for calculating inactivation coefficients (k_d), Equation 4.9.

Time (min.)	0	2.5	5	7.5	10	12.5	20	30	60	120	180	240	300	360	480	720	1440	2880
50 °C	1.00	-	-	-	-	-	-	0.95	1.01	0.99	0.97	0.89	-	0.86	0.94	-	0.62	0.40
55 °C	1.00	-	-	-	-	-	-	0.96	1.00	0.91	0.87	0.84	-	0.83	0.77	-	0.43	-
60 °C	1.00	-	-	-	-	-	-	0.88	0.95	0.97	0.78	0.59	-	0.76	-	0.32	0.12	-
65 °C	1.00	-	-	-	-	-	-	0.63	0.56	0.56	0.37	0.25	0.23	-	-	-	-	-
70 °C	1.00	-	-	-	-	-	-	0.60	0.55	0.21	0.16	-	-	-	-	-	-	-
75 °C	1.00	-	-	-	0.63	-	0.39	0.28	-	-	-	-	-	-	-	-	-	-
80 °C	1.00	0.69	0.62	0.40	0.29	0.19	-	-	-	-	-	-	-	-	-	-	-	-

Table 4.S2: Apparent first-order rate coefficients (k_a) of *S. pasteurii* urease between 20 and 80 °C

Temperature (°C)	**Apparent first-order rate Coefficient (k_a) (1/min)**	**Standard Deviation**
20	0.006	0.000
30	0.015	0.002
40	0.030	0.004
50	0.054	0.009
60	0.075	0.009
70	0.066	0.004
80	0.019	0.007

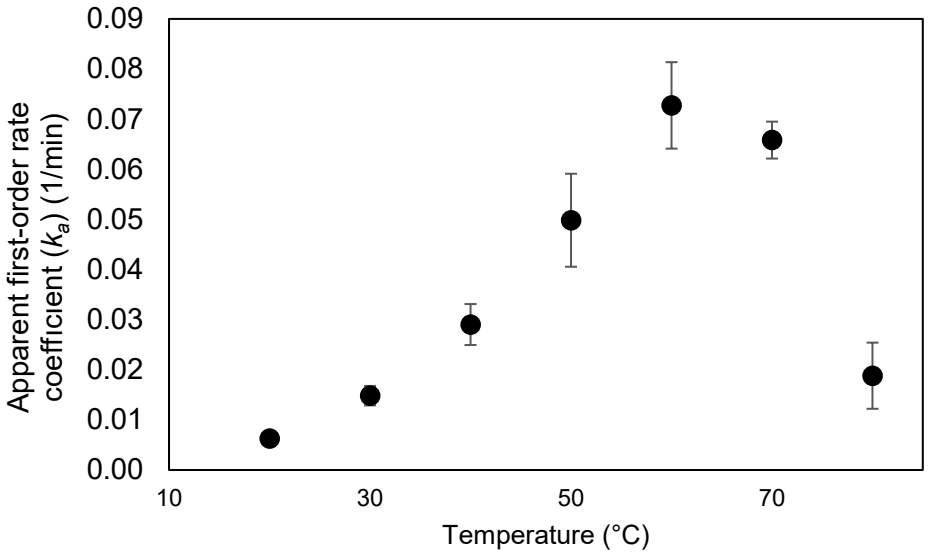

Figure 4.S6: Apparent first-order rate coefficients of *S. pasteurii* urease between 20-80 °C.

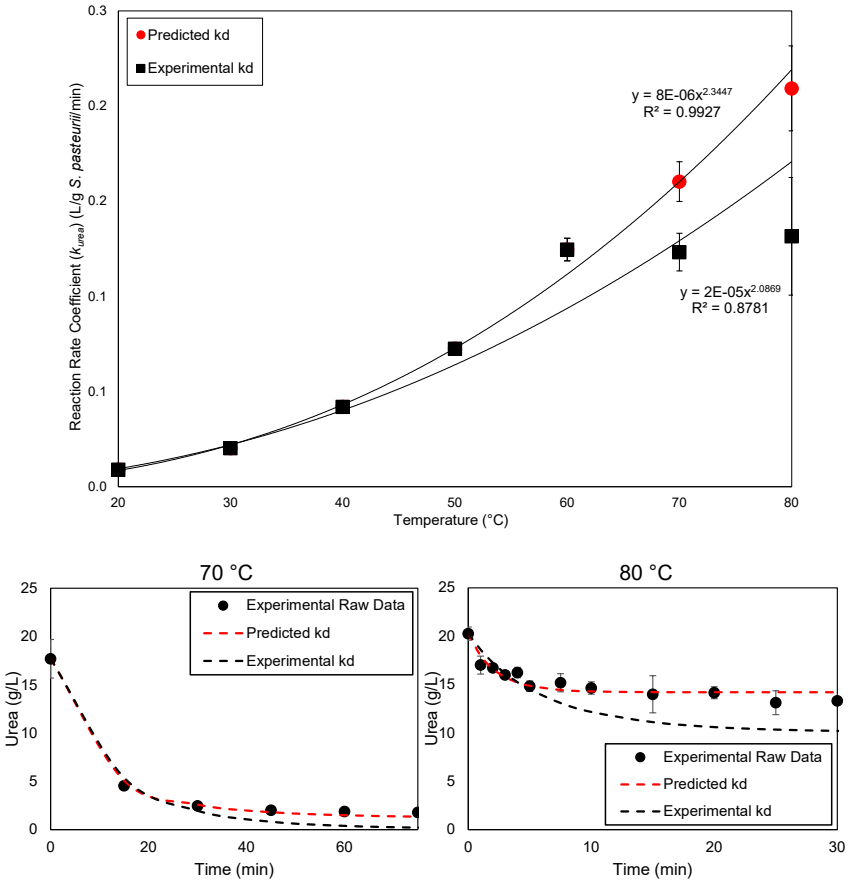

Figure 4.S7: The k_{urea} rate coefficients were calculated using experimental k_d values between 20 °C and 80 °C. k_{urea} values estimated using experimental k_d for temperatures of 70 °C and above did not align with the Arrhenius-type trendline observed for the lower temperature conditions (up to 60 °C (Top figure, black square markers (■)). However, when k_d values were predicted using k_{urea} trendlines between 20-60 °C for temperature conditions 70-80 °C (Top figure, red circle markers (●)), higher regression was achieved (R^2=0.99). Moreover, modeled urea concentrations over the time using the predicted coefficients align with the experimental urea concentration (Bottom left and right figures).

Table 4.S3: Summary of *S. pasteurii*-urease thermal stability and activity between 20-80 °C. First-order inactivation (k_d) and ureolysis rate coefficients (k_{urea}) were calculated considering the effects of thermal inactivation.

T(°C)	T (K)	**Thermal Inactivation**			**Reaction Rate (k_{urea})**	
		Thermal Exposure Period (longest)	k_d (1/min)	Half-lives ($t_{1/2}$) (min)	k_{urea} (L/g *S. pasteurii*/ min)	R^2
20	293.15	n.a.	1.39E-07*	4,992,308*	0.0089	0.98
30	303.15	n.a.	1.90E-06*	365,590*	0.0202	>0.99
40	313.15	n.a.	2.19E-05*	31,637*	0.0420	>0.99
50	323.15	168 hr.	3.18E-04	2,182	0.0725	>0.99
55	328.15	96 hr.	5.87E-04	1,181	-	-
60	333.15	48 hr.	1.50E-03	461	0.1246	>0.99
65	338.15	48 hr.	4.58E-03	151	-	-
70	343.15	6 hr.	1.05E-02	66	0.1233	0.97
75	348.15	4 hr.	4.32E-02	16	-	-
80	353.15	2 hr.	1.29E-01	5	0.1316	0.68

*k_d values for temperatures less than 50°C were predicted using experimental data from 50-80 °C, using the Arrhenius plot (Figure 4.2).

Table 4.S4: Ureolysis rate coefficients normalized to urease weight (k'_{urea}) using the k_{urea} values from Table 4.1 for the current study (*S. pasteurii*) and Feder et al. (2020) (JBM). Presented information in here demonstrated in Figure 4.3.

T(°C)	**Normalized Reaction Rate *(k'urea)* (L/g urease/min)**			
	S. pasteurii (Current Study)		Jack Bean Meal (Feder et al., 2020)	
	Average	Standard Deviation	Average	Standard Deviation
20	8.94E-01	2.43E-02	1.25E+00	1.52E-01
30	2.02E+00	9.47E-02	1.98E+00	2.92E-01
40	4.20E+00	1.83E-01	4.39E+00	5.55E-01
50	7.25E+00	7.88E-02	7.14E+00	3.21E-01
60	1.25E+01	5.97E-01	1.20E+01	5.53E-01
70	1.60E+01	1.04E+00	1.43E+01	1.40E+00
80	2.09E+01	2.23E+00	2.03E+01	2.14E+00

CHAPTER FIVE

IMMOBILIZATION IMPROVES THE STABILITY OF UREASE AGAINST CO_2, pH, AND TEMPERATURE STRESS

Contribution of Authors and Co-Authors

Manuscript in Chapter 5

Author: Arda Akyel

Contributions: Designed and performed experimental work, and analyzed data. Wrote and revised the manuscript.

Co-Author: Ryanne L. Daily

Contributions: Designed and performed experimental work. Wrote and revised the manuscript.

Co-Author: Anna P. Martinson

Contributions: Performed experimental work. Wrote and revised the manuscript.

Co-Author: Adrienne J. Phillips

Contributions: Contributed to experimental design and the manuscript's revision with comments and feedback.

Co-Author: Robin Gerlach

Contributions: Contributed to experimental design and the manuscript's revision with comments and feedback.

Manuscript Information

Arda Akyel, Ryanne L. Daily, Anna P. Martinson, Adrienne J. Phillips, Robin Gerlach

Status of Manuscript:
_X_ Prepared for submission to a peer-reviewed journal
____ Officially submitted to a peer-reviewed journal
____ Accepted by a peer-reviewed journal
_ _ Published in a peer-reviewed journal

Abstract

Urease Induced Calcium Carbonate Precipitation (UICP) has been shown to seal subsurface fractures; however, urease activity is currently limited to circumneutral to slightly alkaline pH ranges (~pH 6-10). Increasing the pH tolerance of urease would expand the range of UICP applications to technologies aimed at sequestering carbon where low pH values and elevated temperatures can be encountered due to increased CO_2 concentrations and depth. In this study, urea hydrolysis (ureolysis) was tested in the presence of pressurized CO_2 and synthetic buffers. In carbonated brines at CO_2 pressures between 0 and 4 MPa (corresponding to pH values of ~4.8 to 8.3), the first-order ureolysis rate coefficients ranked from highest to lowest for the 1.89 MPa, 0.89 MPa, 2.89 MPa, 4 MPa, and 0 MPa systems. Ureolysis reaction rates were also evaluated in the absence of CO_2 in well-buffered systems containing synthetic buffers with pH values ranging between 3-12. Similar ureolytic activities were observed, indicating that neither pressure nor CO_2 affected urea hydrolysis rates. In both sets of experiments, ureolysis rates declined when pH conditions moved further away from circumneutral pH. Separate experiments tested ureolysis at acidic pH values and two different temperatures (20 and 60 °C) with findings indicating that a partial irreversible inactivation of the urease occurred during a one-hour exposure. Finally, urease immobilization tests using a porous ceramic carrier found the carrier protected the urease from low-pH- and high temperature-based inactivation, allowing for the recovery of activity after either readjusting the pH to circumneutral conditions or by decreasing the temperature. These find experiments suggest that urease can be protected from inactivation through immobilization, allowing for the potential delivery of urease into or through unfavorable

environments such as the surroundings of leaky wells in geologic carbon sequestration environments.

Introduction

With anthropogenic carbon dioxide (CO_2) levels on the rise, greenhouse gas mitigation methods such as carbon capture and storage (CCS) are being considered worldwide (Aminu et al., 2017; Stocker et al., 2013; Zahasky & Krevor, 2020). In the case of geological carbon storage, CO_2 is injected into deep subsurface saline reservoirs through existing or newly drilled wells (Akono et al., 2019; Aminu et al., 2017; Kirkland et al., 2021a). Concerns exist that CO_2 could immediately leak back up to the surface, as approximately 15% of newly drilled wells require immediate cement repairs (Aminu et al., 2017; King & King, 2013; Wilson et al., 2003).

Unfortunately, cement injections (termed "cement squeeze jobs") are not always successful in sealing leakage pathways, in particular when microfractures form in the well cements (Montana Emergent Technologies, 2020). Cements are highly viscous suspensions, containing particles generally ranging from 7 to 200 μm (Zhang, 2011). Thus, high injection pressures might be required to seal small fractures, which could potentially exceed equipment capabilities or endanger the well stability. Urease Induced Calcium Carbonate Precipitation (UICP), uses dilute aqueous suspensions with lower viscosity and smaller particle sizes, which can more easily can penetrate small apertures (Cuthbert et al., 2012; Macleod et al., 1988; Phillips et al., 2013b) and promote the precipitation of calcium carbonate minerals (bi-coement).

During UICP, urea is hydrolyzed either enzymatically or thermochemically to produce ammonia and carbonate (Eq. 5.1). Ammonia functions as a Brønsted–Lowry base (Eq. 5.2), increasing the pH and shifting the dissolved inorganic carbon equilibrium towards carbonate (CO_3^{2-}) (Eq. 5.3). In the presence of sufficient calcium, calcium carbonate precipitation occurs (Eq. 5.4).

$$NH_2CONH_2 + H_2O \xrightarrow{\text{Urease}} 2NH_3 + CO_2 \qquad \text{Equation 5.1}$$

$$2NH_3 + 2H_2O \leftrightarrow 2NH_4^+ + 2OH^- \qquad \text{Equation 5.2}$$

$$CO_2 + 2OH^- \leftrightarrow HCO_3^- + OH^- \leftrightarrow CO_3^{2-} + H_2O \qquad \text{Equation 5.3}$$

$$Ca^{2+} + CO_3^{2-} \rightarrow CaCO_3\ (s) \qquad \text{Equation 5.4}$$

The application of UICP-based well-sealing technologies for leaky oil and gas wells has been demonstrated in the field and commercialized (BioSqueeze®, 2022). However, UICP-based well-sealing technologies in deeper subsurface environments may be challenged by elevated temperatures and pH values that significantly differ from the optimal urease range (Feder et al., 2020; Fidaleo & Lavecchia, 2003; Krajewska, 2016). The pH optimum for urease has been described to be between pH 6 and 8, while the temperature optimum is between 45-65 °C (Feder et al., 2020; Fidaleo & Lavecchia, 2003; Krajewska et al., 2012; Lauchnor et al., 2015; Moynihan et al., 1989; Qin & Cabral, 1994). The pH dependence of ureolysis kinetics can described using Equation 5.S3 (Fidaleo & Lavecchia, 2003; Lauchnor et al., 2015; Moynihan et al., 1989; Qin & Cabral, 1994), and urease has been demonstrated to be reasonably active across pH conditions ranging from 5 to 10 (Krajewska, 2016; Lauchnor et al., 2015). At elevated temperatures (>50 °C), urease begins to thermally denature (Feder et al., 2020) and can be

mathematically modeled using Equation 5.S2 (Feder et al., 2020; Illeova et al., 2020; Krajewska, 2016).

Improving the stability of urease would increase the range of possible field applications of UICP, including high-pressure CO_2 storage and sequestration applications such as CCS. Enzyme immobilization has been demonstrated to improve the stability of enzymes in the face of harsh conditions such as temperature and low pH (Alazhari et al., 2018; Frieling, 2019; Krajewska, 2009b; Sheldon, 2007). In recent work, urease immobilization on ceramic carriers allowed this enzyme to withstand elevated temperatures for longer periods of time (Frieling, 2019).

Immobilization is a process in which an enzyme is adsorbed, covalently bound, or otherwise attached to a carrier (porous or non-porous solids) that may serve to protect the enzyme (Garcia-Galan et al., 2011; Kato et al., 2009; Reetz et al., 1996; Smidsrød & Skja, 1990). It is a well-known method with a broad range of applications (Klibanov, 1979; Kujawa et al., 2021). The immobilized enzyme is often better protected from thermal degradation, pH influence, or inactivation by inhibitors such as heavy metals (Klibanov, 1979; Mateo et al., 2007). In research presented here, an immobilization method was investigated to increase the stability of urease against low-pH and elevated temperature exposure.

Previously, we demonstrated that increased pressure alone does not inhibit ureolysis but that high pressure CO_2 can have an effect on the rate of ureolysis (Mitchell et al., 2013). The inhibitory effect of high pressure CO_2 was mostly attributed to a decrease in pH to well below the optimal pH for urease (Mitchell et al., 2013) rather than the pressure enzyme inhibition.

Work presented here evaluates urease activity in aqueous suspensions exposed to a range of pressurized CO_2 conditions, and thus a range of pH values, followed by a more in-depth assessment of urease activity over a range of pH values (pH 3-12) at two different temperatures (22 °C and 60 °C).

The work demonstrates reduced ureolytic activity at acidic and basic pH conditions as well as at elevated temperatures. Some of the ureolytic activity can be recovered when pH conditions are returned to optimal pH conditions; some activity can be permanently lost to the inactivation. The reduction in activity due to non-optimal pH values and elevated temperatures was partially mitigated through the immobilization of urease on a porous ceramic carrier.

Materials & Methods

Urease Source and Preparations

Suspended JBM preparation. Jack Bean Meal (JBM, *Canavalia ensiformis,* J0125, Sigma-Aldrich, MO) was used as the urease source. 5 g/L JBM suspensions were prepared in deionized water (DI, 9.4 MΩ-cm); the suspension was stirred for 16 hours on a magnetic stir plate at 120 rpm and 22 °C to facilitate dissolution (Feder et al., 2020).

Immobilized JBM urease preparation. One type of ceramic carrier (~0.5 mm diameter, SCALEGUARD, Carbo Ceramics, TX) was received without any chemicals loaded onto them. They were washed thoroughly with DI water and dried at 80 °C for 24 hours. Suspended JBM preparations (25 mL) were added to 6 g of ceramic carriers in 125 mL Erlenmeyer flasks and mixed on an orbital shaker at 150 rpm at 22 °C for 24 hours. Following enzyme sorption, the

liquid was decanted, retaining the ceramic carrier with the attached JBM in the flask. Phosphate buffered saline solution (PBS, 25 mL, 8.5 g/L sodium chloride, 0.61 g/L monopotassium phosphate, and 0.96 g/L dipotassium phosphate adjusted to pH 7.0) was added and decanted three times to the ceramic carrier remaining in the flasks to remove residual suspended enzyme; finally, the residual liquid was removed using a micropipette.

Ureolysis In The Presence of Pressurized CO_2

A 50 mL stainless-steel batch reactor was designed to include a high-pressure syringe pump (Teledyne Isco, NE). It was connected to both a high-pressure adapted pH and conductivity probe (Barben Analyzer Technologies, NV) (Daily, 2019) (Figure 5.1). The high-pressure probes were connected to a data logger (National Instruments, TX) and a LabVIEW platform. A pressurized CO_2 gas tank was connected to the high-pressure pump, allowing the system to produce carbonated brines. All reactor system components were connected via flexible ¼" stainless-steel tubing, Swagelok® fittings, and valves (Swagelok, ID) (Daily, 2019).

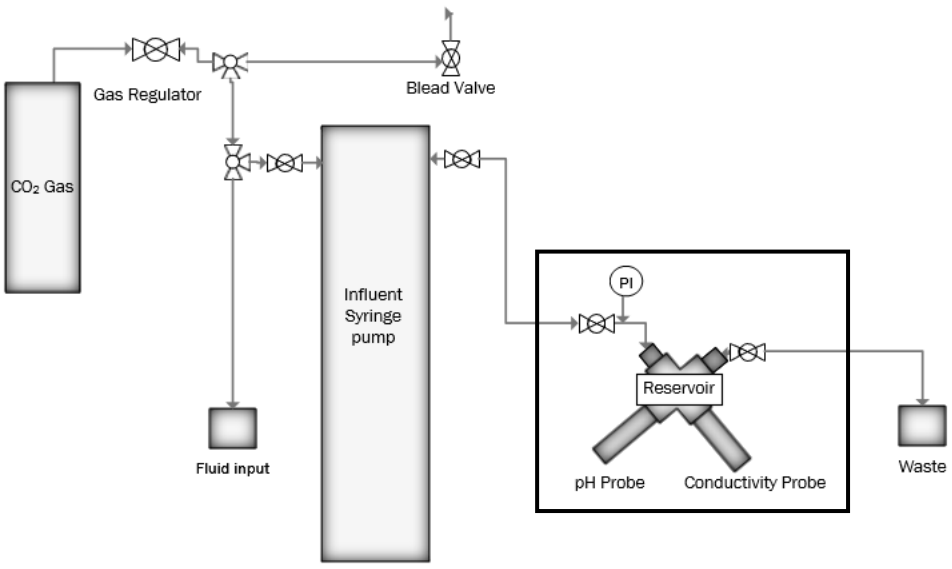

Figure 5.1: Schematic diagram of the high-pressure batch reactor system consisting of a high-pressure syringe pump (Teledyne "syringe pump"), CO_2 tank, stainless steel cross, high-pressure pH and conductivity probes, pressure gauge (pressure indicator, PI), and Swagelok® tubing and valves. The box around the reactor marks the stainless-steel cross and high-pressure probes. The tubing from the syringe pump to the reactor reservoir had a volume of 50 mL, and the reactor reservoir had a volume of 50 mL (Daily, 2019).

For ureolysis rate experiments, 60 mL of the 5 g/L JBM was mixed 1:1 with 60 mL brine (666 mmol/L urea and 374 mmol/L NH_4Cl). The solutions were used in the high-pressure batch reactor at four different pressures, along with an atmospheric pressure control tested at room temperature (22 °C). JBM urease was added to the brine prior to carbonation, and the pH and conductivity were monitored over time. Urea concentrations could not be measured while the reactor was under pressure; thus, conductivity was used as a surrogate to estimate changes in urea concentrations over time (Whiffin et al., 2007); see below for a detailed explanation.

The reactor system was prepared by injecting CO_2 gas to reach the desired pressure (0.89 MPa, 1.89 MPa, 2.89 MPa, or 4 MPa). The batch reactor was isolated from the pump before the pump was filled with JBM-containing brine. The brine was injected into the reactor system at a rate of 20 mL/min until the desired experimental pressure was reached, pushing the CO_2 gas and experimental solutions into the 50 mL reactor. The pump then switched to a constant pressure mode for the duration of the experiment. Each experimental trial lasted 1 to 5 hours, depending on the reaction rate. Each pressure test condition was conducted in triplicate, and conductivity and pH were recorded every minute.

pH-Dependent Ureolysis Rate Studies

Buffers were prepared in DI water amended with 4 g/L urea. The buffers used at each pH value were citrate (pH 3 and 5), acetate (pH 4), 2-(N-morpholino)ethanesulfonic buffer (MES) (pH 6), phosphate (pH 7 and 12), TRIS (pH 8), borate (pH 9), and carbonate (pH 10-11) (Table 5.S1). These buffers were prepared in DI water and filter-sterilized using 0.2 μm Rapid-Flow™ filters (Nalgene, NY). Ten mL of the amended buffers were mixed with 10 mL of 0.5 g/L JBM in 30 mL glass vials, resulting in a final concentration of 2 g/L urea and 0.25 g/L JBM. Lower JBM and urea concentrations than in the pressurized CO_2 studies were chosen for this study to minimize pH changes experienced during the ureolysis reaction. The batch experiments were run in triplicate in a shaking water bath set to 30 °C at 70 rpm. The batch systems were sampled every 15 minutes for 150 minutes.

Low-pH Exposure Studies and Enzyme Stability Improvements

To distinguish between reversible and irreversible enzyme inactivation during the pH exposure experiments, and to develop strategies to protect urease from inactivation, the degree of urease inactivation was assessed at low pH ranges at two different temperatures.

Four different pH conditions (pH 3.7-7.1) were created using acetate and phosphate buffers (Table 5.S2). First, 5 mL of each buffer was transferred into glass vials in triplicate. Second, 5 mL of 10 g/L suspended JBM was added. In the case of the immobilized enzyme, solid carrier particles were added as a source of enzyme, and 5 mL of sterile DI water was added to maintain identical buffer concentrations across treatments. JBM urease (suspended and immobilized) was exposed to each of the pH conditions for one hour at 22 °C or 60 °C to simulate transport into or through acidic zones of an aquifer or a well. The pH was measured in each system after the low-pH exposure at two different temperatures.

Urea solutions (20 g/L) containing pH 7 buffer were added to each of the enzyme-buffer solutions with the goal of achieving a pH of 7 before assessing the remaining ureolytic activity. The change in ureolytic activity was used to assess the degree of urease inactivation due to pH. Glass vials containing the exposed urease suspensions were readjusted to pH ~7 (see Table 5.1 for exact pH values after pH readjustment). Then the samples were placed in a water bath at 30 °C and agitated at 120 rpm to determine the ureolysis rate. Samples were taken for urea analysis at 0, 0.5, 1, 3, 8, 24, and 48 hours. The first-order rate coefficients (k_a) were calculated, and calculations are described more in detail in the next section.

Table 5.1: Actual pH values of the buffer solutions after adding enzyme and urea solutions.

Initial Actual Buffer pH	3.7	4.1	4.7	7.1
After mixing with enzyme solution	3.7 ± 0.0	4.1 ± 0.0	4.7 ± 0.0	7.2 ± 0.1
After mixing with pH 7 buffered urea solution	6.7 ± 0.3	6.9 ± 0.0	6.9 ± 0.0	7.1 ± 0.1

Analytical Tools and Measurements

Reaction Rate Coefficient Calculation. A first-order rate model was used to describe the ureolytic activity (Eq. 5.5) as described in Feder et al. (2020)

$$\frac{dA}{dt} = -k_a[A] \qquad \text{Equation 5.5}$$

After integration, with the appropriate initial condition A=1 at t=0, the integrated form of the model (Eq. 5.6) was used to estimate the first-order rate coefficient (k_a) using a linear trendline in Microsoft Excel.

$$ln(A) = ln(A_0) - k_a t \qquad \text{Equation 5.6}$$

Urea concentration-conductivity correlation curve. Because samples could not be collected while the reactor system was pressured, the change in conductivity over time was measured and used a proxy for ureolysis rates. pH and conductivity probes were calibrated at the beginning of each day of experiments. The production of ionic species (Eq. 5.2-5.3, NH_4^+ and HCO_3^-) from non-ionic substrates (urea and H_2O) results in an increase in overall conductivity, and the rate at which conductivity increases is proportional to the rate at which the urea concentration decreases (Whiffin et al., 2007). A correlation between the change in conductivity to the change in urea concentration was established (R^2=0.98, Figure 5.S1). This correlation was

used to convert the conductivity data (Figure 5.S2, A) into urea concentrations for the 0, 0.89, 1.89, 2.89, and 4 MPa experimental conditions.

Urea concentration analysis. A modified colorimetric urea assay (Jung et al., 1975; Phillips, 2013) was used to determine the urea concentration. Samples were diluted 1:10 in 0.56 M H_2SO_4 (final concentration of 0.5 M) to stop ureolytic activity. Samples were stored in the fridge in 1.5 mL microcentrifuge tubes before the urea assay was performed in a flatbottom 96 well plate, and absorbances (505 nm) were measured in a 96-well plate spectrophotometer (Biotek Synergy HT, VT).

Results and Discussion

Ureolysis in pressurized CO_2 brine

The high-pressure reactor (Figure 5.1) was pressurized with CO_2 at five different pressures (including air at atmospheric pressure control "0 MPa") before assessing ureolysis rates. As expected, initial pH values in the brine were lower at higher CO_2 pressures, with the highest CO_2 pressure treatment (4 MPa of pure phase CO_2) exhibiting an initial pH of 4.8 while the "0 MPa" treatment (no added CO_2) exhibited a pH of 8.6 at the 0-hour timepoint (Figure 5.2, B). Once ureolysis commenced, urea concentrations decreased from the initial concentration of 333 mmol/L to 151, 160, 205, 216, and 269 mmol/L after one hour at CO_2 pressures of 1.89, 0.89, 2.89, 4, and 0 MPa, respectively (Figure 5.2, A). The pH values increased in all treatments (Figure 5.2, B) due to the net generation of hydroxyl ions during ureolysis (*cf.* Eq. 5.2-5.3). The

pH appeared to stabilize after one hour, with only minor increases observed afterward (Figure 5.S2, B).

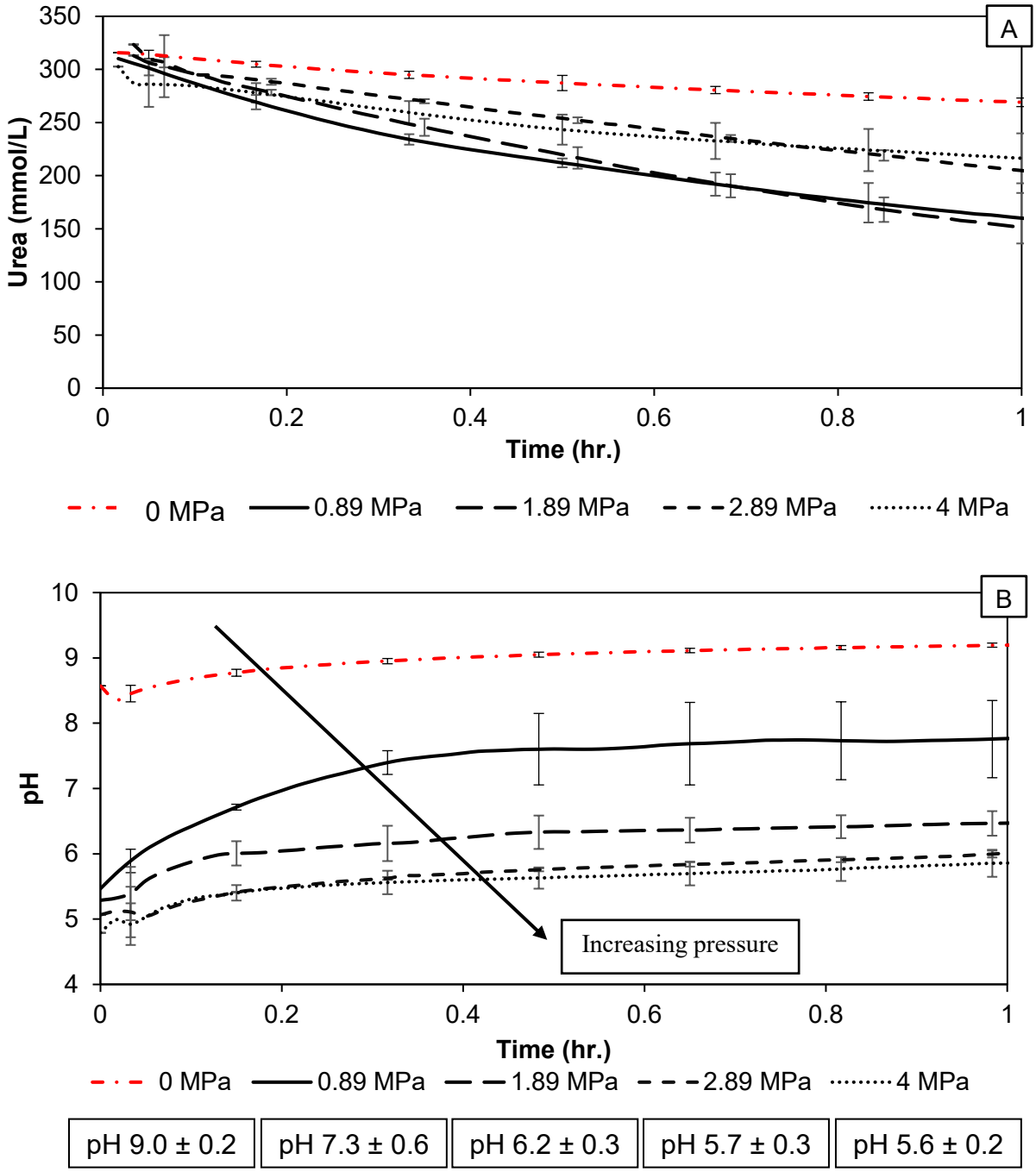

Figure 5.2: (A) Urea concentrations over time estimated by converting *in situ* conductivity into urea concentration according to Equation 5.S1. (B) Change in pH values during ureolysis at various CO_2 pressures. The average pH (+/- standard deviations) for the first hour of each experiment is listed below each treatment in the legend. The black lines represent experimental

conditions with CO_2 at increasing pressures (0.89-4 MPa); the red line (dot-dashed) is the "CO_2-free" control ("0 MPa"), which had atmospheric air at ambient pressure in the headspace.

Ureolytic activities at the different CO_2 pressures were compared using their apparent first-order rate coefficients (k_a) (Figure 5.3). The highest k_a (0.76 ± 0.1 hr^{-1}) was estimated for the 1.89 MPa treatment, with an average pH value of 6.2 ± 0.3 in the one-hour experimental time frame. For statistical analysis of different experiments, ANOVA with post-hoc Tukey testing was applied using the triplicate k_a values for each pressure condition. Data points presented in Figures 5.3, 5.4, and 5.6 that share the same letter (located either above or below the data points) are not statistically significantly different based on a 95% confidence level assumption ($p = 0.05$). Based on these ANOVA with post-hoc Tukey test comparisons, the apparent k_a for the 1.89 MPa experiment was significantly higher than the apparent k_a values for the 0 MPa (k_a 0.16 ± 0.0 hr^{-1}, pH 9.0 ± 0.2) and 4 MPa experiments (0.32 ± 0.1 hr^{-1}, pH 5.6 ± 0.2) but not significantly different from the apparent k_a values for the 2.89 MPa (k_a 0.42 ± 0.0 hr^{-1}, pH 5.7 ± 0.3) and 0.89 MPa (k_a 0.66 ± 0.2 hr^{-1}, pH 7.3 ± 0.6), presumably due to the wide range of pH values experienced during these experiments (*cf.* horizontal error bars in Figure 5.3).

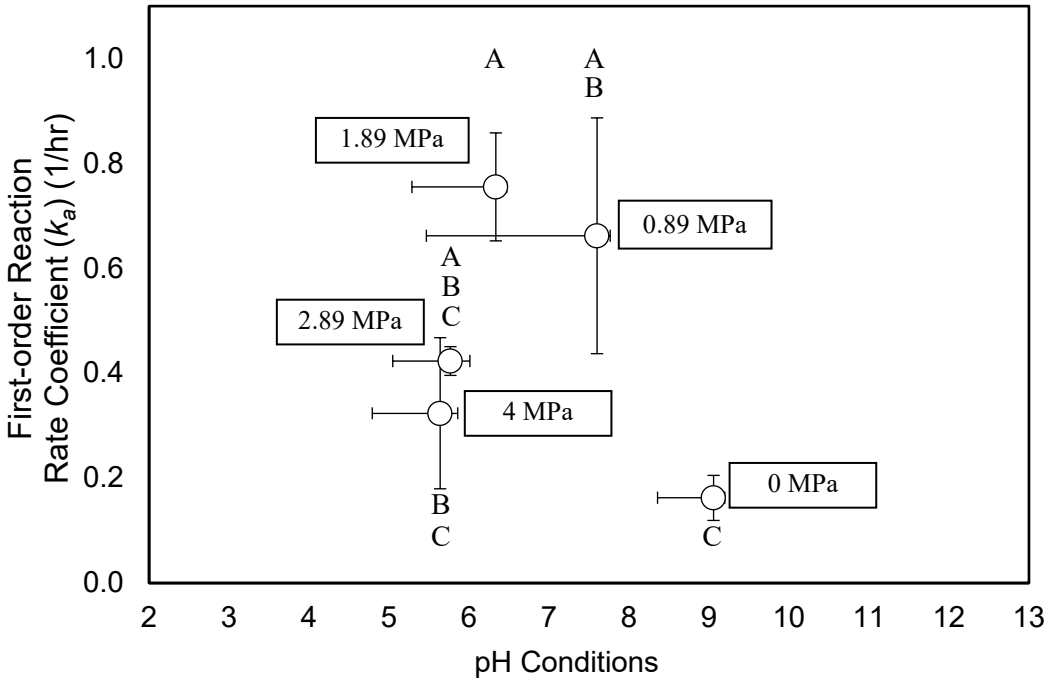

Figure 5.3: First-order urea hydrolysis rate coefficients (k_a) estimated from pressurized CO_2 studies containing 2.5 g/L Jack Bean Meal. Vertical error bars represent one standard deviation of triplicate studies. Median pH values were plotted, and the range of pH values during each experimental timeframe used for first-order rate coefficient estimation is indicated with horizontal error bars. ANOVA with post-hoc Tukey testing was applied using each triplicate data point. Data points that share the same letter (located either above or below the average data points) are not statistically significantly different based on a 95% confidence interval assumption (p = 0.05).

The experiment demonstrates that ureolysis can occur in the presence of pressurized CO_2, indicating a potential for using EICP to seal leaky wellbores in geologic carbon sequestration scenarios. The highest ureolysis rates were observed at intermediate CO_2 pressures (1.89 and 0.89 MPa), while higher and lower CO_2 pressures resulted in lower ureolysis rates (Figure 5.3). The lower rates were hypothesized to result from significantly higher or lower pH values, below the optimal urease range reported previously (pH 6-8) (Figure 5.3) (Cesareo & Langton, 1992;

Krajewska, 2016; Lauchnor et al., 2015). However, the pH shifted up to 2.3 pH units throughout these pressurized CO_2 studies, with the median pH of each treatment close to the upper bound of the observed pH (horizontal error bars in Figure 5.3). This indicates that most urea hydrolysis occurred at pH values higher than the initial pH value. This variation in pH conditions did not allow for a clear distinction between the potential effect of CO_2 and the pH on JBM urease activity. As a result, another set of experiments was conducted in systems with more tightly controlled pH conditions (using synthetically buffered solutions in the absence of pressurized CO_2) over a broader range of pH values.

pH-Dependent Ureolysis

The pressurized CO_2 study demonstrated that ureolysis catalyzed by the JBM urease could occur under pressurized-CO_2 conditions; however, the pH increased significantly over time for each test condition, preventing a distinction between the effect of CO_2 and pH on urease activity from being determined. Hence, at ambient pressure, pH-dependent batch experiments were performed using synthetic buffer systems, in which the pH was largely maintained during the ureolysis reaction. Ureolytic activities were assessed for ten different pH values ranging between 3 and 12, and the median pH value for each treatment was measured along with the range of pH values observed during the experiment (Figure 5.4). The batch tests uncovered that the median pH was closer to the initial pH conditions than the pressurized CO_2 experiments.

To obtain these small changes in pH, strong synthetic buffers with a buffer capacity of 300 mM or greater, along with one-tenth of the urea concentration (2 g/L), were used, in contrast to the pressurized CO_2 studies, which were conducted in the absence of external buffers and

contained 20 g/L urea. As a result, the average value of all standard deviations for the pH values within the experimental timeframe (2.5 hours) was 0.1; the minimal standard deviations for the pH 3, 12, and 13 experiments were not included in this calculation since there was no significant ureolysis observed and the average value of all standard deviations would have become even smaller.

The highest apparent first-order urea hydrolysis rate coefficient (k_a) was observed in the pH 6.4 ± 0.3, MES-buffered system (k_a 1.03 ± 0.02 hr^{-1}) (Figure 5.4), and no activity was observed at pH 11 and 12. Urea (2 g/L) was hydrolyzed entirely within 2.5 hours at pH values between 6 and 9 (*cf*. Figure 5.S3). Incomplete hydrolysis of urea was observed at pH values 3 (6%), 4 (46%), 5 (46%), and 10 (84%) within the experimental time frame, and the lowest measurable k_a was observed at pH 3 (0.06 ± 0.01 hr^{-1}).

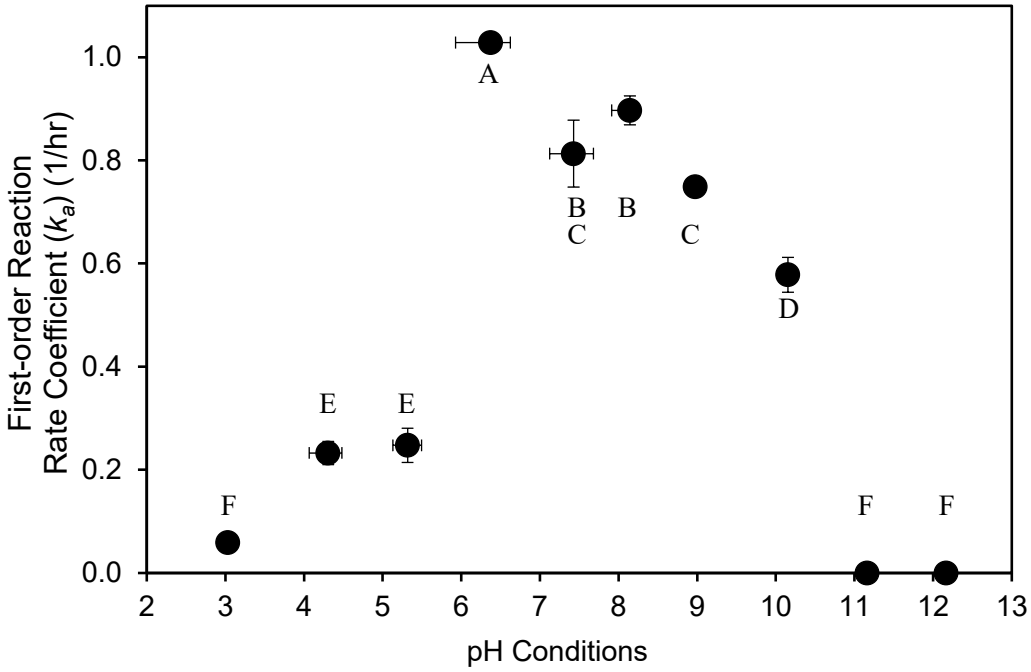

Figure 5.4: First-order urea hydrolysis rate coefficients (k_a) estimated from ambient pressure batch studies using synthetic pH buffers (Table 5.S1 (Buffer recipes), Figure 5.S3 (Raw urea and pH concentrations over time)). Vertical error bars represent one standard deviation from triplicate treatments. Median pH values were plotted, and the range of pH values during the experimental timeframe (2.5 hours) used for first-order rate coefficient estimation are indicated with horizontal error bars. ANOVA with post-hoc Tukey testing was applied using each triplicate data point for the buffered study. Data points that share the same letter (located either above or below the data points) are not statistically significantly different based on a 95% confidence interval assumption (p = 0.05).

These results demonstrate that the pH affects ureolysis, with the highest ureolysis rate coefficient observed at pH 6.4 ± 0.3 (k_a 1.03 ± 0.02 hr^{-1}). This highest rate coefficient was statistically different from the rate coefficients at all other pH values evaluated. When ureolytic activities at pH 7.4 and pH 8.1 were compared, they were found to be not statistically significantly different (at pH 7.4 ± 0.2, k_a = 0.81 ± 0.06 hr^{-1} and at pH 8.1 ± 0.1, k_a = 0.90 ± 0.03 hr^{-1}). Ureolytic activities at pH 4.3 and pH 5.3 were also found to be not statistically significantly different (at pH 4.3 ± 0.1, k_a = 0.23 ± 0.02 $hr^{-1,}$ and at pH 5.3 ± 0.1 k_a = 0.23 ± 0.02 hr^{-1}). When

ureolytic activities at the extremes of the acidic and basic pH conditions utilized in this study were compared, they were found to not be statistically different (at 3.0 ± 0.0 k_a = 0.06 ± 0.01 hr^{-1}, at pH 11.2 ± 0.0 k_a = 0.00 ± 0.00 hr^{-1}, and pH 12.2 ± 0.0 k_a = 0.00 ± 0.00 hr^{-1})

pH conditions heavily influence ureolytic activities

While, in general, k_a values estimated from the ambient pressure systems with synthetic buffers were higher than those from the pressurized CO_2 systems, statistically, there were no differences at similar pH conditions, presumably due to the large variation in pH in the pressurized CO_2 systems which were not well buffered. ANOVA results indicate first-order urea hydrolysis rate coefficients (k_a) not being statistically significantly different from synthetically buffered pH 7.4 ± 0.2 (k_a 0.81 ± 0.06 hr^{-1}), pH 8.1 ± 0.1 (k_a 0.90 ± 0.03 hr^{-1}), pH 9.0 ± 0.0 (k_a 0.75 ± 0.01 hr^{-1}) and pressurized-CO_2 1.89 MPa (k_a 0.76 ± 0.1 hr^{-1}, pH 6.2 ± 0.3), and 0.89 MPa (k_a 0.66 ± 0.2 hr^{-1}, pH 7.3 ± 0.6) experiments. k_a values from buffered pH 4.3 ± 0.1 (k_a 0.23 ± 0.02 hr^{-1}), pH 5.3 ± 0.1 (k_a 0.25 ± 0.03 hr^{-1}) and pressurized-CO_2 4 MPa experiments (0.32 ± 0.1 hr^{-1}, pH 5.6 ± 0.2), and 2.89 MPa (k_a 0.42 ± 0.0 hr^{-1}, pH 5.7 ± 0.3) were also found to be not statistically significantly different (Figure 5.S4).

Several factors might have contributed to higher k_a values estimated from synthetic buffer studies (even though these are not statistically significant). While the presence of CO_2 might have contributed to differences, pressure alone did not affect ureolysis in our previous work (Mitchell et al., 2013). Furthermore, the pressurized CO_2 studies were conducted in the presence of 333 mmol/L (20 g/L) urea and 2.5 g/L JBM solutions, while lower urea (33 mmol/L = 2 g/L) and JBM (0.25 g/L) concentrations were used in the synthetic buffer studies to minimize the

change in pH during the experiments. The pressurized CO_2 studies were conducted in a closed reactor system, while flasks open to the atmosphere were used for the synthetic buffer studies. Ammonium/ammonia and inorganic carbon ($CO_2/HCO_3^-/CO_3^{2-}$) are by-products of urea hydrolysis. Increased ammonium concentrations have been reported to decrease urease activity (Fidaleo & Lavecchia, 2003). In open systems, ammonia can off-gas, thus reducing ammonium concentrations; in closed systems, ammonium/ammonia generated during ureolysis will accumulate and might decrease urease activity (Fidaleo & Lavecchia, 2003). Other differences between the pressurized CO_2 and synthetically buffered studies include the use of different synthetic buffers depending on the desired pH (*cf.* Table 5.S1), while no additional buffer was present in the pressurized CO_2 experiments. Enzymatic activity has been described to be affected by the reaction medium chemistry (Schomburg et al., 2012), including buffers. Only NH_4Cl and CO_2 were present in addition to urea and JBM solutions in the pressurized CO_2 studies. The significant changes in pH values during the pressurized CO_2 studies (Figure 5.3) may have led to changes in the ureolytic activity. While the buffers used in the synthetic buffer experiments along with the lower urea concentrations prevented drastic pH changes and, consequently, the possible denaturation of the enzyme through drastic pH changes (Schomburg et al., 2012), the pressurized and largely unbuffered systems experienced a larger pH change during ureolysis.

The apparent first-order rate coefficients (k_a values) estimated in this work are higher than those reported in most previous studies (*cf.* Table 5.2); however, when the k_a values were normalized to the urease concentration, the values are comparable (Table 5.2). Differences in k_a could be due to differences in temperature and pH conditions tested, which have been reported to

influence ureolytic activity (Feder et al., 2020; Krajewska, 2016). Moreover, in the presence of calcium ions, urease can be entrapped in precipitated calcium carbonate minerals, which can inhibit ureolysis (Cuthbert et al., 2012). When the results of the current studies (buffered and pressurized CO_2) were compared, the buffered test (performed at 30 °C) expressed slightly higher k_a values than pressurized CO_2 experiments (performed at 22 °C) under similar pH conditions. These results agree with prior work demonstrating that higher temperatures generally result in higher ureolytic activity (Feder et al., 2020; Krajewska, 2016; Krajewska et al., 2012). Feder et al. (2020) reported k_a of 0.36 hr^{-1} at 30 °C and 0.25 hr^{-1} at 20 °C with a final pH of 9.3; whereas the current pressurized CO_2 studies reported k_a of 0.16 hr^{-1} at 22 °C and the average pH 9.0 ± 0.2 in a closed system. However, because the buffered experiments used one-tenth of the urease content, when normalized, the k_a values became significantly larger (2143-2943 hr^{-1}(g/L urease)$^{-1}$) than pressurized CO_2 tests (46-217 hr^{-1}(g/L urease)$^{-1}$). Ureolytic activities reported in Handley-Sidhu et al. (2013) are lower than the ones observed in the buffered studies here, even though higher JBM concentrations were used (0.5 g/L JBM). This difference could be due to lower temperatures (10 °C) as well as the presence of calcium (Table 5.2) (Feder et al., 2020; Krajewska, 2018).

Table 5.2: Comparison of urea hydrolysis rate data with previous studies using bacterial whole cells and plant-based ureases. The current study and reported apparent first-order rate coefficients (k_a) and k_a normalized to the amount of urease source (bacteria or jack bean meal) are listed along with the corresponding references.

Urease Source	OD_{600} or JBM conc.	Urease */** (mg/L)	Urea (mmol/L)	Calcium (mmol/L)	Temperature (°C)	Final pH	Apparent k_a (hr^{-1})	Normalized Apparent k_a (hr^{-1}* $(g/Lurease)^{-1}$)	Reference
S. pasteurii	0.07	0.25	6	1.75	20	9.3	0.038	151*	Ferris et al. (2004)
S. pasteurii	0.05	0.18	33-333	20	30	8.7-9.5	0.027-0.035	150-194*	Dupraz et al. (2009b)
S. pasteurii	0.32	1.15	1-722	0	30	9.3	0.35	861*	Lauchnor et al. (2015)
S. pasteurii	0.07	0.25	250	200	20	8.0	0.095	377*	Tobler et al. (2011)
JBM	0.5 g/L	0.7	200	400	10	8.5	0.011	15.7**	Handley-Sidhu et al. (2013)
JBM	2.5 g/L	3.5	333	0	20-30	9.3	0.248-0.355	71-101**	Feder et al. (2020)
JBM	2.5 g/L	3.5	333	0	22	5.9-9.2	0.16-0.76	46-217**	Current Study (Pressurized CO_2)
JBM	0.25 g/L	0.35	33	0	30	3-12.2 (6.7-9.1)	0.0-1.03 (0.75-1.03)	0-2943** (2143-2943)**	Current Study (Buffered)

*Assumes 0.36 (g/L CDW)/$OD600_{nm}$ (Ren et al., 2013) and 1% urease in *S. pasteurii* (Bachmeier et al., 2002)
**Assumes 0.14% urease in JBM (Krajewska, 2009a)

The pH dependency of urea hydrolysis rates of work here was compared with previously published studies and models. Each previously published data set was modeled using Eq. 5.S3, which results in the "bell-shaped" reaction rate curves as a function of pH (Figure 5.5). The trend in various literature studies aligns with our pressurized CO_2 and buffered ureolysis rates. The difference in curve heights in Figure 5.5 of pressurized CO_2 studies and buffered studies, (Lauchnor et al. (2015), and Qin and Cabral (1994)) are due to the amount of enzyme used. Peak

activity (mM/hr) was achieved at pH 6-8, except for Lauchnor et al. (2015), which used intact *S. pasteurii* cells as the urease source compared to cell-free enzymes and reported a peak between pH 8-9 (Figure 5.5).

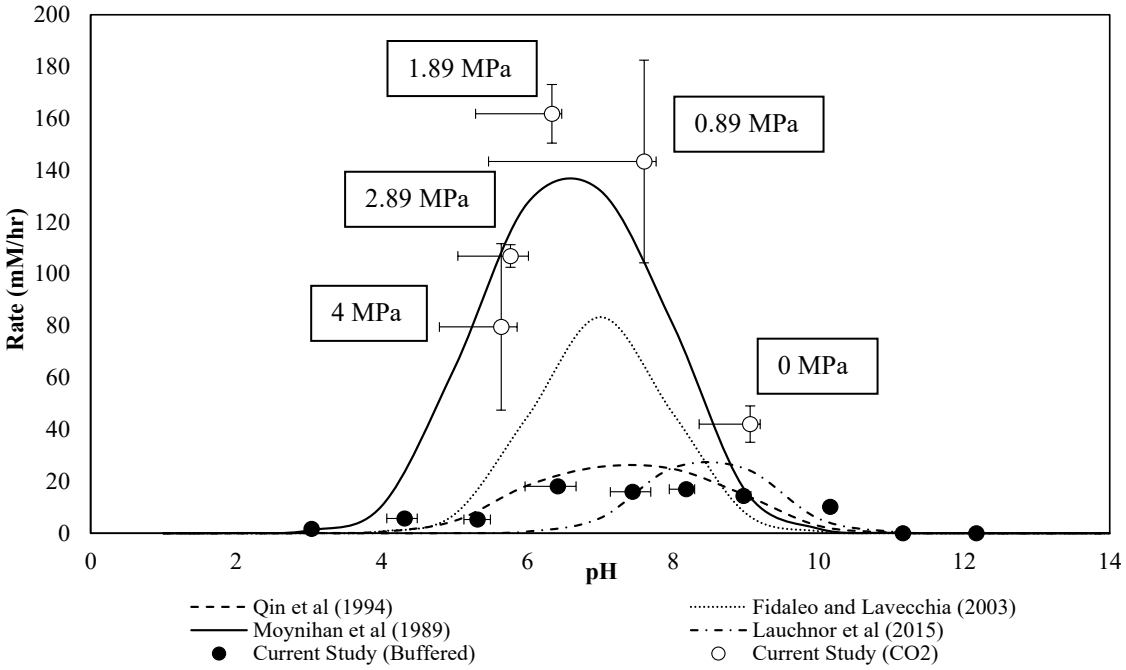

Figure 5.5: Rates of ureolysis vs. pH values are plotted. The rates of ureolysis (mM/hr) from current studies are presented for carbonated brines at 0-4 MPa (○) and buffered (●) studies. Median pH conditions were plotted, and changes in pH during the experiment were indicated with horizontal error bars. Vertical error bars are the standard deviations of the initial ureolysis rates for current studies; buffered experimental error bars, if not visible, are small enough to be hidden behind markers. The initial rates from this study are compared to the models made with Equation 5.S3 using the values of $K_{es,1}$, $K_{es,2}$, $v_{max,}$ and K_m from Qin and Cabral (1994) (dashed), Fidaleo and Lavecchia (2003) (dotted), and Moynihan et al. (1989) (solid). Kinetic parameter (v_{max}, k_m, K_{es}) values are reported in Table 5.S4. Results from the current and the literature demonstrate a reduction in rates further apart from circumneutral pH conditions with a peak around pH 6-8.

Ureolysis clearly occurred across a pH range from 4 to 10. The pressurized CO_2 systems, which experienced greater variations in pH, also exhibited more significant variations in k_a. At high CO_2 pressures, and thus at low initial pH values, initial urea hydrolysis rates were slow,

presumably due to the low pH values, but increased over time once more optimal (meaning higher) pH values developed. The change in pH throughout the experiment led to a broader range of k_a values.

Lower rates of ureolysis at higher and lower pH values were expected, based on the known effect of pH on enzyme activity and enzyme inactivation. Here, both high and low pH conditions can lead to lower rates of ureolysis and permanent enzyme denaturation (Barazorda-Ccahuana et al., 2020; Fidaleo & Lavecchia, 2003; Krajewska, 2016). Unfortunately, work here is unable to determine whether the urease enzyme was permanently inactivated or reversible. Hence, experiments were conducted to estimate the extent of inactivation at low pH values at two different temperatures (22 and 60 °C), and enzyme immobilization was evaluated as a strategy to increase enzyme stability under each test condition.

Immobilization of urease reduces inactivation by low pH and increased temperatures

Suspended and surface-immobilized JBM was exposed to solutions with pH values of 3.7, 4.1, 4.7, and 7.1 at 22 °C and 60 °C for one hour before the pH was re-adjusted to ~ pH 7, and the residual ureolytic activity was assessed at 30 °C (see Table 5.S2 for details). Because the pH was re-adjusted to ~ pH 7 (a near-optimal pH for urease), and the urease activity assessments were conducted at a temperature of 30 °C (a near-optimal temperature for urease), any observed differences in ureolysis rates were considered due to irreversible urease inactivation experienced during the pH and temperature exposure.

Urease immobilization of urease on the porous ceramic carrier used in this work increased the stability of urease during low-pH and elevated temperature exposure (60 °C) (Figure 5.6). For instance, while, at 22 °C, the estimated apparent first-order rate coefficient (k_a) for immobilized urease after a one-hour exposure to pH 4.1 did not change statistically (k_a = 0.50 ± 0.03 hr^{-1}) relative to the k_a after pH 7.2 exposure (0.46 ± 0.02 hr^{-1}). However, the k_a of the suspended urease decreased significantly, to 0.40 ± 0.04 hr^{-1} compared to a k_a of 0.92 ± 0.02 hr^{-1} after a one-hour exposure to 7.2 (Figure 5.6, compare solid blue bars to blue hashed bars). Even after a one-hour exposure to pH 3.7 at 22 °C, the immobilized urease showed no statistically significant decrease in activity relative to the pH 7.2 treatments (k_a = 0.40 ± 0.01 hr^{-1}); in comparison, there was no urease activity after exposure of the suspended urease to pH 3.7 at 22 °C. It should be noted that the overall activity (in terms of estimated apparent first-order rate coefficients) was consistently lower for the immobilized urease treatments, which likely due to the incomplete sorption of urease to the porous ceramic carrier and a results in a lower urease concentration relative to the suspended systems (*cf*. Materials and Methods for details).

Neither suspended nor immobilized urease exposure to pH 4.7 for one hour at 22 °C resulted in a decrease in k_a (Figure 5.6, blue solid and hashed bars), relative to the pH 7.2 treatments, indicating that permanent inactivation (*i.e.*, denaturation) of urease did not occur. Indeed, for both the suspended and immobilized enzyme, the k_a increased slightly after exposure to the acetic acid/acetate buffer at pH 4.7 relative to the pH 7.2 (phosphate buffer) exposure treatments (Figure 5.6). This increase was statistically significant for the immobilized enzyme, while it was not statistically significant for the suspended urease treatments. The increase could

be due to a slightly different chemical environment (Kafarski & Talma, 2018; Schomburg et al., 2012) stemming from the carryover of components from the pH 4.7 treatment (acetic acid/acetate buffer) relative to the phosphate buffer used in the pH 7.2 exposure (Table 5.S2).

Exposing the urease to 60 °C for one hour decreased urease activity relative to the 22 °C treatments, regardless of pH and whether the urease was suspended or immobilized (Figure 5.6, compare red bars to blue bars). This agrees with previous findings by our group and others (Feder et al., 2020; Krajewska, 2016). For instance, at pH 7.2, the 60 °C-exposed suspended JBM urease exhibited only ~50% (0.46 ± 0.03 hr^{-1}) of the activity observed after exposure to pH 7.2 at 22 °C.

As hypothesized, immobilization successfully protected the enzyme (Figure 5.6, compare solid bars with hashed bars for red and blue separately). For instance, while suspended urease activity exposed to pH 7.2 at 60 °C retained approximately 50% of urease activity relative to the 22 °C treatments, the immobilized urease retained approximately 78% (0.36 ± 0.02 hr^{-1}) of its activity. Reduced enzyme inactivation was observed for the immobilized enzyme at each pH and temperature combination. The lone exception was test conditions at pH 3.7 at 60°C, where no remaining activity was observed. Notably, even after exposure to a pH value of 4.1 at 60 °C, some residual activity was detected for immobilized urease, while the suspended urease showed no remaining activity.

In summary, urease immobilization appears to protect the enzyme and reduce inactivation under low-pH and elevated temperature exposure. At the same time, there appears to be a combined effect of temperature and pH, which results in additional inactivation when urease

experiences low pH values at elevated temperatures. These findings agree with previous observations regarding increased urease stability at elevated temperatures after immobilization (Daniel, 1996; Frieling, 2019; Krajewska, 2009b; Moynihan et al., 1989)

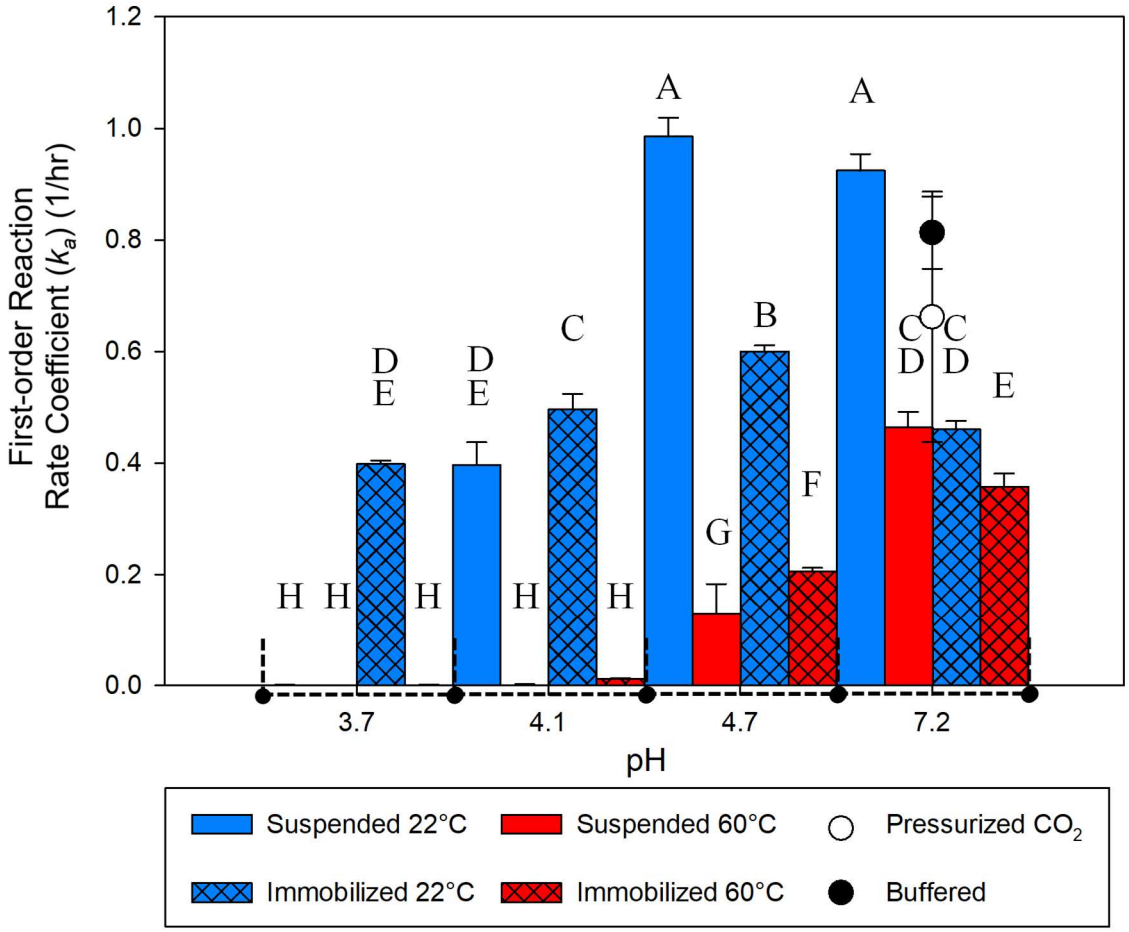

Figure 5.6: Apparent first-order ureolysis rate coefficients (k_a) after one-hour exposure to low pH conditions at two different temperatures (22 °C and 60 °C). Assessment of the residual activity were performed at ~ pH 7 and 30 °C, *cf.* Table 5.1 and Materials and Methods for details). Apparent first-order rate coefficient (k_a) (y-axis) of suspended urease represented by solid bars and immobilized urease represented by hashed bars; data are tabulated in Table 5.S3. k_a values from pressurized CO_2 (open circles, data from pH 7.6 treatments, Figure 5.3), and buffered pH experiments (black circles, data from pH 7.4 treatments, Figure 5.4) were added for comparison. ANOVA with post-hoc Tukey testing was applied to the data set. Data points not statistically significantly different (95% CI) were labeled using the same letters.

Conclusions

Ureolysis can occur under pressure and in the presence of CO_2, indicating the principal feasibility of using ureolytically induced calcium carbonate precipitation (UICP) for sealing leakage pathways in geologic carbon storage situations where CO_2-affected brine might be present (Kirkland et al., 2021a). Increased CO_2 pressure resulted in successively lower pH values, which are known to negatively affect urease activity (Haghi et al., 2017; Kirkland et al., 2021a). There is no clear evidence that increased pressure (0-4 MPa) or the CO_2 itself had a negative effect on urease activity. The dependency of urease activity on pH has been reported before (Barazorda-Ccahuana et al., 2020; Krajewska, 2016), and the study presented with pressurized CO_2 and unpressurized experiments here confirm these previous observations.

Work here sheds additional light on whether the changes in urease activity due to pH and temperature exposure are due to reversible (meaning only inhibitory) processes, or result in irreversible inactivation of urease. It appears that exposure of suspended urease at approximately room temperature (22 °C) to a pH as low as 4.7 for one hour does not result in irreversible inactivation of the enzyme. However, pH values of 4.1 and lower result in a significant decrease in suspended urease activity, signifying enzyme denaturation. The extent of irreversible inactivation of urease increases if the enzyme is exposed to a combined pH and temperature stress: If urease is exposed to 60 °C for one hour, even at a pH of 4.7, partial inactivation of urease is observed, and urease is completely inactivated when exposed to pH values of 3.7 or 4.1 at 60 °C for one hour.

Immobilization of urease (demonstrated here using a porous ceramic carrier) partially protects urease from temperature- and pH-dependent inactivation, thus expanding the range of potential UICP applications. Immobilization could be a useful urease delivery tool, expanding the range of temperature and pH conditions in which UICP can occur. In the future, the effect of different materials for enzyme immobilization may need to be investigated in more detail to develop customized combinations for specific applications in the subsurface and elsewhere. Furthermore, the loading of the enzyme onto surfaces should be investigated with the goal of optimizing the amount of enzyme covering the carrier surface.

Acknowledgments

Funding: This work was supported by the U.S. Department of Energy, grant Numbers DE-FE0026513 and DE-SC0010099. Any opinions, findings, conclusions or recommendations expressed herein are those of the authors and do not necessarily reflect the views of the DOE. Additional support was provided by Montana State University's Center for Biofilm Engineering, Thermal Biology Institute, Norm Asbjornson College of Engineering, and Vice President for Research, Graduate Education, and Economic Development, as well as through the National Science Foundation (NSF) (Award #2036867) FMSG: Biologically Assembled and Recycled Construction and Structural Materials (BRICS). The authors acknowledge Al Parker at the Center for Biofilm Engineering, Montana State University for his assistance in the statistical analysis.

Supplemental Information

Pressurized CO_2 Brine Studies urea/conductivity correlation

Urea concentration/conductivity correlation curve. The change in conductivity was correlated to changes in urea concentrations in order to estimate urea concentrations in closed, pressurized systems using conductivity measurements. Independent experiments were performed at 2.89 MPa (420 psi) and terminated at four different time points (1, 2, 3, and 5 hrs), resulting in different residual urea concentrations. The conductivity was recorded directly before the system was depressurized, and the remaining urea concentrations were determined immediately. The change in urea concentration relative to the change in conductivity was then plotted, and a linear regression was used to fit a correlation curve. (Figure 5.S1). Equation 5.S1 is the equation for the correlation line seen in Figure 5.S1:

$$DU = 7.5207 \, x \, DC - 0.735 \qquad \text{Equation 5.S1}$$

where DU is the change in urea concentration (mmol/L) and DC is the change in conductivity (mS/cm). This equation was used to convert the conductivity measurements recorded throughout the pressurized CO_2 experiments to urea concentrations for rate analysis. The R^2 value for this line was 0.98, indicating an adequate correlation.

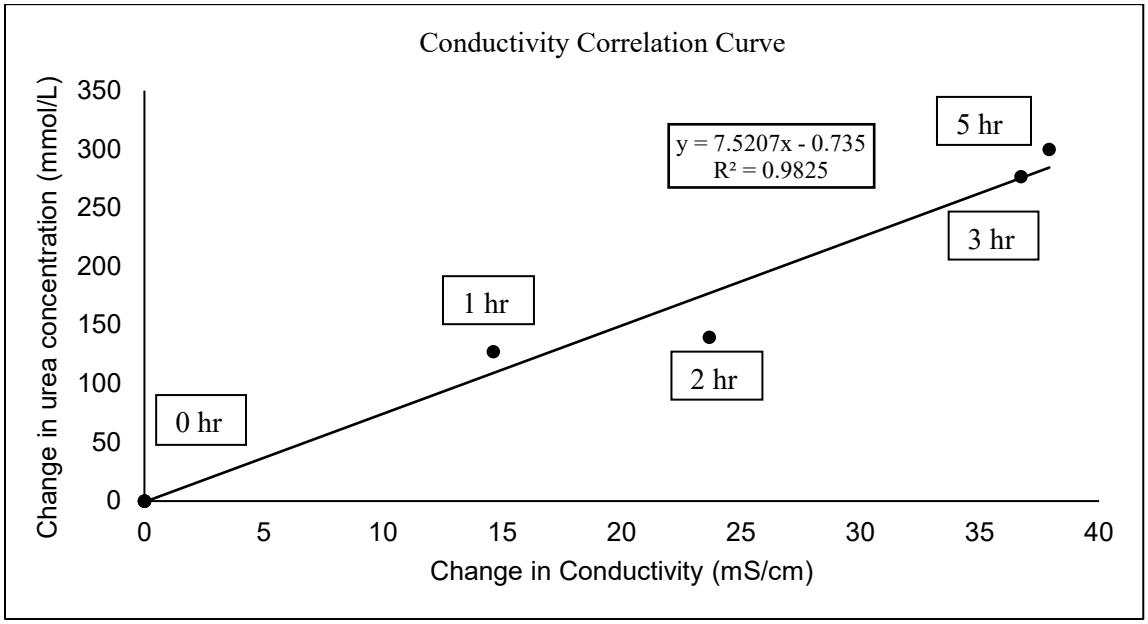

Figure 5.S1: Change in conductivity over change in urea concentrations obtained for a closed system with a CO_2 pressure of 2.89 MPa. The correlation equation was used to estimate urea concentrations and thus ureolysis rates over time in the high-pressure reactor based on the *in situ* conductivity measurements.

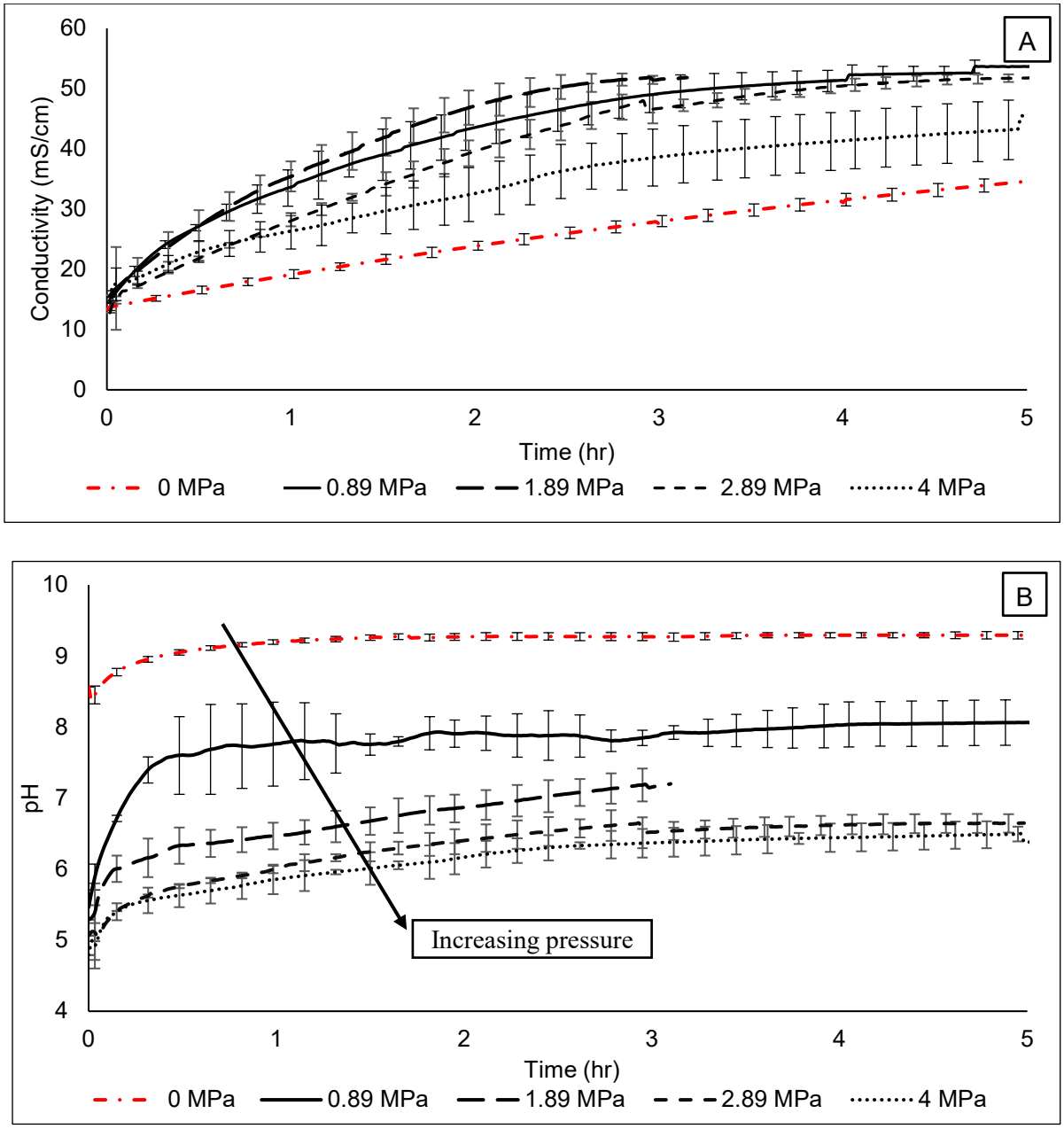

Figure 5.S2: (A) Conductivity changes over time in high-pressure reactors at the different tested CO_2 pressures. (B) Change in pH conditions during ureolysis reactions, at the different CO_2 pressures.

Ureolysis with synthetic pH Buffers

Table 5.S1: Synthetic buffers prepared for pH-dependent ureolysis rate studies. The buffers contained 4 g/L urea and were diluted 1:2 at the beginning of each study with 0.5 g/L JBM suspension to result in final concentrations 50% of the indicated buffer strength, 2 g/L urea, and 0.25 g/L JBM.

pH	Conjugate Acid	Conjugate Base	Buffer Type
3	Citric acid monohydrate (246 mmol/L)	Trisodium citrate dihydrate (54 mmol/L)	Citrate
4	Acetic Acid (55 mmol/L)	Sodium acetate trihydrate (245 mmol/L)	Acetate
5	Citric acid monohydrate (106 mmol/L)	Trisodium citrate dihydrate (195 mmol/L)	Citrate
6	MES (300 mmol/L)	-	MES
7	Monosodium phosphate (100 mmol/L)	Disodium phosphate (347 mmol/L)	Phosphate
8	Tris-HCl (133 mmol/L)	Tris Base (163 mmol/L)	Tris
9	Boric Acid (296 mmol/L)	-	Boric
10	Sodium carbonate (487 mmol/L)	Sodium bicarbonate (121 mmol/L)	Carbonate
11	Sodium carbonate (730 mmol/L)	Sodium bicarbonate (29 mmol/L)	Carbonate
12	-	Disodium phosphate (566 mmol/L)	Phosphate

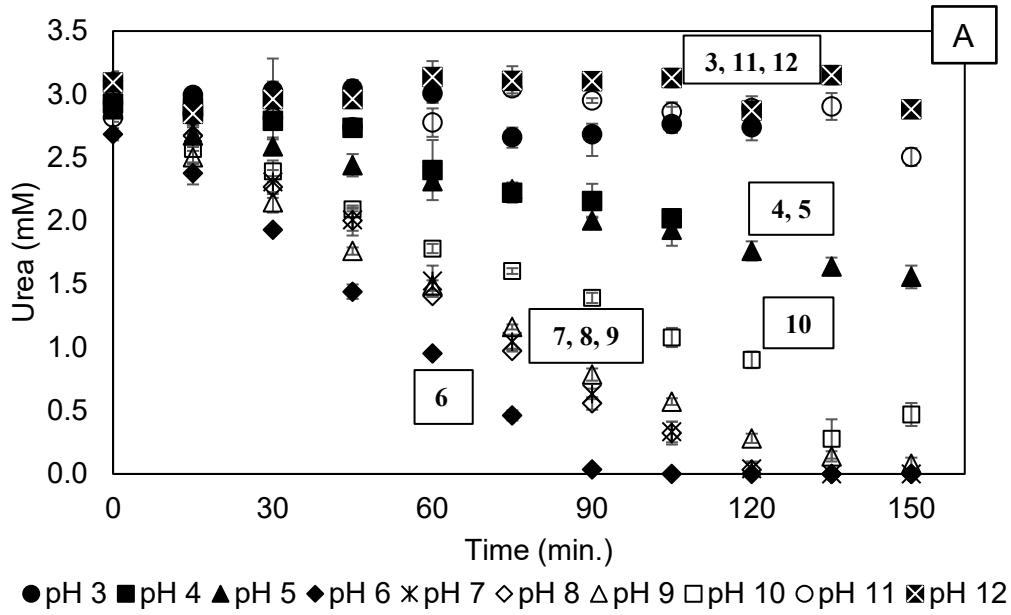

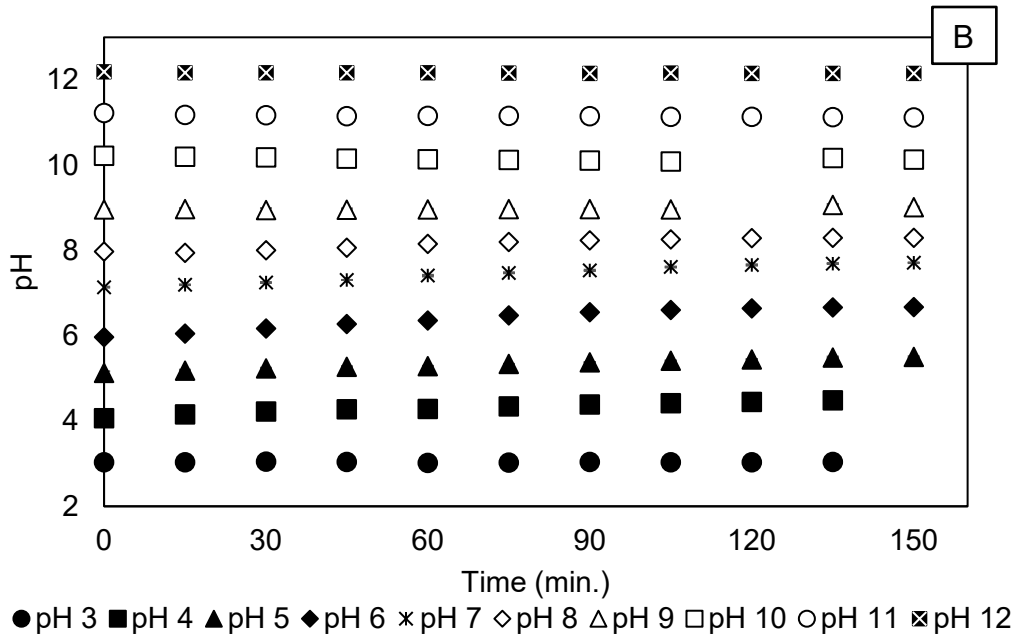

Figure 5.S3: (A) Urea concentration (mmol/L) over time (hours) for all pH values tested. pH ranged from 3 to 12. The fast reaction was observed at 6, while no significant ureolysis was observed at pH values 3,11 and 12. (B) Change in pH was tracked for 150 minutes; with the help of synthetic buffers and lower initial urea concentration (2 g/L or 33 mM) the pH values remained relatively stable while ureolysis occurred (average standard deviation of pH changes is 0.1).

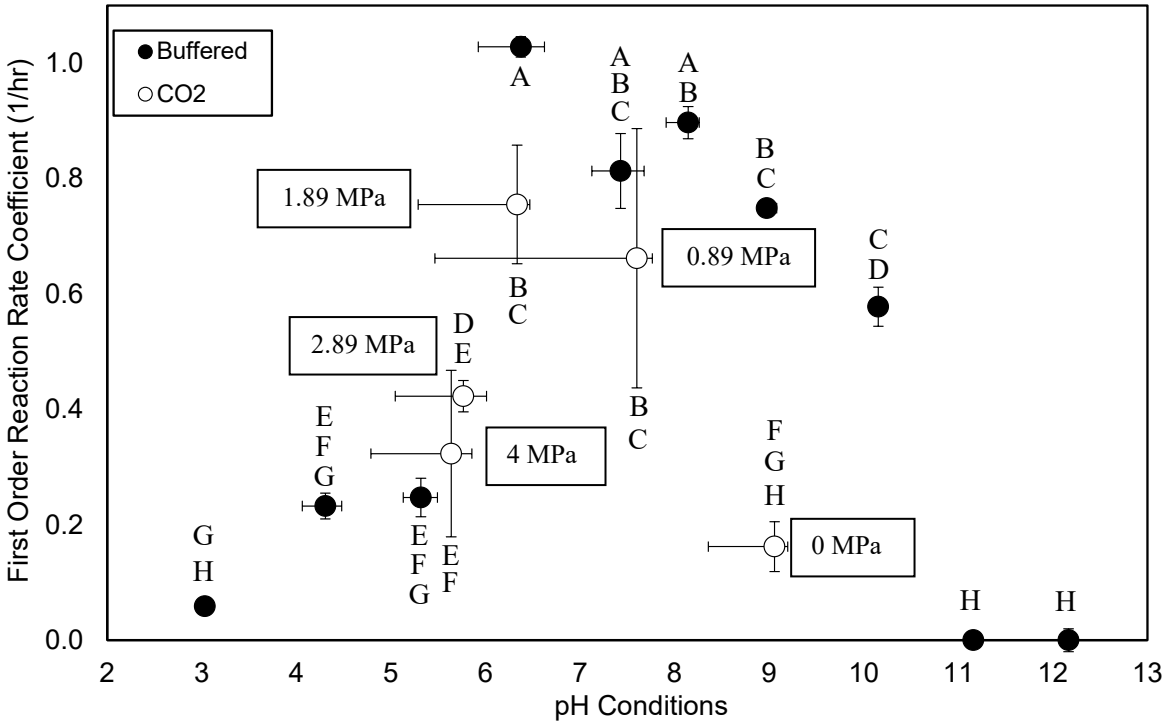

Figure 5.S4: First-order reaction rate coefficients (k_a) of pressurized CO_2 studies (○), constant pH buffered studies (●). Vertical error bars represent one standard deviation of triplicates. Median pH values were plotted, and the range of pH values during the experiment timeframe used for first-order rate coefficient estimation are indicated with horizontal error bars. ANOVA with post-hoc Tukey testing was applied using each triplicate data point for both the CO_2 study and the buffered study alone and then compared to each other. Data points that share the same letter (located either above or below the data points) are not statistically significantly different based on a 95% confidence interval assumption (p = 0.05).

Urease Activity After Low-pH Exposure Studies

Table 5.S2: Synthetic buffers prepared for pH exposure studies. The buffers contained 40 g/L urea and were diluted 1:2 at the beginning of each study with 5 g/L JBM suspension to result in final concentrations 50% of the indicated buffer strength, 20 g/L urea and 2.5 g/L JBM.

Targeted pH	**Conjugate Acid**	**Conjugate Base**	**Buffer Type**
3.7	Glacial Acetic acid (280 mmol/L)	Sodium acetate trihydrate (30 mmol/L)	Acetate
4.1	Glacial Acetic acid (300 mmol/L)	Sodium acetate trihydrate (90 mmol/L)	Acetate
4.7	Glacial Acetic acid (245 mmol/L)	Sodium acetate trihydrate (280 mmol/L)	Acetate
7.1	Monosodium phosphate monohydrate (100 mmol/L)	Sodium phosphate dibasic anhydrous (138 mmol/L)	Phosphate

$$A = A_0 e^{-k_d \cdot t} \text{ or } a = e^{-k_d \cdot t} \text{ where } a = \frac{E}{E_0} = \frac{A}{A_0} \qquad \text{Equation 5.S2}$$

Nomenclature

k_d – inactivation rate coefficient (1/min)
E – concentration of enzyme source (g JBM/L)
A_0 – initial activity of urease (no heat inactivation) (g/(L*min))
A – activity of urease after heat inactivation (g/(L*min))
t – time (min)

a – normalized activity of enzyme (A/A_0) (unitless)

Table 5.S3: First-order reaction coefficients were calculated at circumneutral pH conditions after a one-hour exposure to low-pH conditions at two different temperatures (20 °C and 60 °C). pH 7 exposures for one hour were included as controls.

pH	**Temperature**	**Enzyme Form**	**First-Order Rate Coefficient (hr^{-1})**
7.1 ± 0.1 (Control)	22 °C	Suspended	0.924 ± 0.030
		Immobilized	0.460 ± 0.015
	60 °C	Suspended	0.464 ± 0.028
		Immobilized	0.357 ± 0.024
4.7 ± 0.0	22 °C	Suspended	0.985 ± 0.034
		Immobilized	0.600 ± 0.011
	60 °C	Suspended	0.130 ± 0.053
		Immobilized	0.206 ± 0.006
4.1 ± 0.0	22 °C	Suspended	0.396 ± 0.041
		Immobilized	0.496 ± 0.028
	60 °C	Suspended	0.001 ± 0.001
		Immobilized	0.011 ± 0.002
3.7 ± 0.0	22 °C	Suspended	0.000 ± 0.001
		Immobilized	0.398 ± 0.006
	60 °C	Suspended	0.000 ± 0.000
		Immobilized	0.000 ± 0.001

Literature Comparisons

Data obtained from the literature were modeled using Equation 5.S3, which resulted in the "bell-shaped" reaction rate curves as a function of pH (Figure 5.5) and allowed us to compare our results with the literature.

$$\frac{d[urea]}{dt} = \left(\frac{V_{max}[urea]}{(K_m + [urea])\left(1 + \frac{[H^+]}{K_{es,1}} + \frac{K_{es,2}}{[H^+]}\right)} \right) \quad \text{Equation 5.S3}$$

Where $[H^+]$ is the hydrogen ion concentration, $[urea]$ is the concentration of urea, v_{max} is the maximum rate of reaction (without pH control), K_m is the half-saturation coefficient, and $K_{es,1}$ and $K_{es,2}$ are the acid-base dissociation constants for protonation and deprotonation of the enzyme/substrate complex (Fidaleo & Lavecchia, 2003; Lauchnor et al., 2015). The maximum and minima in each curve depend on the values of $K_{es,1}$ and $K_{es,2}$. Equation 5.S3 can be used to predict the theoretical pH optima of enzymes and assumes that there is only one active form of the protonated enzyme and that the K_m is not dependent on pH (Dixon et al., 1980; Fidaleo & Lavecchia, 2003).

Table 5.S4: Reported kinetic parameters for pH-dependent ureolysis

Urease Source	v_{max} (mmol/L/h)	K_m (mmol/L)	$K_{es,1}$ (pKes,1)	$K_{es,2}$ (pKes,2)	References
0.1 g/L JBM	109	3.21	7.59×10^{-07} (6.12)	1.26×10^{-08} (7.9)	Fidaleo and Lavecchia (2003)
0.01 g/L JBM	27.81	2.47	2.14×10^{-06} (5.67)	8.51×10^{-10} (9.02)	Qin and Cabral (1994)
Immobilized JBM	150	3.21	7.94×10^{-06} (5.81)	7.94×10^{-09} (8.1)	Moynihan et al. (1989)
S. pasteurii	200	305	1.58×10^{-08} (7.8)	6.61×10^{-10} (9.18)	Lauchnor et al. (2015)

CHAPTER SIX

CONCLUSIONS AND OUTLOOK

Conclusions

Ureolysis-induced calcium carbonate ($CaCO_3$) precipitation (UICP) is a promising technology that takes advantage of urea hydrolysis. During UICP, the enzyme urease hydrolyzes urea, and in the presence of calcium (Ca^{2+}), calcium carbonate precipitates can form; this process is also known as biocementation or engineered biomineralization. Urease is found in several bacterial and plant cells. Calcium carbonate precipitates can reduce permeability and porosity in porous media such as soils and rocks and increase particle binding, enabling a wide range of engineering applications, such as the production of building materials, soil stabilization, or subsurface application. An example of a subsurface application is sealing subsurface leakage pathways which can occur during carbon dioxide sequestration, where ureolytic biomineralization can be challenged by low-pH and elevated temperature conditions. Improved enzyme capabilities are essential for the application of biomineralization technology.

In this dissertation, the ureolysis rates and stability of the enzyme responsible for UICP application were investigated, and strategies were developed to improve the stability of the suspended form of urease. Improved enzyme capabilities can become essential for applying biomineralization technology in some fields where biomineralization has to occur under extreme temperature or pH conditions. The enzyme catalyzing the biological reaction has a limited pH and temperature range; hence pH and temperature tolerance of Jack Bean Meal (JBM) and

Sporosarcina pasteurii (*S. pasteurii*) ureases reaction rate (k_a & k_{urea}) and inactivation rate (k_d) constants were modeled for various temperature and pH conditions. In addition, the immobilization technique was used to improve the enzyme stability; pH and temperature tolerances of urease were re-evaluated, and stability improvements were observed after immobilization**.**

When *S. pasteurii* whole cells were exposed to 60 °C for 30 minutes, bacterial cells lost the ability to be cultured on agar plates. When ureolytic activity was tested after exposing cells to 60 °C for one hour, urease was still active even though cells were not able to reproduce. It was demonstrated that it is possible to extract urease from bacterial cells using sonication for cell disruption. *S. pasteurii* extracted urease thermal stability and reaction rates were evaluated at temperatures between 20-80 °C.

In addition to bacterial-based urease, plant-based enzyme sources were investigated because of the potential limitations in using bacteria, such as *S. pasteurii*, in higher temperature applications since *S. pasteurii* has been shown to not grow above 40 °C. It was also demonstrated that *S. pasteurii* extracted urease and JBM urease exhibited an increase in urea hydrolysis rate with increasing temperature; however, above 60 °C, inactivation of urease began occurring quite rapidly.

S. pasteurii and JBM ureases are capable of hydrolyzing urea even at elevated temperature conditions up to 80 °C, even though cells (*S. pasteurii*) are not growing. Eventually, the enzyme becomes thermally inactivated when cells are exposed to elevated temperature conditions. First-order rate coefficients (k_{urea}) of JBM and *S. pasteurii* were compared. Since

S. pasteurii urease content (1% g/g) was significantly higher than JBM (0.14% g/g) (Bachmeier et al., 2002; Krajewska, 2009a), the observed *S. pasteurii* rate coefficients were significantly higher. However, ureolysis with both resources followed the same trend in change in rate coefficients against temperature conditions.

Urease activity and stability were investigated in the presence of pressurized CO_2 and buffered pH solutions. Urease has a limited range of pH conditions where activity is retained; urease activity was explored at various pH conditions (pH 3-12), including low-pH conditions that can mimic carbon sequestration sites if the urease enzyme is to be used in a carbon sequestration application to seal leakage pathways. JBM urease was stressed at various acidic and basic pH conditions. The stability of urease was investigated with suspended and immobilized enzymes. Surface immobilization is well known to stabilize enzymes (Klibanov, 1979; Krajewska, 2009b; Sipehia et al., 1988). The research was performed using the immobilization of urease to increase the temperature and pH tolerance of the enzyme in Chapter 5. pH exposure studies were performed with immobilized and suspended ureases at low-pH conditions (for one hour), and later pH conditions were brought back to circumneutral pH conditions. Ureolytic activity declined when pH conditions were further away from the circumneutral pH conditions in both directions on the pH scale. pH- and temperature-dependent inactivation of urease becomes more prominent below pH 4.7. Immobilized urease was better protected from inhibition at low-pH conditions, even at pH 3.7 at room temperature conditions. When low-pH and elevated temperature (60 °C) stress were applied at the same time, higher inhibition on enzyme activity was observed.

This dissertation's research and development activities contribute to developing environmentally friendly methods, products, and economic competitiveness. Biological manufacturing methods, such as engineered mineral precipitation, can significantly reduce energy-intensive cement manufacturing activities and contribute to resource and climate conservation. The findings of this dissertation will contribute to the foundation of the ureolytic biomineralization technology, and it will be a step toward achieving successful applications.

Outlook

While the results in this dissertation demonstrate ureolytic activity at various temperature and pH ranges, it should be noted that urease activity may not be directly correlated with mineral formation. Urease can be inhibited by environmental conditions such as temperature or pH. In addition to urease inhibition for mineral formation, supersaturation is required for calcium carbonate precipitation to occur (see, *e.g.*, Connolly and Gerlach (2015)). Compounds such as organics (proteins, organic acids, chelators, etc.) can inhibit precipitation reactions (Aggarwal et al., 2013; Arp et al., 2001; Bentov et al., 2010).

Ureolysis rates can differ in the presence of calcium ions due to the mineralization reaction. Moreover, entrapment of urease in precipitated calcium carbonate is possible (Cuthbert et al., 2012), and this factor can be combined with the inactivation of urease due to pH and elevated temperature. The enzyme stability and reaction rates should be investigated in the presence of calcium.

In this dissertation, both JBM urease and *S. pasteurii* extracted urease were successfully immobilized on ceramic carriers. While ceramic carriers were able to improve the stability of JBM urease at elevated temperature conditions and low pH values, these ceramic carriers are not the most abundant material, and other carriers may provide similar or better enzyme stability. Investigation of other materials might allow the cost-effective immobilization of urease. For instance, tons of materials are used daily only once and cannot be recycled efficiently and practically, such as some types of plastics. Discovering new enzyme carriers for the right task can potentially make the process a more sustainable option. If we can immobilize urease on abundant materials, such as used hard-to-recycle plastics, we can reuse materials that go to landfills. Stabilization of plastics using biomineralization may reduce microplastic proliferation; however, this claim should be evaluated. Hard-to-recycle plastics such as polyvinyl chloride (PVC), polypropylene (PP), and polystyrene (PS) can be investigated for the immobilization of ureases. Plastics can be used in biomineralization applications without direct contact with water or water streams to reduce microplastic proliferation, such as in building materials. In addition to plastics, additional ceramic carriers can be investigated, for certain applications, to provide additional stability improvements. Ceramic materials can be used as thermal insulators; larger diameter ceramics may have different porosity, and greater thermal mass per particle may improve enzyme thermal stability by slowing the heat transfer. Suppose the immobilization material can act like a thermal barrier between enzymes and the environment. In that case, slowing down heat transfer at elevated temperatures may help reduce enzymes' thermal inactivation for a period.

While untreated *S. pasteurii* urease could not be immobilized, urease extracted from *S. pasteurii* using a sonication-based method was able to be immobilized on ceramic carriers (Appendix D). The sonication method allowed us to extract urease from *S. pasteurii* in small volumes (40 mL). Different enzyme extraction approaches can be considered for cost and time-efficient scalability. There are at least three standard methods of disrupting bacterial cells to release urease: modified flow-through sonication, French-press, and freeze-drying.

Optimizing enzyme concentration and immobilization material should maximize the enzyme loading efficiency on each enzyme carrier material. If untreated materials do not allow immobilization (adsorption) like ceramic carriers, additional treatment such as gaseous plasma can be applied for potential covalent bonding to immobilize urease (Sipehia et al., 1988). Increasing the stability of urease using immobilization can help biomineralization reactions and be used for other enzymes. Immobilized enzymes can help reduce the total use of enzymes by increasing stability and allowing repeated use; through a collection of enzyme-loaded particles for numerous applications.

Any protein can degrade over time, and storage optimization studies should be performed. A ready-to-use enzyme that is more resilient to stresses would expand the application range of the technology. Suspended urease has a limited lifespan as its activity decreases with time, even when stored at 4 °C. It can be tested whether the immobilization of the enzyme improves storage stability during 4 °C and 22 °C storage. The storability of these enzymes should be investigated for 180 days (and longer, if appropriate). Inactivation models presented in previous chapters (Chapters 3 & 4) can be used to model the storage inactivation and predict

further inactivation longer than 180 days. First-order inactivation rate coefficients (k_d) should be calculated, and the inactivation model can be used to predict activity for storage times longer than 180 days.

UICP is a promising technology that can solve many environmental challenges; however, at the same time, environmental conditions can stress the protein structure of the enzyme. Environmental stresses can lead to inhibition or denaturation of urease. Field conditions should be mimicked in the laboratory environment, and the stability of urease should be evaluated with and without calcium carbonate.

Achieved advancements in this dissertation will contribute to developing advanced biomineralization technologies, which can benefit society with a wide range of applications, including hydraulic fracturing, enhanced oil recovery, dust suppression, and groundwater remediation.

REFERENCES CITED

Abdel-Gawwad, H.A. 2017. Performance of bio-mortar under elevated temperatures. *Journal of Thermal Analysis and Calorimetry*, **130**(3), 1439-1444.

Abdul-Wahab, S.A., Al-Rawas, G.A., Ali, S., Al-Dhamri, H. 2016. Assessment of greenhouse CO_2 emissions associated with the cement manufacturing process. *Environmental Forensics*, **17**(4), 338-354.

Achal, V., Kawasaki, S. 2016. Biogrout: A Novel Binding Material for Soil Improvement and Concrete Repair. *Frontiers in Microbiology*, **7:314**.

Achal, V., Mukherjee, A. 2015. A review of microbial precipitation for sustainable construction. *Construction and Building Materials*, **93**, 1224-1235.

Achal, V., Mukherjee, A., Kumari, D., Zhang, Q. 2015. Biomineralization for sustainable construction – A review of processes and applications. *Earth-Science Reviews*, **148**, 1-17.

Adamson, J. 2006. Preparation of Conductivity and pH Solutions, Vol. 2018, UK Environmental Change Network. Bailrigg Lancaster.

Aggarwal, K.P., Narula, S., Kakkar, M., Tandon, C. 2013. Nephrolithiasis: Molecular Mechanism of Renal Stone Formation and the Critical Role Played by Modulators. *BioMed Research International*, **2013**, 292953.

Akono, A.-T., Druhan, J.L., Dávila, G., Tsotsis, T., Jessen, K., Fuchs, S., Crandall, D., Shi, Z., Dalton, L., Tkach, M.K., Goodman, A.L., Frailey, S., Werth, C.J. 2019. A review of geochemical–mechanical impacts in geological carbon storage reservoirs. *Greenhouse Gases: Science and Technology*, **9**(3), 474-504.

Akyel, A., Coburn, M., Phillips, A.J., Gerlach, R. 2022. Key Applications of Biomineralization. in: *Mineral Formation by Microorganisms*, (Eds.) A. Berenjian, M. Seifan, Springer International Publishing. Cham, pp. 347-387.

Alazhari, M., Sharma, T., Heath, A., Cooper, R., Paine, K. 2018. Application of expanded perlite encapsulated bacteria and growth media for self-healing concrete. *Construction and Building Materials*, **160**, 610-619.

Almajed, A., Lemboye, K., Arab, M.G., Alnuaim, A. 2020. Mitigating wind erosion of sand using biopolymer-assisted EICP technique. *Soils and Foundations*, **60**(2), 356-371.

Alsaba, M., Nygaard, R., Hareland, G., Contreras, O. 2014. Review of Lost Circulation Materials and Treatments with an Updated Classification, 2014 AADE Fluids Technical Conference and Exhibition, Houston, TX.

Alvarado, V., Manrique, E. 2010. Enhanced Oil Recovery: An Update Review. *Energies*, **3**(9), 1529-1575.

Aminu, M.D., Nabavi, S.A., Rochelle, C.A., Manovic, V. 2017. A review of developments in carbon dioxide storage. *Applied Energy*, **208**, 1389-1419.

Anthon, G.E., Barrett, D.M. 2002. Kinetic parameters for the thermal inactivation of quality-related enzymes in carrots and potatoes. *Journal of Agricultural and Food Chemistry*, **50**(14), 4119-4125.

Arias, D., Cisternas, L.A., Rivas, M. 2017. Biomineralization Mediated by Ureolytic Bacteria Applied to Water Treatment: A Review. *Crystals*, **7**(11).

Arp, G., Reimer, A., Reitner, J. 2001. Photosynthesis-Induced Biofilm Calcification and Calcium Concentrations in Phanerozoic Oceans. *Science*, **292**(5522), 1701-1704.

Aymard, C., Belarbi, A. 2000. Kinetics of thermal deactivation of enzymes: a simple three parameters phenomenological model can describe the decay of enzyme activity, irrespectively of the mechanism. *Enzyme and Microbial Technology*, **27**(8), 612-618.

Bachmeier, K.L., Williams, A.E., Warmington, J.R., Bang, S.S. 2002. Urease activity in microbiologically-induced calcite precipitation. *Journal of Biotechnology*, **93**(2), 171-181.

Bagal, J., Onadeko, G., Hazel, P., Dagestad, V. 2016. Annular Barrier as an Alternative to Squeezes in Challenging Wells: Technology Review and Case Histories. *SPE/AAPG Africa Energy and Technology Conference, Nairobi City, Kenya*.

Baines, S.J., Worden, R.H. 2004. The long-term fate of CO_2 in the subsurface: natural analogues for CO_2 storage. *Geological Society, London, Special Publications*, **233**(1), 59-85.

Bang, S.S., Lippert, J.J., Yerra, U., Mulukutla, S., Ramakrishnan, V. 2010. Microbial calcite, a bio-based smart nanomaterial in concrete remediation. *International Journal of Smart and Nano Materials*, **1**(1), 28-39.

Barazorda-Ccahuana, H.L., Gómez, B., Mas, F., Madurga, S. 2020. Effect of pH on the Supramolecular Structure of Helicobacter pylori Urease by Molecular Dynamics Simulations. *Polymers*, **12**(11), 2713.

Barkouki, T.H., Martinez, B.C., Mortensen, B.M., Weathers, T.S., De Jong, J.D., Ginn, T.R., Spycher, N.F., Smith, R.W., Fujita, Y. 2011. Forward and Inverse Bio-Geochemical Modeling of Microbially Induced Calcite Precipitation in Half-Meter Column Experiments. *Transport in Porous Media*, **90**(1), 23.

Basilisk. 2020. Basilisk Info sheet no. 4, https://www.basiliskconcrete.com/en/downloads/, March 10, 2021. 20200205 ed.

Bauer, S., Beyer, C., Dethlefsen, F., Dietrich, P., Duttmann, R., Ebert, M., Feeser, V., Görke, U., Köber, R., Kolditz, O., Rabbel, W., Schanz, T., Schäfer, D., Würdemann, H., Dahmke, A. 2013. Impacts of the use of the geological subsurface for energy storage: an investigation concept. *Environmental Earth Sciences*, **70**(8), 3935-3943.

Behnood, A. 2018. Soil and clay stabilization with calcium- and non-calcium-based additives: A state-of-the-art review of challenges, approaches and techniques. *Transportation Geotechnics*, **17**, 14-32.

Bentov, S., Weil, S., Glazer, L., Sagi, A., Berman, A. 2010. Stabilization of amorphous calcium carbonate by phosphate rich organic matrix proteins and by single phosphoamino acids. *Journal of Structural Biology*, **171**(2), 207-215.

bioMASON. 2020. bioLITH® Overview Information, https://biomason.com/, November 01, 2020.

BioSqueeze®. 2022. https://biosqueeze.com/, Vol. 2022.

Boothroyd, I.M., Almond, S., Qassim, S.M., Worrall, F., Davies, R.J. 2016. Fugitive emissions of methane from abandoned, decommissioned oil and gas wells. *Science of The Total Environment*, **547**, 461-469.

Boquet, E., Boronat, A., Ramos-Cormenzana, A. 1973. Production of Calcite (Calcium Carbonate) Crystals by Soil Bacteria is a General Phenomenon. *Nature*, **246**(5434), 527-529.

Bosch, C., Meiser, W. 1922. Process of manufacturing urea, US1429483A, Patent. Germany.

Boukadi, F., Yaghi, B., Al-Hadrami, H., Bemani, A.L.I., Babadagli, T., De Mestre, P. 2004. A Comparative Study of Lost Circulation Materials. *Energy Sources*, **26**(11), 1043-1051.

Bouwer, E.J., Rijnaarts, H. H. M., Cunningham, A. B., Gerlach, R. 2000. *Biofilms II: Process Analysis and Applications*. John Wiley & Sons.

Brown, D., Sadiq, R., Hewage, K. 2014. An overview of air emission intensities and environmental performance of grey cement manufacturing in Canada. *Clean Technologies and Environmental Policy*, **16**(6), 1119-1131.

Castanier, S., Le Métayer-Levrel, G., Orial, G., Loubière, J.-F., Perthuisot, J.-P. 2000. Bacterial Carbonatogenesis and Applications to Preservation and Restoration of Historic Property. in: *Of Microbes and Art: The Role of Microbial Communities in the Degradation and*

Protection of Cultural Heritage, (Eds.) O. Ciferri, P. Tiano, G. Mastromei, Springer US. Boston, MA, pp. 203-218.

Castro-Alonso, M.J., Montañez-Hernandez, L.E., Sanchez-Muñoz, M.A., Macias Franco, M.R., Narayanasamy, R., Balagurusamy, N. 2019. Microbially Induced Calcium Carbonate Precipitation (MICP) and Its Potential in Bioconcrete: Microbiological and Molecular Concepts. *Frontiers in Materials*, **6**(126).

Cecchi, G., Marescotti, P., Di Piazza, S., Lucchetti, G., Mariotti, M.G., Zotti, M. 2018. Gypsum Biomineralization in Sulphide-rich Hardpans by a Native Trichoderma harzianum Rifai Strain. *Geomicrobiology Journal*, **35**(3), 209-214.

Cesareo, S.D., Langton, S.R. 1992. Kinetic properties of Helicobacter pylori urease compared with jack bean urease. *FEMS Microbiology Letters*, **99**(1), 15-21.

Connolly, J.M. 2015. *Biofilm-induced carbonate precipitation at the pore-scale*. Bozeman, Montana : Montana State University, Bozeman, Montana.

Connolly, J.M., Gerlach, R. 2015. Microbially Induced Carbonate Precipitation in the Subsurface Fundamental Reactions and Transport Processes. Third Edition ed. in: *Handbook of Porous Media*, CRC Press Taylor & Francis Group, pp. 891-922.

Cunningham, A.B., Class, H., Ebigbo, A., Gerlach, R., Phillips, A.J., Hommel, J. 2019. Field-scale modeling of microbially induced calcite precipitation. *Computational Geosciences*, **23**(2), 399-414.

Cunningham, A.B., Gerlach, R., Spangler, L., Mitchell, A.C., Parks, S., Phillips, A. 2011. Reducing the risk of well bore leakage of CO_2 using engineered biomineralization barriers. *Energy Procedia*, **4**, 5178-5185.

Cunningham, A.B., Phillips, A.J., Troyer, E., Lauchnor, E., Hiebert, R., Gerlach, R., Spangler, L. 2014. Wellbore leakage mitigation using engineered biomineralization. *Energy Procedia*, **63**, 4612-4619.

Cunningham, A.B., Sharp, R.R., Caccavo, F., Gerlach, R. 2007. Effects of starvation on bacterial transport through porous media. *Advances in Water Resources*, **30**(6), 1583-1592.

Cuthbert, M.O., McMillan, L.A., Handley-Sidhu, S., Riley, M.S., Tobler, D.J., Phoenix, V.R. 2013. A Field and Modeling Study of Fractured Rock Permeability Reduction Using Microbially Induced Calcite Precipitation. *Environmental Science & Technology*, **47**(23), 13637-13643.

Cuthbert, M.O., Riley, M.S., Handley-Sidhu, S., Renshaw, J.C., Tobler, D.J., Phoenix, V.R., Mackay, R. 2012. Controls on the rate of ureolysis and the morphology of carbonate precipitated by S. Pasteurii biofilms and limits due to bacterial encapsulation. *Ecological Engineering*, **41**, 32-40.

Daily, R. 2019. A Study of Bio-Mineralization For The Application of Reducing Leakage Potential of Geologically Stored CO_2.

Daniel, R.M. 1996. The upper limits of enzyme thermal stability. *Enzyme and Microbial Technology*, **19**(1), 74-79.

Davies, R., Teall, O., Pilegis, M., Kanellopoulos, A., Sharma, T., Jefferson, A., Gardner, D., Al-Tabbaa, A., Paine, K., Lark, R. 2018. Large Scale Application of Self-Healing Concrete: Design, Construction, and Testing. *Frontiers in Materials*, **5**(51).

De Muynck, W., De Belie, N., Verstraete, W. 2010. Microbial carbonate precipitation in construction materials: A review. *Ecological Engineering*, **36**(2), 118-136.

De Muynck, W., Debrouwer, D., De Belie, N., Verstraete, W. 2008. Bacterial carbonate precipitation improves the durability of cementitious materials. *Cement and Concrete Research*, **38**(7), 1005-1014.

De Muynck, W., Leuridan, S., Van Loo, D., Verbeken, K., Cnudde, V., De Belie, N., Verstraete, W. 2011. Influence of pore structure on the effectiveness of a biogenic carbonate surface treatment for limestone conservation. *Applied and environmental microbiology*, **77**(19), 6808-6820.

DeJong, J.T., Fritzges, M.B., Nusslein, K. 2006. Microbially induced cementation to control sand response to undrained shear. *Journal of Geotechnical and Geoenvironmental Engineering*, **132**(11), 1381-1392.

DeJong, J.T., Kavazanjian, E. 2019. Bio-mediated and Bio-inspired Geotechnics. in: *Geotechnical Fundamentals for Addressing New World Challenges*, (Eds.) N. Lu, J.K. Mitchell, Springer International Publishing. Cham, pp. 193-207.

DeJong, J.T., Soga, K., Banwart, S.A., Whalley, W.R., Ginn, T.R., Nelson, D.C., Mortensen, B.M., Martinez, B.C., Barkouki, T. 2011. Soil engineering in vivo: harnessing natural biogeochemical systems for sustainable, multi-functional engineering solutions. *J R Soc Interface*, **8**(54), 1-15.

Denninger, K., Eustes, A., Visser, C., Baker, W., Bolton, D., Bell, J., Bell, S., Jacobs, A., Nagandran, U., Tilley, M. 2015. Optimizing geothermal drilling: Oil and gas technology

transfer. *Transactions, Geothermal Resources Council*, GRC Transactions, Vol. 39, 2015.

Dhami, N.K., Alsubhi, W.R., Watkin, E., Mukherjee, A. 2017. Bacterial Community Dynamics and Biocement Formation during Stimulation and Augmentation: Implications for Soil Consolidation. *Front Microbiol*, **8**, 1267.

Dixon, N.E., Riddles, P.W., Gazzola, C., Blakeley, R.L., Zerner, B. 1980. Jack bean urease (EC 3.5. 1.5). V. On the mechanism of action of urease on urea, formamide, acetamide, N-methylurea, and related compounds. *Canadian journal of biochemistry*, **58**(12), 1335-1344.

Dupraz, C., Reid, R.P., Braissant, O., Decho, A.W., Norman, R.S., Visscher, P.T. 2009a. Processes of carbonate precipitation in modern microbial mats. *Earth-Science Reviews*, **96**(3), 141-162.

Dupraz, S., Parmentier, M., Ménez, B., Guyot, F. 2009b. Experimental and numerical modeling of bacterially induced pH increase and calcite precipitation in saline aquifers. *Chemical Geology*, **265**(1), 44-53.

Dusseault, M.B., Gray, M.N., Nawrocki, P.A. 2000. Why Oilwells Leak: Cement Behavior and Long-Term Consequences, Beijing, China, November 2000. *International Oil and Gas Conference and Exhibition in China*.

Ebigbo, A., Phillips, A., Gerlach, R., Helmig, R., Cunningham, A.B., Class, H., Spangler, L.H. 2012. Darcy-scale modeling of microbially induced carbonate mineral precipitation in sand columns. *Water Resources Research*, **48**(7).

EIA, U.S.E.I.A. 2016. Oil wells drilled horizontally are among the highest-producing wells, https://www.eia.gov/, March 01 2021.

EIA, U.S.E.I.A. 2020. U.S. Oil and Natural Gas Wells by Production Rate, https://www.eia.gov/, March 01 2021.

El Mountassir, G., Minto, J.M., van Paassen, L.A., Salifu, E., Lunn, R.J. 2018. Applications of Microbial Processes in Geotechnical Engineering. *Advances in Applied Microbiology, Vol 104*, **104**, 39-91.

Emmons, P.H., Sordy, D.J. 2006. The State of the Concrete Repair Industry, and a Vision for its Future, pp. 7-14.

Erşan, Y.Ç., Hernandez-Sanabria, E., Boon, N., de Belie, N. 2016a. Enhanced crack closure performance of microbial mortar through nitrate reduction. *Cement and Concrete Composites*, **70**, 159-170.

Erşan, Y.Ç., Verbruggen, H., De Graeve, I., Verstraete, W., De Belie, N., Boon, N. 2016b. Nitrate reducing $CaCO_3$ precipitating bacteria survive in mortar and inhibit steel corrosion. *Cement and Concrete Research*, **83**, 19-30.

Feder, M.J., Akyel, A., Morasko, V.J., Gerlach, R., Phillips, A.J. 2020. Temperature-dependent inactivation and catalysis rates of plant-based ureases for engineered biomineralization. *Engineering Reports*, **3**(2), e12299.

Ferguson, G. 2015. Deep Injection of Waste Water in the Western Canada Sedimentary Basin. *Groundwater*, **53**(2), 187-194.

Ferris, F.G., Phoenix, V., Fujita, Y., Smith, R.W. 2004. Kinetics of calcite precipitation induced by ureolytic bacteria at 10 to 20 degrees C in artificial groundwater. *Geochimica Et Cosmochimica Acta*, **68**(8), 1701-1710.

Fidaleo, M., Lavecchia, R. 2003. Kinetic study of enzymatic urea hydrolysis in the pH range 4-9. *Chemical and Biochemical Engineering Quarterly*, **17**(4), 311-318.

Forsberg, C., Rogers, H.J. 1971. Autolytic Enzymes in Growth of Bacteria. *Nature*, **229**(5282), 272-273.

Frieling, Z. 2019. Urease immobilization for advancing enzyme-induced calcium carbonate precipitation applications, Bozeman, Montana : Montana State University. Bozeman, Montana.

Fujita, Y., Taylor, J.L., Gresham, T.L.T., Delwiche, M.E., Colwell, F.S., McLing, T.L., Petzke, L.M., Smith, R.W. 2008. Stimulation Of Microbial Urea Hydrolysis In Groundwater To Enhance Calcite Precipitation. *Environmental Science & Technology*, **42**(8), 3025-3032.

Gagné, F. 2014. Chapter 2 - Tissue Preparation and Subcellular Fractionation Techniques. in: *Biochemical Ecotoxicology*, (Ed.) F. Gagné, Academic Press. Oxford, pp. 21-31.

Garcia-Galan, C., Berenguer-Murcia, Á., Fernandez-Lafuente, R., Rodrigues, R.C. 2011. Potential of different enzyme immobilization strategies to improve enzyme performance. *Advanced Synthesis & Catalysis*, **353**(16), 2885-2904.

Gardner, D., Lark, R., Jefferson, T., Davies, R. 2018. A survey on problems encountered in current concrete construction and the potential benefits of self-healing cementitious materials. *Case Studies in Construction Materials*, **8**, 238-247.

Gat, D., Ronen, Z., Tsesarsky, M. 2016. Soil Bacteria Population Dynamics Following Stimulation for Ureolytic Microbial-Induced $CaCO_3$ Precipitation. *Environmental Science & Technology*, **50**(2), 616-624.

Gerlach, R. 2001. Transport and activity of dissimilatory metal-reducing bacteria in porous media for the remediation of heavy metals and chlorinated hydrocarbons, Vol. Doctor of Philosophy, Montana State University.

Gomez, M.G., Graddy, C.M.R., DeJong, J.T., Nelson, D.C. 2019. Biogeochemical Changes During Bio-cementation Mediated by Stimulated and Augmented Ureolytic Microorganisms. *Scientific Reports*, **9**(1), 11517.

Gomez, M.G., Martinez, B.C., DeJong, J.T., Hunt, C.E., deVlaming, L.A., Major, D.W., Dworatzek, S.M. 2015. Field-scale bio-cementation tests to improve sands. *Proceedings of the Institution of Civil Engineers - Ground Improvement*, **168**(3), 206-216.

Gowthaman, S., Iki, T., Nakashima, K., Ebina, K., Kawasaki, S. 2019. Feasibility study for slope soil stabilization by microbial induced carbonate precipitation (MICP) using indigenous bacteria isolated from cold subarctic region. *SN Applied Sciences*, **1**(11), 1480.

Grancic, P., Illeova, V., Polakovic, M., Sefcik, J. 2012. Thermally induced inactivation and aggregation of urease: Experiments and population balance modelling. *Chemical Engineering Science*, **70**, 14-21.

Haber, F. 1905. *Thermodynamik technischer Gasreaktionen: Sieben Vorlesungen, Universität Karlsruhe. R. Oldenburg. München, Berlin.* R. Oldenburg.

Haghi, R.K., Chapoy, A., Peirera, L.M.C., Yang, J., Tohidi, B. 2017. pH of CO_2 saturated water and CO_2 saturated brines: Experimental measurements and modelling. *International Journal of Greenhouse Gas Control*, **66**, 190-203.

Hamdan, N., Jr, E.K. 2016. Enzyme-induced carbonate mineral precipitation for fugitive dust control. *Géotechnique*, **66**(7), 546-555.

Hamdan, N., Kavazanjian, E., Rittmann, B.E., Karatas, I. 2017. Carbonate Mineral Precipitation for Soil Improvement Through Microbial Denitrification. *Geomicrobiology Journal*, **34**(2), 139-146.

Hamdan, N., Zhao, Z., Mujica, M., Kavazanjian, E., He, X. 2016. Hydrogel-Assisted Enzyme-Induced Carbonate Mineral Precipitation. *Journal of Materials in Civil Engineering*, **28**(10), 04016089.

Handley-Sidhu, S., Sham, E., Cuthbert, M.O., Nougarol, S., Mantle, M., Johns, M.L., Macaskie, L.E., Renshaw, J.C. 2013. Kinetics of urease mediated calcite precipitation and permeability reduction of porous media evidenced by magnetic resonance imaging. *International Journal of Environmental Science and Technology*, **10**(5), 881-890.

Harrison, W.E.L.K.V.U.S.D.o.E.I.O.O.O.G.S. 1986. *Temperature-gradient information for several boreholes drilled in Oklahoma*. Oklahoma Geological Survey, the University of Oklahoma, Norman, Okla.

He, J., Chu, J., Liu, H. 2014. Undrained shear strength of desaturated loose sand under monotonic shearing. *Soils and Foundations*, **54**(4), 910-916.

Henley, J.P., Sadana, A. 1984. A mathematical analysis of enzyme stabilization by a series-type mechanism: Influence of chemical modifiers. *Biotechnology and Bioengineering*, **26**(8), 959-969.

Herigstad, B., Hamilton, M., Heersink, J. 2001. How to optimize the drop plate method for enumerating bacteria. *Journal of Microbiological Methods*, **44**(2), 121-129.

Heveran, C.M., Williams, S.L., Qiu, J., Artier, J., Hubler, M.H., Cook, S.M., Cameron, J.C., Srubar, W.V. 2020. Biomineralization and Successive Regeneration of Engineered Living Building Materials. *Matter*, **2**(2), 481-494.

Hodges, T.M., Lingwall, B.N. 2020. Laboratory Study in the Treatment of Burned Soils with Microbial Augmentation for Erosion Control. in: *Geo-Congress 2020*, pp. 20-28.

Hommel, J., Akyel, A., Frieling, Z., Phillips, A.J., Gerlach, R., Cunningham, A.B., Class, H. 2020. A Numerical Model for Enzymatically Induced Calcium Carbonate Precipitation. *Applied Sciences*, **10**(13), 4538.

Hommel, J., Lauchnor, E., Gerlach, R., Cunningham, A.B., Ebigbo, A., Helmig, R., Class, H. 2016. Investigating the Influence of the Initial Biomass Distribution and Injection Strategies on Biofilm-Mediated Calcite Precipitation in Porous Media. *Transport in Porous Media*, **114**(2), 557-579.

Hommel, J., Lauchnor, E., Phillips, A., Gerlach, R., Cunningham, A.B., Helmig, R., Ebigbo, A., Class, H. 2015. A revised model for microbially induced calcite precipitation: Improvements and new insights based on recent experiments. *Water Resources Research*, **51**(5), 3695-3715.

Illeova, V., Polakovic, M., Stefuca, V., Acai, P., Juma, M. 2003. Experimental modelling of thermal inactivation of urease. *Journal of Biotechnology*, **105**(3), 235-243.

Illeova, V., Sefcik, J., Polakovic, M. 2020. Thermal inactivation of jack bean urease. *International Journal of Biological Macromolecules*, **151**, 1084-1090.

IPCC. 2014. Intergovernmental Panel on Climate Change Fifth Assessment Report, https://www.ipcc.ch/, March 01 2021.

IPCC. 2018. Summary for Policymakers, https://www.ipcc.ch/, March 01 2021.

Jonkers, H.M. 2011. Healing agent for self-healing cementious material, WO 2011126361 (A1), Patent.

Jonkers, H.M. 2009. Healing agent in cement-based materials and structures, and process for its preparation, WO 2009093898 (A1), Patent.

Jonkers, H.M., Mors, R.M. 2016. Process for the production of cementitious material, WO 2016010434 (A1), Patent.

Jonkers, H.M., Thijssen, A., Muyzer, G., Copuroglu, O., Schlangen, E. 2010. Application of bacteria as self-healing agent for the development of sustainable concrete. *Ecological Engineering*, **36**(2), 230-235.

Joshi, S., Goyal, S., Mukherjee, A., Reddy, M.S. 2017. Microbial healing of cracks in concrete: a review. *Journal of Industrial Microbiology & Biotechnology*, **44**(11), 1511-1525.

Jung, D., Biggs, H., Erikson, J., Ledyard, P.U. 1975. New Colorimetric reaction for end-point, continuous-flow, and kinetic measurement of urea. *Clin Chem*, **21**(8), 1136-40.

Kafarski, P., Talma, M. 2018. Recent advances in design of new urease inhibitors: A review. *Journal of advanced research*, **13**, 101-112.

Kalkan, E. 2020. A Review on the Microbial Induced Carbonate Precipitation (MICP) for Soil Stabilization. in: *International Journal of Earth Sciences Knowledge and Applications*, Vol. 2. www.ijeska.com, pp. 38-47.

Kato, M., Shoda, N., Yamamoto, T., Shiratori, R., Toyo, T. 2009. Development of a silica-based double-network hydrogel for high-throughput screening of encapsulated enzymes. *Analyst*, **134**(3), 577-581.

Khodadadi, T.H., Kavazanjian, E., van Paassen, L., DeJong, J. 2017. Bio-Grout Materials: A Review. *Grouting 2017: Grouting, Drilling, and Verification*(288), 1-12.

King, G.E., King, D.E. 2013. Environmental Risk Arising From Well-Construction Failure—Differences Between Barrier and Well Failure, and Estimates of Failure Frequency Across

Common Well Types, Locations, and Well Age. *SPE Production & Operations*, **28**(04), 323-344.

Kirkland, C.M., Akyel, A., Hiebert, R., McCloskey, J., Kirksey, J., Cunningham, A.B., Gerlach, R., Spangler, L., Phillips, A.J. 2021a. Ureolysis-induced calcium carbonate precipitation (UICP) in the presence of CO_2-affected brine: A field demonstration. *International Journal of Greenhouse Gas Control*, **109**, 103391.

Kirkland, C.M., Hiebert, R., Hyatt, R., McCloskey, J., Kirksey, J., Thane, A., Cunningham, A.B., Gerlach, R., Spangler, L., Phillips, A.J. 2021b. Direct Injection of Biomineralizing Agents to Restore Injectivity and Wellbore Integrity. *SPE Production & Operations*, **36**(01), 216-223.

Kirkland, C.M., Norton, D., Firth, O., Eldring, J., Cunningham, A.B., Gerlach, R., Phillips, A.J. 2019. Visualizing MICP with X-ray μ-CT to enhance cement defect sealing. *International Journal of Greenhouse Gas Control*, **86**, 93-100.

Kirkland, C.M., Thane, A., Hiebert, R., Hyatt, R., Kirksey, J., Cunningham, A.B., Gerlach, R., Spangler, L., Phillips, A.J. 2020. Addressing wellbore integrity and thief zone permeability using microbially-induced calcium carbonate precipitation (MICP): A field demonstration. *Journal of Petroleum Science and Engineering*, **190**, 107060.

Klibanov, A.M. 1979. Enzyme stabilization by immobilization. *Analytical Biochemistry*, **93**, 1-25.

Krajewska, B. 2016. A combined temperature-pH study of urease kinetics. Assigning pK(a) values to ionizable groups of the active site involved in the catalytic reaction. *Journal of Molecular Catalysis B-Enzymatic*, **124**, 70-76.

Krajewska, B. 2018. Urease-aided calcium carbonate mineralization for engineering applications: A review. *Journal of Advanced Research*, **13**, 59-67.

Krajewska, B. 2009a. Ureases I. Functional, catalytic and kinetic properties: A review. *Journal of Molecular Catalysis B-Enzymatic*, **59**(1-3), 9-21.

Krajewska, B. 2009b. Ureases. II. Properties and their customizing by enzyme immobilizations: A review. *Journal of Molecular Catalysis B-Enzymatic*, **59**(1-3), 22-40.

Krajewska, B., van Eldik, R., Brindell, M. 2012. Temperature- and pressure-dependent stopped-flow kinetic studies of jack bean urease. Implications for the catalytic mechanism. *Journal of biological inorganic chemistry : JBIC : a publication of the Society of Biological Inorganic Chemistry*, **17**(7), 1123-1134.

Kudryavtsev, V.A., Spooner, N.J.C., Gluyas, J., Fung, C., Coleman, M. 2012. Monitoring subsurface CO_2 emplacement and security of storage using muon tomography. *International Journal of Greenhouse Gas Control*, **11**, 21-24.

Kujawa, J., Głodek, M., Li, G., Al-Gharabli, S., Knozowska, K., Kujawski, W. 2021. Highly effective enzymes immobilization on ceramics: Requirements for supports and enzymes. *Science of The Total Environment*, **801**, 149647.

Kumari, D., Pan, X., Lee, D.-J., Achal, V. 2014. Immobilization of cadmium in soil by microbially induced carbonate precipitation with Exiguobacterium undae at low temperature. *International Biodeterioration & Biodegradation*, **94**, 98-102.

Lauchnor, E.G., Schultz, L.N., Bugni, S., Mitchell, A.C., Cunningham, A.B., Gerlach, R. 2013. Bacterially Induced Calcium Carbonate Precipitation and Strontium Coprecipitation in a Porous Media Flow System. *Environmental Science & Technology*, **47**(3), 1557-1564.

Lauchnor, E.G., Topp, D.M., Parker, A.E., Gerlach, R. 2015. Whole cell kinetics of ureolysis by Sporosarcina pasteurii. *Journal of Applied Microbiology*, **118**(6), 1321-1332.

Lee, Y.S., Park, W. 2018. Current challenges and future directions for bacterial self-healing concrete. *Applied Microbiology and Biotechnology*, **102**(7), 3059-3070.

Li, M., Cheng, X., Guo, H. 2013. Heavy metal removal by biomineralization of urease producing bacteria isolated from soil. *International Biodeterioration & Biodegradation*, **76**, 81-85.

Li, M., Fu, Q.-L., Zhang, Q., Achal, V., Kawasaki, S. 2015. Bio-grout based on microbially induced sand solidification by means of asparaginase activity. *Scientific reports*, **5**, 16128-16128.

Li, Y., Wang, X., Li, Y.Z., Duan, J.S., Jia, H.N., Ding, H.R., Lu, A.H., Wang, C.Q., Nie, Y., Wu, X.L. 2019. Coupled anaerobic and aerobic microbial processes for Mn-carbonate precipitation: A realistic model of inorganic carbon pool formation. *Geochimica Et Cosmochimica Acta*, **256**, 49-65.

Macleod, F.A., Lappin-Scott, H.M., Costerton, J.W. 1988. Plugging of a model rock system by using starved bacteria. *Appl Environ Microbiol*, **54**(6), 1365-72.

Mansour, A., Dahi Taleghani, A., Salehi, S., Li, G., Ezeakacha, C. 2019. Smart lost circulation materials for productive zones. *Journal of Petroleum Exploration and Production Technology*, **9**(1), 281-296.

Marbun, B. 2013. Evaluation of Non Productive Time Of Geothermal Drilling Operations - Case Study In Indonesia.

Martinez, B.C., DeJong, J.T., Ginn, T.R., Montoya, B.M., Barkouki, T.H., Hunt, C., Tanyu, B., Major, D. 2013. Experimental Optimization of Microbial-Induced Carbonate Precipitation for Soil Improvement. *Journal of Geotechnical and Geoenvironmental Engineering*, **139**(4), 587-598.

Marvasi, M., Mastromei, G., Perito, B. 2020. Bacterial Calcium Carbonate Mineralization *in situ* Strategies for Conservation of Stone Artworks: From Cell Components to Microbial Community. *Frontiers in Microbiology*, **11**(1386).

Mateer, J.G., Marshall, E.K. 1916. The urease content of certain beans, with special reference to the jack bean. *Journal of Biological Chemistry*, **25**(2), 297-305.

Mateo, C., Palomo, J.M., Fernandez-Lorente, G., Guisan, J.M., Fernandez-Lafuente, R. 2007. Improvement of enzyme activity, stability and selectivity via immobilization techniques. *Enzyme and microbial technology*, **40**(6), 1451-1463.

McKenzie, L.M., Witter, R.Z., Newman, L.S., Adgate, J.L. 2012. Human health risk assessment of air emissions from development of unconventional natural gas resources. *Science of The Total Environment*, **424**, 79-87.

Miot, J., Benzerara, K., Morin, G., Kappler, A., Bernard, S., Obst, M., Férard, C., Skouri-Panet, F., Guigner, J.-M., Posth, N., Galvez, M., Brown, G.E., Guyot, F. 2009a. Iron biomineralization by anaerobic neutrophilic iron-oxidizing bacteria. *Geochimica et Cosmochimica Acta*, **73**(3), 696-711.

Miot, J., Benzerara, K., Obst, M., Kappler, A., Hegler, F., Schädler, S., Bouchez, C., Guyot, F., Morin, G. 2009b. Extracellular Iron Biomineralization by Photoautotrophic Iron-Oxidizing Bacteria. *Applied and Environmental Microbiology*, **75**(17), 5586-5591.

Mitchell, A.C., Dideriksen, K., Spangler, L.H., Cunningham, A.B., Gerlach, R. 2010. Microbially Enhanced Carbon Capture and Storage by Mineral-Trapping and Solubility-Trapping. *Environmental Science & Technology*, **44**(13), 5270-5276.

Mitchell, A.C., Espinosa-Ortiz, E.J., Parks, S.L., Phillips, A.J., Cunningham, A.B., Gerlach, R. 2019. Kinetics of calcite precipitation by ureolytic bacteria under aerobic and anaerobic conditions. *Biogeosciences*, **16**(10), 2147-2161.

Mitchell, A.C., Ferris, F.G. 2006a. Effect of strontium contaminants upon the size and solubility of calcite crystals precipitated by the bacterial hydrolysis of urea. *Environmental Science & Technology*, **40**(3), 1008-1014.

Mitchell, A.C., Ferris, F.G. 2006b. The Influence of Bacillus pasteurii on the nucleation and growth of calcium carbonate. *Geomicrobiology Journal*, **23**(3-4), 213-226.

Mitchell, A.C., Phillips, A., Schultz, L., Parks, S., Spangler, L., Cunningham, A.B., Gerlach, R. 2013. Microbial $CaCO_3$ mineral formation and stability in an experimentally simulated high pressure saline aquifer with supercritical CO_2. *International Journal of Greenhouse Gas Control*, **15**, 86-96.

Montana Emergent Technologies. 2020. BioSqueeze® - The silver bullet for the oil and gas industry, https://biosqueeze.com/, March 08, 2021.

Mortensen, B.M., Haber, M.J., DeJong, J.T., Caslake, L.F., Nelson, D.C. 2011. Effects of environmental factors on microbial induced calcium carbonate precipitation. *J Appl Microbiol*, **111**(2), 338-49.

Moynihan, H.J., Lee, C.K., Clark, W., Wang, N.H.L. 1989. Urea Hydrolysis by Immobilized Urease in a Fixed-Bed Reactor - Analysis and Kinetic Parameter-Estimation. *Biotechnology and Bioengineering*, **34**(7), 951-963.

Mugwar, A.J., Harbottle, M.J. 2016. Toxicity effects on metal sequestration by microbially-induced carbonate precipitation. *Journal of Hazardous Materials*, **314**, 237-248.

Mujah, D., Shahin, M.A., Cheng, L. 2017. State-of-the-Art Review of Biocementation by Microbially Induced Calcite Precipitation (MICP) for Soil Stabilization. *Geomicrobiology Journal*, **34**(6), 524-537.

National Research Council. 2005. *Contaminants in the Subsurface: Source Zone Assessment and Remediation*. The National Academies Press, Washington, DC.

Nayberg, T.M. 1987. Laboratory study of lost circulation materials for use in both oil-based and water-based drilling muds. *SPE (Society of Petroleum Engineers) Drill. Eng.; (United States)*, Medium: X; Size: Pages: 229-236.

Nazel, T. 2016. Bioconsolidation of Stone Monuments. An Overview. *Restoration of Buildings and Monuments*, **22**(1), 37.

Nemati, M., Voordouw, G. 2003. Modification of porous media permeability, using calcium carbonate produced enzymatically *in situ*. *Enzyme and Microbial Technology*, **33**(5), 635-642.

NORSOK Standard. 2013. Well integrity in drilling and well operations. NORSOK D-010:2013.

O'Donnell, S.T., Kavazanjian, E., Rittmann, B.E. 2017a. MIDP: Liquefaction Mitigation via Microbial Denitrification as a Two-Stage Process. II: MICP. *Journal of Geotechnical and Geoenvironmental Engineering*, **143**(12), 04017095.

O'Donnell, S.T., Rittmann, B.E., Kavazanjian, E. 2017b. MIDP: Liquefaction Mitigation via Microbial Denitrification as a Two-Stage Process. I: Desaturation. *Journal of Geotechnical and Geoenvironmental Engineering*, **143**(12), 04017094.

Omoregie, A.I., Palombo, E.A., Ong, D.E.L., Nissom, P.M. 2019. Biocementation of sand by Sporosarcina pasteurii strain and technical-grade cementation reagents through surface percolation treatment method. *Construction and Building Materials*, **228**, 116828.

Pacala, S., Socolow, R. 2004. Stabilization Wedges: Solving the Climate Problem for the Next 50 Years with Current Technologies. *Science*, **305**(5686), 968-972.

Papadakis, V.G., Vayenas, C.G., Fardis, M. 1989. A reaction engineering approach to the problem of concrete carbonation. *AIChE Journal*, **35**(10), 1639-1650.

Peng, J., Liu, Z.M. 2019. Influence of temperature on microbially induced calcium carbonate precipitation for soil treatment. *Plos One*, **14**(6).

Perito, B., Marvasi, M., Barabesi, C., Mastromei, G., Bracci, S., Vendrell, M., Tiano, P. 2014. A Bacillus subtilis cell fraction (BCF) inducing calcium carbonate precipitation: Biotechnological perspectives for monumental stone reinforcement. *Journal of Cultural Heritage*, **15**(4), 345-351.

Pham, V.P., Paassen, L.A.v., Star, W.R.L.v.d., Heimovaara, T.J. 2018. Evaluating Strategies to Improve Process Efficiency of Denitrification-Based MICP. *Journal of Geotechnical and Geoenvironmental Engineering*, **144**(8), 04018049.

Phillips, A.J. 2013. *Biofilm-induced calcium carbonate precipitation application in the subsurface*. Bozeman, Montana : Montana State University, Bozeman, Montana.

Phillips, A.J., Cunningham, A.B., Gerlach, R., Hiebert, R., Hwang, C.C., Lomans, B.P., Westrich, J., Mantilla, C., Kirksey, J., Esposito, R., Spangler, L. 2016. Fracture Sealing with Microbially-Induced Calcium Carbonate Precipitation: A Field Study. *Environmental Science & Technology*, **50**(7), 4111-4117.

Phillips, A.J., Gerlach, R., Cunningham, A.B., Spangler, L.H., Akyel, A., Kirkland, C.M., Hiebert, D.R. 2022. Ureolysis-Induced Calcium Carbonate Precipitation for Sealing Channels and Other Uses.

Phillips, A.J., Gerlach, R., Lauchnor, E., Mitchell, A.C., Cunningham, A.B., Spangler, L. 2013a. Engineered applications of ureolytic biomineralization: a review. *Biofouling*, **29**(6), 715-733.

Phillips, A.J., Lauchnor, E., Eldring, J., Esposito, R., Mitchell, A.C., Gerlach, R., Cunningham, A.B., Spangler, L.H. 2013b. Potential CO_2 Leakage Reduction through Biofilm-Induced Calcium Carbonate Precipitation. *Environmental Science & Technology*, **47**(1), 142-149.

Phillips, A.J., Troyer, E., Hiebert, R., Kirkland, C., Gerlach, R., Cunningham, A.B., Spangler, L., Kirksey, J., Rowe, W., Esposito, R. 2018. Enhancing wellbore cement integrity with microbially induced calcite precipitation (MICP): A field scale demonstration. *Journal of Petroleum Science and Engineering*, **171**, 1141-1148.

Polakovič, M., Vrábel, P. 1996. Analysis of the mechanism and kinetics of thermal inactivation of enzymes: Critical assessment of isothermal inactivation experiments. *Process Biochemistry*, **31**(8), 787-800.

Polakovic, M., Vrabel, P., Bales, V. 1998. Approaches for improved identification of mechanisms of enzyme inactivation. in: *Stability and Stabilization of Biocatalysts*, (Eds.) A. Ballesteros, F.J. Plou, J.L. Iborra, P.J. Halling, Vol. 15, Elsevier Science Bv. Amsterdam, pp. 77-82.

Qabany, A.A., Soga, K., Santamarina, C. 2012. Factors Affecting Efficiency of Microbially Induced Calcite Precipitation. *Journal of Geotechnical and Geoenvironmental Engineering*, **138**(8), 992-1001.

Qin, Y., Cabral, J.M.S. 1994. Kinetic studies of the urease-catalyzed hydrolysis of urea in a buffer-free system. *Applied Biochemistry and Biotechnology*, **49**(3), 217-240.

Rahman, Z., Singh, V.P. 2020. Bioremediation of toxic heavy metals (THMs) contaminated sites: concepts, applications and challenges. *Environmental Science and Pollution Research*.

Reddy, M.S. 2013. Biomineralization of calcium carbonates and their engineered applications: a review. *Frontiers in Microbiology*, **4**.

Reetz, M.T., Zonta, A., Simpelkamp, J. 1996. Efficient immobilization of lipases by entrapment in hydrophobic sol-gel materials. *Biotechnology and Bioengineering*, **49**(5), 527-534.

Ren, Q., Henes, B., Fairhead, M., Thöny-Meyer, L. 2013. High level production of tyrosinase in recombinant Escherichia coli. *BMC Biotechnol*, **13**, 18.

Rice, K.C., Bayles, K.W. 2008. Molecular control of bacterial death and lysis. *Microbiology and molecular biology reviews : MMBR*, **72**(1), 85-109.

Rivadeneyra, M.A., Ramos-Cormenzana, A., Delgado, G., Delgado, R. 1996. Process of Carbonate Precipitation by Deleya halophila. *Curr Microbiol*, **32**(6), 308-13.

Rodriguez-Navarro, C., Rodriguez-Gallego, M., Ben Chekroun, K., Gonzalez-Muñoz, M.T. 2003. Conservation of Ornamental Stone by Myxococcus xanthus-Induced Carbonate Biomineralization. *Applied and Environmental Microbiology*, **69**(4), 2182-2193.

Ryparová, P., Tesárek, P., Schreiberová, H., Prošek, Z. 2020. The effect of temperature on bacterial self-healing processes in building materials. *IOP Conference Series: Materials Science and Engineering*, **726**, 012012.

Sadana, A. 1991. *Biocatalysis : fundamentals of enzyme deactivation kinetics*. Prentice Hall, Englewood Cliffs, N.J.

Sadana, A. 1988. Enzyme deactivation. *Biotechnol Adv*, **6**(3), 349-446.

Sadat-Shojai, M., Ershad-Langroudi, A. 2009. Polymeric coatings for protection of historic monuments: Opportunities and challenges. *Journal of Applied Polymer Science*, **112**(4), 2535-2551.

Schomburg, K.T., Ardao, I., Götz, K., Rieckenberg, F., Liese, A., Zeng, A.-P., Rarey, M. 2012. Computational biotechnology: Prediction of competitive substrate inhibition of enzymes by buffer compounds with protein–ligand docking. *Journal of Biotechnology*, **161**(4), 391-401.

Seifan, M., Samani, A.K., Berenjian, A. 2016. Bioconcrete: next generation of self-healing concrete. *Applied Microbiology and Biotechnology*, **100**(6), 2591-2602.

Sen, R. 2008. Biotechnology in petroleum recovery: The microbial EOR. *Progress in Energy and Combustion Science*, **34**(6), 714-724.

Sharma, T.K., Alazhari, M., Heath, A., Paine, K., Cooper, R.M. 2017. Alkaliphilic Bacillus species show potential application in concrete crack repair by virtue of rapid spore production and germination then extracellular calcite formation. *J Appl Microbiol*, **122**(5), 1233-1244.

Sheldon, R.A. 2007. Enzyme Immobilization: The Quest for Optimum Performance. *Advanced Synthesis & Catalysis*, **349**(8-9), 1289-1307.

Sipehia, R., Chawla, A.S., Daka, J., Chang, T.M.S. 1988. Immobilization of enzymes on polypropylene bead surfaces by anhydrous ammonia gaseous plasma technique. *Journal of Biomedical Materials Research*, **22**(5), 417-422.

Skorupa, D.J., Akyel, A., Fields, M.W., Gerlach, R. 2019. Facultative and anaerobic consortia of haloalkaliphilic ureolytic micro-organisms capable of precipitating calcium carbonate. *Journal of Applied Microbiology*.

Smidsrød, O., Skja, G. 1990. Alginate as immobilization matrix for cells. *Trends in biotechnology*, **8**, 71-78.

Stocker, T.F., Qin, D.P., Gian-Kasper , Tignor, M., Allen, S.K., Boschung, J., Nauels, A., Xia, Y.B., Vincent, Midgley, P.M. 2013. Climate change 2013: The physical science basis. *Cambridge University Press*.

Stocks-Fischer, S., Galinat, J., Bang, S.S. 1999. Microbiological precipitation of $CaCO_3$. *Soil Biol. Biochem.*, **31**(11), 1563-1571.

Stumm, W., Morgan, J.J. 2013. Aquatic Chemistry : Chemical Equilibria and Rates in Natural Waters.

Sujoy, B., Aparna, A. 2013. Enzymology, immobilization and applications of urease enzyme. *International Research Journal of Biological Sciences*, **2**(6), 51-56.

Tepe, M., Arslan, S., Koralay, T., Mercan Dogan, N. 2019. Precipitation and characterization of $CaCO_3$ of Bacillus amyloliquefaciens U17 strain producing urease and carbonic anhydrase. *Turkish Journal of Biology*, **43**(3), 198-208.

Thomas, S. 2008. Enhanced Oil Recovery - An Overview. *Oil & Gas Science and Technology - Rev. IFP*, **63**(1), 9-19.

Tiano, P., Biagiotti, L., Mastromei, G. 1999. Bacterial bio-mediated calcite precipitation for monumental stones conservation: methods of evaluation. *Journal of Microbiological Methods*, **36**(1), 139-145.

Tobler, D.J., Cuthbert, M.O., Greswell, R.B., Riley, M.S., Renshaw, J.C., Handley-Sidhu, S., Phoenix, V.R. 2011. Comparison of rates of ureolysis between Sporosarcina pasteurii and an indigenous groundwater community under conditions required to precipitate large volumes of calcite. *Geochimica Et Cosmochimica Acta*, **75**(11), 3290-3301.

Tobler, D.J., Maclachlan, E., Phoenix, V.R. 2012. Microbially mediated plugging of porous media and the impact of differing injection strategies. *Ecological Engineering*, **42**, 270-278.

Tourney, J., Ngwenya, B.T. 2009. Bacterial extracellular polymeric substances (EPS) mediate $CaCO_3$ morphology and polymorphism. *Chemical Geology*, **262**(3), 138-146.

Townsend-Small, A., Ferrara, T.W., Lyon, D.R., Fries, A.E., Lamb, B.K. 2016. Emissions of coalbed and natural gas methane from abandoned oil and gas wells in the United States. *Geophysical Research Letters*, **43**(5), 2283-2290.

Troyer, E., Berninghaus, A., Gerlach, R., Foreman, C., Joyce, J., West, C., Phillips, A.J. 2017. Biomineralized Art: Using Microbes and Minds to Make Mountains. *51st U.S. Rock Mechanics/Geomechanics Symposium*.

UN environment. 2017. GLOBAL STATUS REPORT, https://www.worldgbc.org/, March 01 2021.

Van Lith, Y., Warthmann, R., Vasconcelos, C., Mckenzie, J.A. 2003. Sulphate-reducing bacteria induce low-temperature Ca-dolomite and high Mg-calcite formation. *Geobiology*, **1**(1), 71-79.

van Paassen, L. 2011. Bio-Mediated Ground Improvement: From Laboratory Experiment to Pilot Applications. in: *Geo-Frontiers 2011*, pp. 4099-4108.

van Paassen, L., Ghose, R., van der Linden, T.J.M., van der Star, W.R.L., van Loosdrecht, M.C.M. 2010a. Quantifying Biomediated Ground Improvement by Ureolysis: Large-Scale Biogrout Experiment. *Journal of Geotechnical and Geoenvironmental Engineering*, **136**(12), 1721-1728.

van Paassen, L.A., Daza, C.M., Staal, M., Sorokin, D.Y., van der Zon, W., van Loosdrecht, M.C.M. 2010b. Potential soil reinforcement by biological denitrification. *Ecological Engineering*, **36**(2), 168-175.

Van Tittelboom, K., De Belie, N., De Muynck, W., Verstraete, W. 2010. Use of bacteria to repair cracks in concrete. *Cement and Concrete Research*, **40**(1), 157-166.

Villa, F., Gulotta, D., Toniolo, L., Borruso, L., Catto, C., Cappitelli, F. 2020. Aesthetic Alteration of Marble Surfaces Caused by Biofilm Formation: Effects of Chemical Cleaning. *Coatings*, **10**(2).

Wang, J., Dewanckele, J., Cnudde, V., Van Vlierberghe, S., Verstraete, W., De Belie, N. 2014a. X-ray computed tomography proof of bacterial-based self-healing in concrete. *Cement and Concrete Composites*, **53**, 289-304.

Wang, J.Y., Soens, H., Verstraete, W., De Belie, N. 2014b. Self-healing concrete by use of microencapsulated bacterial spores. *Cement and Concrete Research*, **56**, 139-152.

Wang, L., Paassen, L.A.v., Kavazanjian, E. 2020. Feasibility Study on Liquefaction Mitigation of Fraser River Sediments by Microbial Induced Desaturation and Precipitation (MIDP). in: *Geo-Congress 2020*, pp. 121-131.

Wang, L., van Paassen, L., Gao, Y., He, J., Gao, Y., Kim, D. 2021. Laboratory Tests on Mitigation of Soil Liquefaction Using Microbial Induced Desaturation and Precipitation. 520-534.

Whiffin, V.S., van Paassen, L.A., Harkes, M.P. 2007. Microbial carbonate precipitation as a soil improvement technique. *Geomicrobiology Journal*, **24**(5), 417-423.

Wiktor, V., Jonkers, H.M. 2016. Bacteria-based concrete: from concept to market. *Smart Materials and Structures*, **25**(8), 084006.

Wiktor, V., Jonkers, H.M. 2011. Quantification of crack-healing in novel bacteria-based self-healing concrete. *Cement and Concrete Composites*, **33**(7), 763-770.

Wiktor, V.A.C., Jonkers, H.M. 2014. Bio-based repair method for concrete, WO 2014185781 (A1), Patent.

Wilson, E.J., Johnson, T.L., Keith, D.W. 2003. Regulating the Ultimate Sink: Managing the Risks of Geologic CO_2 Storage. *Environmental Science & Technology*, **37**(16), 3476-3483.

Wong, C.L., Mo, K.H., Yap, S.P., Alengaram, U.J., Ling, T.-C. 2018. Potential use of brick waste as alternate concrete-making materials: A review. *Journal of Cleaner Production*, **195**, 226-239.

Xiao, J., Wang, Z., Tang, Y., Yang, S. 2010. Biomimetic mineralization of $CaCO_3$ on a phospholipid monolayer: from an amorphous calcium carbonate precursor to calcite via vaterite. *Langmuir*, **26**(7), 4977-83.

Yadav, A., Vineeth Reddy, K., Muzzaffar Khan, M., Kalyan Kumar, G., Bandhu, A. 2020. Bio-treatment of Fly Ash. Singapore. Springer Singapore. pp. 505-517.

Yang, J., Pan, X., Zhao, C., Mou, S., Achal, V., Al-Misned, F.A., Mortuza, M.G., Gadd, G.M. 2016. Bioimmobilization of Heavy Metals in Acidic Copper Mine Tailings Soil. *Geomicrobiology Journal*, **33**(3-4), 261-266.

Yudhowijoyo, A., Rafati, R., Sharifi Haddad, A., Raja, M.S., Hamidi, H. 2018. Subsurface methane leakage in unconventional shale gas reservoirs: A review of leakage pathways and current sealing techniques. *Journal of Natural Gas Science and Engineering*, **54**, 309-319.

Yudkin, J. 1937. Cell structure and enzymic activity. *The Biochemical journal*, **31**(7), 1065-1068.

Zahasky, C., Krevor, S. 2020. Global geologic carbon storage requirements of climate change mitigation scenarios. *Energy & Environmental Science*, **13**(6), 1561-1567.

Zambare, N.M., Naser, N.Y., Gerlach, R., Chang, C.B. 2020. Mineralogy of microbially induced calcium carbonate precipitates formed using single cell drop-based microfluidics. *Scientific Reports*, **10**(1), 17535.

Zeng, C., Veenis, Y., Hall, C.A., Stallings Young, E., Van der Star, W.R.L., Zheng, J., Van Paassen, L.A. 2021. Experimental and numerical analysis of a field trial application on microbially induced calcite precipitation for ground stabilization. *Journal for Geotechnical and Geo-environmental Engineering*.

Zhang, H. 2011. 4 - Cement. in: *Building Materials in Civil Engineering*, (Ed.) H. Zhang, Woodhead Publishing, pp. 46-423.

Zhang, W., Zheng, Q., Ashour, A., Han, B. 2020. Self-healing cement concrete composites for resilient infrastructures: A review. *Composites Part B: Engineering*, **189**, 107892.

Zhao, Y., Yao, J., Yuan, Z., Wang, T., Zhang, Y., Wang, F. 2017. Bioremediation of Cd by strain GZ-22 isolated from mine soil based on biosorption and microbially induced carbonate precipitation. *Environmental Science and Pollution Research*, **24**(1), 372-380.

APPENDICES

APPENDIX A

ADDITIONAL RESEARCH: FACULTATIVE AND ANAEROBIC CONSORTIA OF HALOALKALIPHILIC UREOLYTIC MICRO-ORGANISMS CAPABLE OF PRECIPITATING CALCIUM CARBONATE

Abstract

Aims: Development of biomineralization technologies has largely focused on microbially induced carbonate precipitation (MICP) via *Sporosarcina pasteurii* ureolysis; however, as an obligate aerobe, the general utility of this organism is limited. Here, facultative and anaerobic haloalkaliphiles capable of ureolysis were enriched, identified and then compared to *S. pasteurii* regarding biomineralization activities.

Methods and results: Anaerobic and facultative enrichments for haloalkaliphilic and ureolytic micro-organisms were established from sediment slurries collected at Soap Lake (WA). Optimal pH, temperature and salinity were determined for highly ureolytic enrichments, with dominant populations identified via a combination of high-throughput SSU rRNA gene sequencing, clone libraries and Sanger sequencing of isolates. The enrichment cultures consisted primarily of Sporosarcina- and Clostridium-like organisms. Ureolysis rates and direct cell counts in the enrichment cultures were comparable to the *S. pasteurii* (strain ATCC 11859) type strain.

Conclusions: Ureolysis rates from both facultatively and anaerobically enriched haloalkaliphiles were either not statistically significantly different to, or statistically significantly higher than, the *S. pasteurii* (strain ATCC 11859) rates. Work here concludes that extreme environments can harbour highly ureolytic active bacteria with potential advantages for large scale applications, such as environments devoid of oxygen.

Significance and impact of the study: The bacterial consortia and isolates obtained add to the possible suite of organisms available for MICP implementation, therefore potentially improving the economics and efficiency of commercial biomineralization.

Citation

Skorupa, D. J., Akyel, A., Fields, M. W., Gerlach, R. Facultative and anaerobic consortia of haloalkaliphilic ureolytic micro-organisms capable of precipitating calcium carbonate. *Journal of Applied Microbiology*. 2019 Nov;127(5):1479-1489. https://doi.org/10.1111/jam.14384

APPENDIX B

ADDITIONAL RESEARCH: A NUMERICAL MODEL FOR ENZYMATICALLY INDUCED CALCIUM CARBONATE PRECIPITATION

Abstract

Enzymatically induced calcium carbonate precipitation (EICP) is an emerging engineered mineralization method similar to others such as microbially induced calcium carbonate precipitation (MICP). EICP is advantageous compared to MICP as the enzyme is still active at conditions where microbes, e.g., *Sporosarcina pasteurii*, commonly used for MICP, cannot grow. Especially, EICP expands the applicability of ureolysis-induced calcium carbonate mineral precipitation to higher temperatures, enabling its use in leakage mitigation deeper in the subsurface than previously thought to be possible with MICP. A new conceptual and numerical model for EICP is presented. The model was calibrated and validated using quasi-1D column experiments designed to provide the necessary data for model calibration and can now be used to assess the potential of EICP applications for leakage mitigation and other subsurface modifications.

Citation

Hommel, J.; Akyel, A.; Frieling, Z.; Phillips, A.J.; Gerlach, R.; Cunningham, A.B.; Class, H. A Numerical Model for Enzymatically Induced Calcium Carbonate Precipitation. *Applied Sciences.* 2020, *10*, 4538. https://doi.org/10.3390/app10134538

APPENDIX C

ADDITIONAL RESEARCH: UREOLYSIS-INDUCED CALCIUM CARBONATE PRECIPITATION (UICP) IN THE PRESENCE OF CO_2-AFFECTED BRINE: A FIELD DEMONSTRATION

Abstract

Biomineralization is an emerging biotechnology for subsurface engineering applications like remediating leaky wellbores. The process relies on ureolysis to induce precipitation of calcium carbonate in undesired flow paths. In geologic storage of CO_2, there is a potential for leakage and low pH conditions, thus, ureolysis-induced calcium carbonate precipitation (UICP) was tested at field scale to seal a channel in the wellbore cement annulus in the presence of CO_2-affected brine. Conventional oil field methods were used to deliver UICP-promoting fluids downhole to the treatment zone approximately 1000 feet (305 m) below ground surface (bgs). Over 4 days, 242 L (64 gal) of heat-treated *Sporosarcina pasteurii* cultures (22 bailers) and 329 L (87 gal) of urea – calcium chloride solution (30 bailers) were injected. The UICP treatment resulted in a 94% reduction of injectivity and ultrasonic well logging showed a noticeable increase in the percentage of solids in the channel outside the casing, including more than 30 m (100 ft) above the injection point. Subsequent well logging 11 months after the field demonstration showed that a significant portion of the new solids remained but the seal was compromised following sustained pumping. The results of this experiment suggest that UICP can be promoted in the presence of CO_2-affected brine to seal leakage pathways. Additional research is required to optimize long term seal integrity to ensure storage of CO_2 in geologic carbon sequestration scenarios.

Citation

Kirkland, C.M., Akyel, A., Hiebert, R., McCloskey, J., Kirksey, J., Cunningham, A.B., Gerlach, R., Spangler, L., Phillips, A.J. 2021. Ureolysis-induced calcium carbonate precipitation (UICP) in the presence of CO_2-affected brine: A field demonstration. *International Journal of Greenhouse Gas Control*, 109, 103391. https://doi.org/10.1016/j.ijggc.2021.103391

APPENDIX D

IMMOBILIZATION OF UREASE FROM SPOROSARCINA PASTEURII ON CERAMIC CARRIERS

Immobilization of Urease from *Sporosarcina pasteurii* on Ceramic Carriers

S. pasteurii and enzyme extract from *S. pasteurii* culture were attempted to immobilize on ceramic carriers.

For crude cell immobilization, on 25 mL *S. pasteurii,* 15 mL BHI growth medium was added, and the total volume was brought to 40 mL. 25 mL of the cell suspension were mixed with 6 g ceramic carriers (SCALEGUARD, Carbo Ceramics, TX) for 24 hours. After 24 hours, cells were removed from ceramic carriers and rinsed with 25 mL PBS buffer twice.

For enzyme extract, 25 mL cell suspension was treated with the sonication protocol defined in Chapter 4 (6 min. sonication, 2 min. cooling, repeated 5 times). The total volume was brought to 40 mL using the enzyme extraction buffer during the sonication process. After sonication treatments, the enzyme solution was filtered through a 0.2 μm filter. 25 mL of enzyme solution was mixed with 6 g ceramic carriers for 24 hours. After 24 hours, the enzyme solution was removed from ceramic carriers and rinsed with 25 mL PBS buffer twice.

Batch kinetic studies were run using both ceramic carriers by adding 25 mL of 20 g/L urea solution at 40 °C, 115 rpm for 2 hours. Enzyme extract immobilized ceramic carriers hydrolyzed 1.09 mmol. The whole-cell immobilization attempted ceramic carriers hydrolyzed 0.21 mmol urea in 2 hours (Figure D.1). Results indicate whole *S. pasteurii* cells may not be able to attach to ceramic carriers; however, when urease is extracted from whole cells, the enzyme can be immobilized on ceramic carriers similar to jack bean meal urease (demonstrated in Chapter 5).

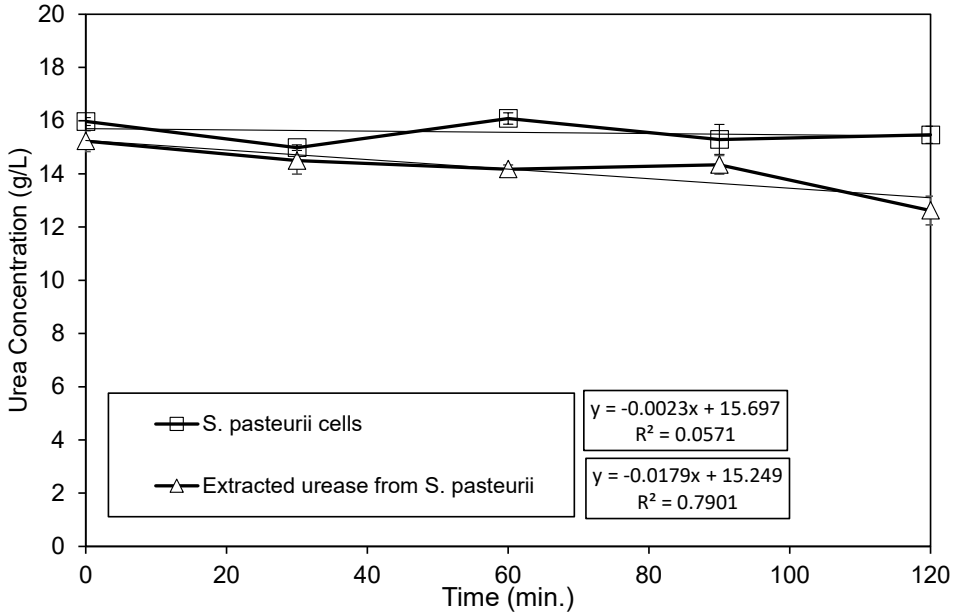

Figure D.1: Ureolysis reactions were tracked using two different ceramic carriers that were attempted to be immobilized with urease extract from *S. pasteurii* and whole *S. pasteurii* cells. The ureolytic activity of two potential enzyme sources was tracked for 2 hours at 40 °C.

APPENDIX E

pH STABILITY OF UREASE PRESENT IN *S. PASTEURII* WHOLE CELLS

pH Stability of Urease Present in *S. pasteurii* Whole Cells

Overnight grown (16 hr) *S. pasteurii* culture was concentrated three times using centrifuging at 5,000 x *g* for 10 minutes at 4 °C. Concentrated *S. pasteurii* whole cells were exposed to pH conditions similar to Jack Bean Meal (JBM) urease described in Chapter 5 (*Low-pH Exposure Studies section*). Four different pH conditions (pH 3.7-7.1) were created using acetate and phosphate buffers (Table 5.S2). First, 5 mL of each buffer was transferred into glass vials in triplicate. Second, 5 mL of three times concentrated *S. pasteurii* whole cells were added.

Cells were exposed for one hour to pH conditions. The pH was measured in each system after the pH exposure (Table E.1). Urea solutions containing pH 7 buffer were added to each of the cell-buffer solutions to achieve a pH of 7 before assessing the remaining ureolytic activity.

Initial pH results showed a higher inhibition to ureolytic activity when whole *S. pasteurii* cells were exposed to the same pH conditions compared to JBM (Figure E.1). Further investigation about the pH stability experiments were performed using JBM urease in Chapter 5 due to higher ureolytic activity after low-pH exposure.

Table E.1: Actual pH values of the buffer solutions after adding *S. pasteurii* cells and urea solutions.

Initial Actual Buffer pH	3.7	4.1	4.7	7.1
After mixing with enzyme solution	3.7 ± 0.0	4.1 ± 0.0	4.7 ± 0.0	7.2 ± 0.0
After mixing with pH 7 buffered urea solution	7.0 ± 0.0	7.0 ± 0.0	7.0 ± 0.0	7.2 ± 0.1

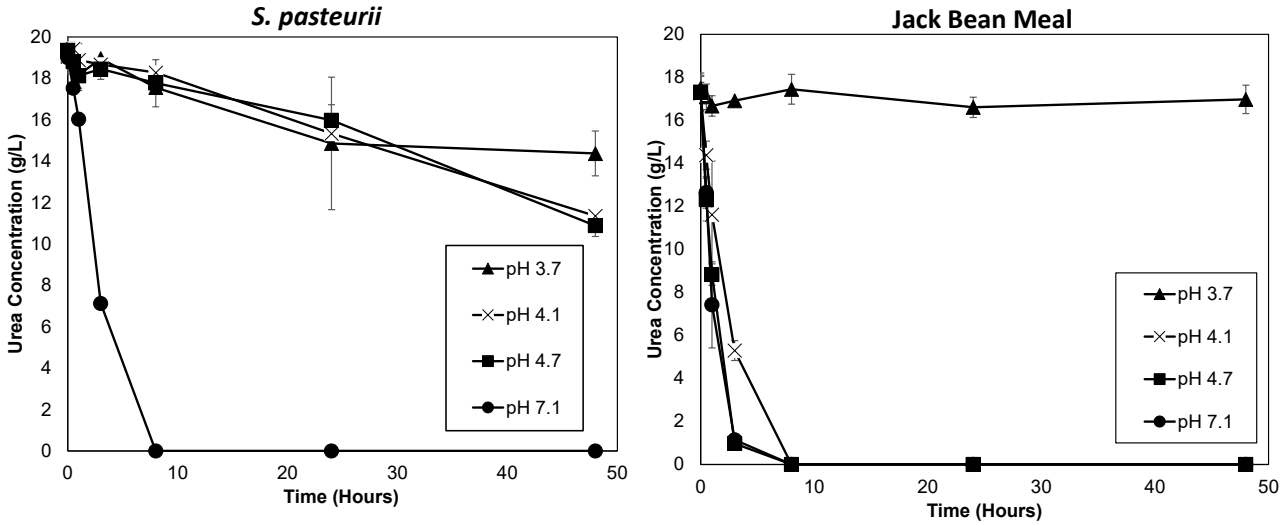

Figure E.1: Change in urea concentration over time were presented for 1-hour exposed urease sources to pH conditions between pH 3.7-7.1. The figure on the left is for *S. pasteurii* whole cells, and the figure on the right is for Jack Bean Meal (JBM).